Methodologies for Mapping the Spatial Extent and Fragmentation of Grassland Using Optical Remote Sensing

GAIRIK ROY
Bachelor of Technology (Honours),
West Bengal University of Technology, India 2009

A Thesis
Submitted to the School of Graduate of the University of Lethbridge in
Partial Fulfillment of the Requirements for the Degree

MASTER OF SCIENCE

Department of Physics & Astronomy
University of Lethbridge
Alberta Terrestrial Imaging Centre
Lethbridge, Alberta, CANADA

ABSTRACT

Grassland is an important part of the ecosystem in the Canadian prairies and its loss and fragmentation affect biodiversity, as well as water and carbon fluxes at local and regional levels. Over the years, native grasslands have been lost to agricultural activities, urban development and oil and gas exploration. This research reports on new methodologies developed for mapping the spatial extent of native grasslands to an unprecedented level of detail and assessing how the grasslands are fragmented. The test site is in the Newell County region of Alberta (NCRA). 72 Landsat and 34 SPOT images from 1985 to 2008 were considered for the analysis. With an airport runway used as a pseudo-invariant feature (PIF), relative radiometric correction was applied to 17 Landsat and 8 SPOT images that included the same airport runway. All the images were classified using the Support Vector Machine (SVM) classification algorithm into grassland, crop, water and road infrastructure classes. The classification results showed an average of 98.2 % overall accuracy for Landsat images and SPOT images. Spatial extents and their temporal change were estimated for all the land cover classes after classifying the images. Fragmentation statistics were obtained using FRAGSTATS 3.3 software that calculated land cover pattern metrics (patch, class and landscape). Based on the available satellite image data, it is found that in Newell County there is almost no significant change found in the grassland and road infrastructure land cover in over two decades. Also, the fragmentation results suggest that fragmentation of grassland was not due to the result of road infrastructure.

ACKNOWLEDGEMENTS

I would like to thank my thesis supervisor, Dr. Philippe Teillet, who provided encouragement, guidance, infrastructure, funding and many very unique opportunities throughout the course of my program. Working with Dr. Phil has been a very intellectually stimulating and rewarding experience. I would also like to thank all the committee members, Dr. Karl Staenz, Dr. Anne M. Smith and Dr. Adriana Predoi-Cross for their help, encouragement and expertise. I would like to extend a special thanks to Dr Anne M. Smith for her suggestions and expert opinions and also for driving from Agriculture and Agri-Food Canada (AAFC) Lethbridge to the University to meet me and give comments on the results. I gratefully acknowledge Dr. Zhijie Wang for his guidance and Ms. Xiaomeng Ren for her help with data analysis problems. I would also like to thank my labmates Ilya Parshakov, Subir Chowdhury and all the employees of Alberta Terrestrial Imaging Centre (ATIC) for helping and encouraging me.

Finally, I am grateful to my family for their support, blessings and encouragement through everything.

TABLE OF CONTENTS

LIST OF TABLES

LIST OF FIGURES

LIST OF ACRONYMS

AESRD - Alberta Environment and Sustainable Resource Development
ATIC – Alberta Terrestrial Imaging Corporation
ATS – Alberta Township Survey
CV – Coefficient of Variation
ETM – Enhanced Thematic Mapper
ETM+ – Enhanced Thematic Mapper Plus
GCP – Ground Control Point
GIS – Geographic Information System
GRIP – Government-Related Initiatives Program
GVI – Grassland Vegetation Inventory
HRV – Haute Resolution Visible
LPI – Largest Patch Index
LSI – Landscape Shape Index
LWIR- Long-Wave Infrared
MERIS – Medium Resolution Imaging Spectrometer
MODIS – Moderate Resolution Imaging Spectroradiometer
MSFE – Macka State Forest Enterprise
MSS – Multi-Spectral Scanner
MWIR- Mid-Wave Infrared
NCRA – Newell County Region of Alberta
NIR – Near Infrared
NP – Number of Patches
NPBI – Native Prairie Baseline inventory
PAFRAC – Perimeter-Area Fractal Dimension
PFRA - Prairie Farm Rehabilitation Administration
PIF – Pseudo-Invariant Feature
RADAR – Radio Detection and Ranging
ROI – Regions Of Interest
SVM – Support Vector Machine
SWIR – Short-Wave Infrared
TIR – Thermal Infrared
TM – Theamtic Mapper
TOA – Top-Of-Atmosphere
USGS – United States Geological Survey
VNIR – Visible and Near Infrared

1 INTRODUCTION

Rangeland is an important contributor to Alberta's economy and to its environmental health. Approximately 95,500 km², or 16 %, of Alberta's land area belongs to rangeland (Castelli et al., 2005). It consists of vast natural landscapes in the form of grasslands, shrublands, woodlands, wetlands and deserts. Most rangeland areas are located in arid and semi-arid environments and, therefore, are very sensitive to climatic influences (James et al., 2003). Rangeland is described as non-forested, native vegetation and is highlighted by grasslands, savannas, and shrublands (e.g., Hunt et al., 2003). Rangeland is an important part of the environment as it reduces soil erosion, sustains animal life with food and shelter, and acts as an ecological buffer zone (Lund, 2007). One of the most important uses of Alberta's rangeland is by the cattle industry for feeding livestock. The industry in Alberta is a $30 billion industry[1] annually and up to 20 % of the feed used for livestock comes from grazing rangeland areas. Human activities, such as camping, canoeing, and kayaking, also take place on rangeland. While providing feed to domestic livestock is important for Alberta's economy, rangeland areas also host a collection of native plants and animal life (Mitchell and Somoliak, 1971; Owens and Myers, 1973; Olsen, 1994). Rangeland health is important as it affects the ecological and economic well-being of plants, animals, and economies that depend on the sustainable management of rangeland.

Native grasslands are a major part of rangeland. They play a significant role in water quality, soil conservation, wildlife habitat and recreation (Marsett et al., 2006). On

[1] "Why Conserve Rangelands: Economic Vitality." Southern Alberta Land Trust Society. Accessed on December 31, 2012 http://www.salts-landtrust.org.

the Canadian Prairies, there are approximately 10 M hectares in the natural grassland region, of which 49 % is in the dry mixed sub-region of Alberta. Over time, native grasslands have been lost to cultivated agriculture, urban development, and oil and gas exploration. Some research has been done to map native grassland change over time. Maps are an invaluable tool for planning the future of grassland areas. Mapping large areas such as grassland is both costly and time-consuming (Ustin et al., 2004). The loss of grasslands can contribute to climate change, decreased biodiversity and economic loss. Changes in the spatial extent and health of these ecosystems can have significant implications for the release of carbon dioxide (Janzen et al., 1997) as well as for wildlife habitats.

Most studies of landscape fragmentation have been conducted in forests (Cakir et al., 2007) or in agricultural lands, places where the anthropogenic impacts on landscape connectivity are particularly evident as a result of large-scale conversion of one land-cover type to another. Agricultural systems have a long history of fragmentation - the conversion of forests and grasslands to cropland by its very nature creates fragmented environments (Hobbs et al., 2008). The economic impact of grassland loss is not known. From an agricultural point of view, the loss of grassland or reduction in grassland health can have a very important effect on Canada's billion-dollar cattle industry. With respect to the Prairie Farm Rehabilitation Administration (PFRA) community pastures in Saskatchewan and Manitoba, approximately $30 M in direct economic activity is generated annually with a further $60 M in indirect activity. A 10 % reduction in the stocking rate, whether as a result of 'wholesale' elimination, fragmentation or health degradation of the grassland, would constitute a $12 M loss (Luciuk et al., 2003)[2].

In an agricultural context, land-use change detection using traditional remote sensing methods of image differencing and principal component analysis can be confounded by changes in agronomic practices as well as the seasonal dynamics of crops both within and across years (Smith and Kloppenburg., 2010). Post-classification methods in which the differences in classified images are derived rely heavily on the accuracy of the classification and yield estimations of land-use change that are often under or over estimated. Combinations of spectroradiometric change and post-classification methods can minimize the errors that occur in image-based land-cover change analysis (Yuan et al., 1998).

Despite the importance of native grasslands, quantifiable estimates of their spatial extent and rate of change due to anthropogenic activity are not readily available because of the expense of collecting the data. The Native Prairie Baseline Inventory (NPBI) was compiled by Alberta Environment and Sustainable Resource Development (AESRD) in 1992-1993 and provides information on native prairie on a quarter-section basis[3]. But many changes and developments have taken place since then. Currently, AESRD is involved in the development of a more detailed database called the Grassland Vegetation Inventory (GVI). Both NPBI and GVI are based upon acquisition of digital air photos and manual interpretation, which is time-consuming and costly and is hardly sustainable in

[2] Luciuk, G.M., Bristol, B., Weins, T.W., and Boyle, D.M., 2003, The potential impact of endangered species legislation on federal grazing lands and the livestock industry. http://www.agr.gc.ca/pfra/pub/endang.htm, (accessed June 2011).

[3] Native Prairie Vegetation Baseline Inventory. http://www.albertapcf.org/background.htm, (accessed on December 31, 2012).

the future. Satellite remote sensing offers a more affordable and timely option to bringing such inventories up to date.

In 2009, Agricultural and Agri-Food Canada started a Government Related Initiatives Program (GRIP) project to develop Earth observation tools for mapping the spatial extent and health of grasslands in Western Canada using optical remote sensing and RADAR (radio detection and ranging). The research in this thesis concerns the estimation of spatial extent of grasslands and their rate of change due to different activities and how the grasslands are fragmented, which results from road infrastructure or oil and gas exploration. This research includes satellite images from more than 2 decades and also addresses the fragmentation statistics analysis of native grasslands unlike the GRIP project. These two aspects distinguish the research in this thesis from the GRIP project.

1.1 Grassland Region Native Prairie

The grassland region native prairie of Alberta approximates some 9,694,650 ha of land, of which 2,857,480 ha are under Crown ownership, while 4,143,960 ha, nearly 43% of the region, remains native prairie. Within these native areas, 2,328,630 ha are under Crown ownership, while 1,815,060 ha are on privately owned[4]. The natural grassland region is further subdivided into four sub-regions. These are Dry Mixed Grass, Mixed Grass, Northern Fescue, and Foothills Fescue.

[4] http://www.albertapcf.org/native-prairie-inventories/npvi

1.2 Native Prairie Vegetation

Any parcel of land in Alberta can be located by its legal and land description. Legal and land descriptions are based on the Alberta Township Survey (ATS) system. It is a grid network dividing the province into equal-sized parcels of land. This way, Alberta is divided into 40 townships and 30 ranges. The Newell County Region of Alberta (NCRA) area falls into townships 15-16 and ranges 12-13. The map in Figure 1.1 provides an overview of where the predominant areas of native prairie remain in southern Alberta. The map includes only those areas having more than 75% native vegetation.

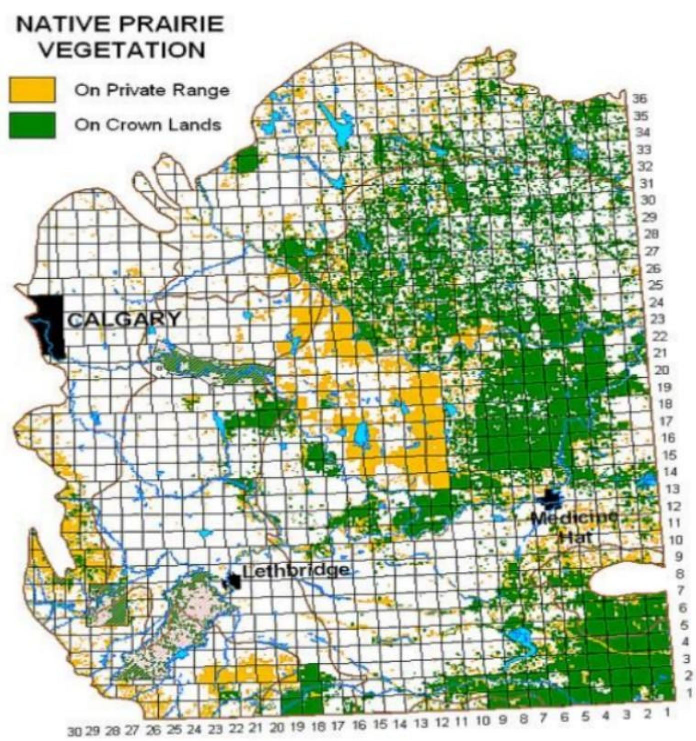

Figure 1.1: Native prairie vegetation map for southern Alberta. (Source: NPBI[5]).

[5] http://www.albertapcf.org/native-prairie-inventories/npvi

1.3 Rangeland Management

Rangeland management is the planning of land-use policies and practices to improve the health and productivity of rangeland areas (Stoddart, 1967). Often, management groups work toward policies that have conservationist goals or may modify land to increase its productivity (Smyth and Dumanski, 1993). In policy development, scientific researchers often contribute to problem identification, strategy formulation in problem solving, setting standards and implementing policy, and monitoring and evaluating existing strategies (Norse and Tschirley, 2000). There are a number of important topics in which policies are being developed and in which rangeland composition plays a large role (Rasmussen and Brunson, 1996; Pyke and Herrick, 2003).

Rangeland management operations have required research to develop new monitoring methods to help improve the health of rangeland. Multispectral, hyperspectral and geographic information system (GIS) data have been successfully combined to monitor grazing gradients for an area of rangeland (Harris et al., 2003).

1.3.1 Rangeland Management Goals

One of AESRD's main interests is the management of rangeland on Alberta's public land[6]. With about 340,000 ha of grazing land used by livestock producers under various forms of dispositions, this management task is a significant responsibility that AESRD shares with ranchers and farmers.

---

[6] Grazing and Range Management
http://www.srd.alberta.ca/LandsForests/GrazingRangeManagement/Default.aspx

Key goals of rangeland management are to maintain[7]:

- A diversity of native plant species, especially deep-rooted and productive forms;
- Vigorous healthy plants with well-developed root systems; and
- Adequate vegetative cover to protect soils from erosion and to conserve scarce moisture.

1.3.2 Rangeland Management Principles

Rangeland management principles are applied to maintain or foster healthy productive rangeland. These include[8]:

- Balancing livestock demands with the available forage supply; the rancher harvests forage to produce red meat but leaves adequate ungrazed residue to protect plants and soil.
- Promoting even livestock distribution by using tools like fencing, salt placement and water development to spread the grazing over the landscape.
- Avoiding grazing rangeland during vulnerable periods; early spring grazing can stress range plants when energy reserves are depleted as new growth is initiated.
- Providing effective rest periods after grazing to allow range plants to recover from the stresses of grazing.

On Alberta rangeland, a planned and balanced cycle of forage harvest and renewal is required to protect this resource and sustain the many benefits that it provides. There is a connection between rangeland management and native grassland as it is a part

[7] http://www.srd.alberta.ca/LandsForests/GrazingRangeManagement/Default.aspx
[8] http://www.srd.alberta.ca/LandsForests/GrazingRangeManagement/Default.aspx

of rangeland, and spatial extent and current and future status of native grassland is not currently available in the prairie region of Canada.

1.4 Remote Sensing

A broad definition of modern-day remote sensing would include human and machine vision, astronomy, space probes, the majority of medical imaging, non-destructive testing, sonar, observing Earth from a distance, and still other areas (Schott, 2007). Some of these activities can be considered the greatest achievements of humankind (Teillet, 2010). Remote sensing can be defined as a technology to acquire information about an object by detecting energy reflected or emitted by that object when the distance between the object and the sensor is much greater than any linear dimension of the sensor (Teillet et al., 2001).

Remotely sensed data of the Earth's surface are acquired using active or passive means (Jensen, 2007). Active sensors provide their own energy source for illumination. They emit radiation that is directed towards the target to be investigated. The radiation reflected from that target is detected and measured by the sensor. For example, RADAR is an active sensor that uses a high-powered radio transmitter/receiver system to transmit a signal that is subsequently reflected by a distant object and the returned signal is detected by the receiver. Passive remote sensing measures electromagnetic energy that is either emitted or reflected by a target. In optical remote sensing, the sensors record energy in the visible, near infrared, short-wave and thermal infrared bands with wavelengths ranging from 0.3 μm to 15 μm.

Optimal management of rangeland systems has been a goal of conservation groups, researchers, and producers for a number of years (Stoddart, 1967), prompting research in ecosystem modelling (Hanson et al., 1988; Welk, 2004). Hunt et al. (2003) provided an overview of the impacts that remote sensing technologies can have on range management. Rangeland managers have been introduced to use of remote sensing products and tools that help in decision making (Butterfield and Malmstrom, 2006; Marsett et al., 2006). For example,the use of Landsat data was introduced in land management decisions and weed control for livestock grazing operations (Butterfield and Malmstrom, 2006).

Grassland condition is very important economically, but it also reflects the number of grazers rangeland can support. It is crucial ecologically, as it indicates the integrity of wildlife habitat (Guo, 2003). Remote sensing has been used before as an approach to monitor grassland health (Guo, 2003) and change (Smith et al., 2009) in western Canada.

1.4.1 Remote Sensing Applications

One of the key roles of remote sensing is to help address some of today's societal issues. Some of the issues are climate change, water supply, food production, environment, natural resources, and sustainability. Remote sensing technology has been applied in these areas in different fields such as agriculture, water management, forestry, land cover, and many more.

1.4.2 Advantages

The advantages of remote sensing are:

- Spatial coverage – Remote sensing allows the acquisition of large amounts of data on a timely basis. However, cloud cover can interfere with timely data acquisition by optical sensors.
- Change detection - Remote sensing covers the same areas repeatedly and can be used to detect changes.
- Spectral coverage – Remote sensing collects data in different wavelength regions of the electromagnetic spectrum not available to human vision or standard photographic systems.
- Spatial resolution – Different remote sensing systems collect data with different footprints (different scales). At small scales, regional phenomena invisible from the ground are clearly visible in remote sensing image data. Examples include faults and other geological structures, a classic example of seeing the forest instead of the trees.
- Digital image data – Remote sensing provides consistent interpretation of the data if sound methods of digital image processing are applied.
- Cost effective - Remote sensing is a cost-effective technique when repeated fieldwork is not required and also a large number of users can share and use the same data.

1.5 Optical Remote Sensing

Optical sensors measure radiation in visible to near infrared (VNIR; 300 nm - 1000 nm), short-wave infrared (SWIR; 1000 nm - 3000 nm), mid-wave infrared (MWIR; 3000 nm – 8000 nm) and long-wave infrared (LWIR; 8000 nm – 15000 nm) wavelength ranges of the electromagnetic spectrum. The MWIR and LWIR are the Thermal infrared (TIR). Because optical sensors typically have lower spatial resolution in the TIR, it is more difficult to extract linear features, e.g., roads, in this wavelength range. Depending on the number of spectral bands used, optical remote sensing can be classified into the following categories:

- Panchromatic imaging systems: Only one wide band is used to detect radiation within a broad range of visible wavelengths. Imagery acquired in this single spectral band will necessarily be in black and white. Examples of imaging systems that include a panchromatic band are SPOT Haute Resolution Visible (HRV) and IKONOS.

- Multispectral imaging systems: Multispectral imaging systems use multichannel detectors and record radiation in multiple bands (3 or more bands, 60-nm wide or wider, which are not necessarily contiguous). Examples are the Landsat Thematic Mapper (TM) and SPOT HRV.

- Superspectral imaging systems: Such systems consist of more than 10 spectral bands that tend to be narrow, which helps to capture finer spectral characteristics of the targets. Examples of this kind of optical remote sensing system are the Moderate Resolution Imaging Spectroradiometer (MODIS) and the Medium Resolution Imaging Spectrometer (MERIS).

• Hyperspectral imaging systems (also known as imaging spectrometers): These are more advanced optical remote sensing systems that record image data in hundreds of narrow contiguous spectral bands. Hyperspectral remote sensing helps to provide information for applications such as mineral exploration, agriculture (crop maturity, moisture level, etc.), coastal management, etc. An example of this type of system is the EO-1 Hyperion.

Optical satellite image data are analysed using digital image analysis, which encompasses a wide variety of techniques. For example, among many thousands of published studies, image classification techniques were compared to spectral vegetation indices for land cover mapping, modelling and analysis of landscape, including fragmentation, for a study area in western Honduras (Southworth et al., 2004). The study area typifies many regions of tropical developing countries, where a complex interaction of social and environmental factors has given rise to a dynamic mosaic of patches of reforestation and deforestation.

1.6 Fragmentation and its Implication

Monitoring land cover change and understanding its dynamics is increasingly important in sustainable development and management of ecosystems. Users from grassland, agriculture and land development communities are interested in the study of fragmentation of grassland. Fragmentation dissects the Earth's surface into spatially isolated parts, rearranges the structure of ecosystems and shapes their functions worldwide. Thus, fragmentation has a major impact in global change. Most scientific studies consider humans the cause of fragmentation of Earth's ecosystems (Hobbs et al., 2008). The state of the Earth's ecosystems cannot be fully understood without carefully considering the coupling between human societies and biological and physical processes. To that end, revealing the effects of fragmentation on people, as well as their roles in driving it, emerges as a critical part of understanding global change (MEA, 2005).

The term fragmentation is used to imply the disconnecting of areas of the landscape from one another. As a result, it restricts access of people and animals to heterogeneity in resources, particularly vegetation and water.

The main reason for the fragmentation of rangeland is conversion of one land cover type to another, which decouples a formerly intact landscape (Hobbs et al., 2008). Another type of fragmentation is compression. It occurs when the activity and mobility of animals or people contracts to isolated pockets within landscapes in the vicinity of settlements (Roth and Fratkin, 2005). Fragmentation of rangeland occurs most often as a result of changes in land tenure. These changes are made to facilitate protection or control of some key portion of the ecosystem, to implement private property rights, or to promote economic intensification (Galaty and Johnson, 1990; Perkins and Thomas, 1993). The research in this thesis is focused on grassland, because currently in the Canadian prairies, there is no information available about spatial extent and current and future status of grassland, and also, how grassland is fragmentated over the decades.

Remote sensing techniques were used to monitor forest cover area located in Macka State Forest Enterprise (MSFE), located in northeast Turkey, from 1975 to 2000 (Cakir et al., 2007) and the spatial and temporal changes in forest cover analysed using GIS and FRAGSTATS. The latter is a fragmentation analysis software package that will be described in Chapter 3. Forest cover changes were detected from a time series of satellite images including Landsat Multi-Spectral Scanner (MSS) in 1975, Landsat TM in 1987, and Landsat Enhanced Thematic Mapper Plus (ETM+) in 2000.

1.7 Objectives

Rangeland differs from grasslands in terms of landscape. Rangeland landscapes include grasslands, shrublands, and woodlands, whereas grasslands commonly consist of grasses and other non-woody plants. This research is more focused towards grasslands than rangeland, as the spatial extent and current and future status of native grasslands are not currently available in the prairie region of Canada and, therefore, are of considerable interest. The study is similar to the GRIP project for spatial extent estimation but adds a change analysis dimension by using 25 years of multispectral satellite imagery. Also, this research is new in terms of fragmentation statistics analysis for grassland areas. These new methodologies have the potential to help the grassland community of western Canada with respect to better usage of grasslands in the future.

The objectives of this research are to use a time series of optical satellite image data to:

- Estimate the spatial extent of native grasslands using multi-year, multi-spectral satellite imagery and, then, to estimate quantitatively the rate and location of grassland change; and
- Estimate the fragmentation of grassland as a result of road infrastructures due to oil and gas exploration and other transportation.

The land cover types of interest for this research include grassland, road infrastructure, crops, and water.

1.8 Hypotheses

There are two main hypotheses tested in this thesis. The first is that remote sensing can provide a unique opportunity to assess and monitor changes in spatial extent as well as fragmentation of grasslands as a result of road infrastructure due to oil and gas exploration and other transportation purposes. The second hypothesis is that better results can be achieved in terms of spatial extent and fragmentation from SPOT-derived land cover over land cover derived from Landsat because of SPOT's higher spatial resolution.

2 STUDY AREA AND DATA SETS

2.1 Study Area

The study area used for this research is in the NCRA. The area is located northwest of Medicine Hat, Alberta at 50° 18´ N and 111° 38´ W and at an elevation of 750 m above sea level. The region has below 1% water incursions (all within 100 m length in size), but it has some petroleum development infrastructure. The main NCRA study area is a 13 km by 13 km region delimited by the following corner coordinates: (5576600 m N, 448600 m E), (5563600 m N, 448600 m E), (5563600 m N, 461600 m E) and (5576600 m N, 461600 m E).

The NCRA study area of interest is shown in Figure 2.1. This area was selected because it is the largest area common to all images considered for this research.

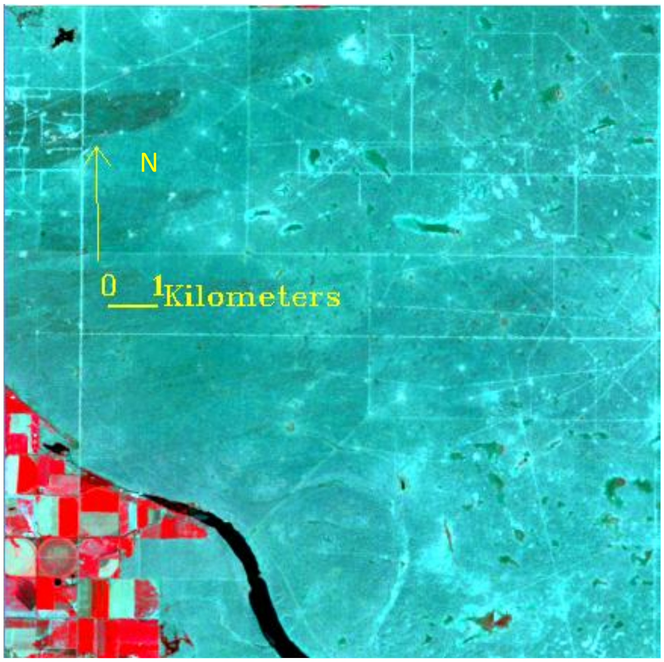

Figure 2.1: Landsat-5 TM July 2, 1987 image of NCRA, 13 km by 13 km, showing the near infrared (NIR) band in red (TM 4), the red band in green (TM 3) and the green band in blue (TM 2). (Source: Natural Resources Canada).

2.2 Data Sets

Satellite digital image data from two satellite systems, Landsat TM and SPOT HRV, were available for the NCRA, where the land cover consists mainly of grassland. The SPOT image data were provided to the University of Lethbridge for research purposes by the Alberta Terrestrial Imaging Corporation (ATIC-Corp). The Landsat image data were downloaded from the United States Geological Survey (USGS) website.

Specifically, the data set consists of 72 Landsat-5 TM images (hereafter referred to as Landsat images) and 34 SPOT HRV images (hereafter referred to as SPOT images). SPOT images were map rectified (UTM zone 12, NAD 83) using ground control points (GCPs) from entire images because the NCRA study area only included a small number of GCPs. The accuracy level of the SPOT HRV images was half a pixel. The Landsat images were downloaded from the USGS website, so these images were already map rectified.

The Landsat images have six spectral bands in the solar reflective spectrum: blue, green, red, near-infrared (NIR), and two shortwave infrared bands (SWIR 1 and SWIR 2). The Landsat images have 30-m spatial resolution, and radiometric and geometric processing level L1. Details of these Landsat technical features are well documented and they can be found on the USGS web site[9].

The SPOT images have three or four spectral bands in the solar reflective spectrum (green, red, NIR bands and, for the later SPOT sensors, a SWIR 1 band) and a 20-m spatial resolution. SPOT-5 sensor images have 10-m spatial resolution. In this study, SPOT-5 images were resampled to 20-m resolution by using nearest neighbor resampling method. The SPOT images have radiometric and geometric processing level 1A[10]. SPOT-1, 2 and 3 offer a 10-m spatial resolution panchromatic band and SPOT-5 offers a 2.5 to 5-m panchromatic band. SPOT-1,2,4 and 5 sensor images were used in this research. No panchromatic imagery was available in the data sets used in this research.

Radiometric correction was performed on the Landsat and SPOT images and it is described in Chapter 3.

---

[9] http://edcsns17.cr.usgs.gov/helpdocs/landsat/product_descriptions.html
[10] http://www.astrium-geo.com/en/195-preprocessing-levels-and-location-accuracy

2.3 NPBI Data Sets

In this research, initially, the NPBI database was used to gather knowledge about the land cover. The NPBI database was created in 1992-93 by AESRD. Each quarter-section of land is interpreted in terms of the percentage area of native vegetation present using the land cover classes given in Table 2.1.

Table 2.1: Native Prairie Baseline Inventory (NPBI) generalized vegetation classification system.

Class	Percent of quarter-section covered by native vegetation (%)
1	100-75
2	74-51
3	50-26
4	25-1
5	<1

The vegetation is grouped into the cover types presented in Table 2.2, with each cover type interpreted to within 5%.

Table 2.2: Native vegetation group cover types defined in the Native Prairie Baseline Inventory.

Vegetation cover type	Designation
Trees	T
Shrubs	S
Graminoid	G
Lake	L
Riparian	R
Wetland	W

Figure 2.2 shows the ArcGIS shapefile of Class 1 of the 13-km by 13-km NCRA study area, i.e., with 75-100% native vegetation. It contains township and quarter section lines.

Figure 2.2: Quarter-sections in the 13-km by 13-km NCRA study area with 75% or more native vegetation.

3 METHODOLOGIES

This chapter presents the methods used to map the spatial extent and determine the fragmentation of grassland based on a time series of optical remote sensing data. Image preprocessing techniques are described, including identification of pseudo-invariant features (PIFs), radiometric correction, and image analysis. Image classification and fragmentation analysis methods using support vector machine (SVM) and FRAGSTATS software, respectively, are also described. A flow chart of the methodologies is given in Figure 3.1.

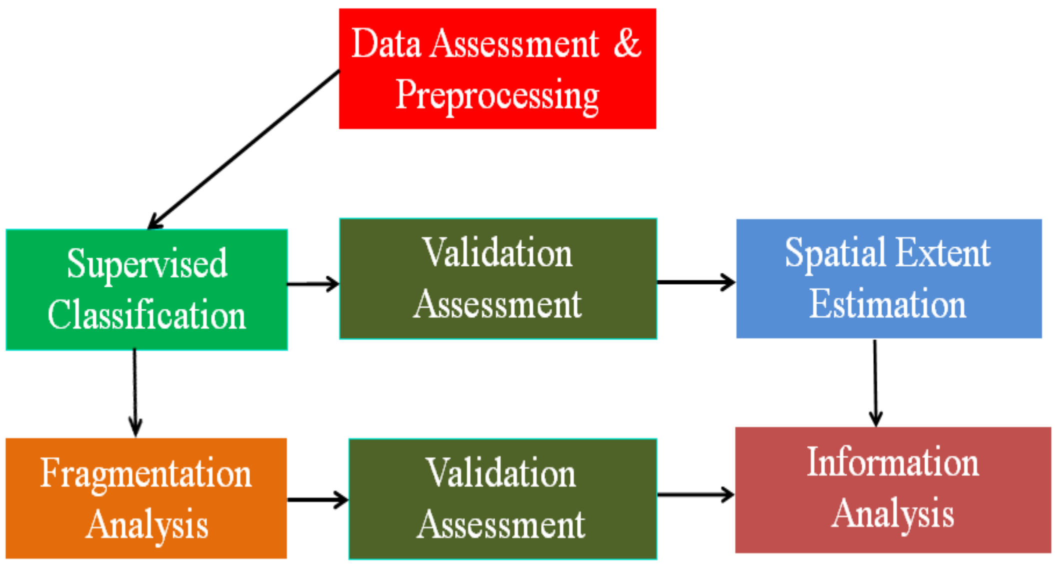

Figure 3.1: A flowchart describing the logical data flow of the methodologies applied in this research.

3.1 Software

Processing and analysis of digital images were carried out using the ITT Corporation[11] digital image analysis software ENVI. FRAGSTATS 3.3 software was used for computing fragmentation statistics based on a wide variety of landscape metrics for categorical map patterns. The original FRAGSTATS software (version 2) was released in to the public domain in 1995 in association with the publication of a United States Department of Agriculture (USDA) technical report (McGarigal and Marks, 1995). The program was completely revamped in 2002[12]. It is a stand-alone program written in Microsoft Visual C++ for use in the Windows Operating environment. It accepts raster images in a variety of formats as input, including ArcGrid, ascii, 16 or 32 bit binary, ERDAS, and IDRISI image files.

3.2 Radiometric Correction

Multitemporal remotely sensed images are very important for change detection and understanding the behaviour of an area and its land cover and land use change, especially in agricultural applications. However, to assure a reliable use of this kind of data, a radiometric correction step is necessary. Optical sensors measure radiance, but for analyzing target characteristics, surface reflectance is preferred. Reflectance (ρ) is obtained by dividing radiance (L) by the irradiance (I) (Price, 1994) :

$$\rho = \frac{\mathrm{L}}{\mathrm{I}} \tag{1}$$

[11] Formerly International Telephone and Telegraph.

[12] **McGarigal, K., SA Cushman, MC Neel, and E Ene. 2002.** FRAGSTATS: Spatial Pattern Analysis Program for Categorical Maps. Computer software program produced by the authors at the University of Massachusetts, Amherst. Available at the following web site: http://www.umass.edu/landeco/research/fragstats/fragstats.html.

Thus, first, a radiometric calibration step converts the digital count of a pixel to radiance in physical units using sensor radiometric calibration coefficients. Radiances can then be converted to top-of-atmosphere (TOA) reflectance using established transformation equations. The additional step of retrieving surface reflectances is non-trivial and involves atmospheric models or empirical normalisation methods (Richter, 1990; Song et al., 2001). The main problem is the difficulty of obtaining an atmospheric characterization on any given image acquisition date. A common normalisation approach is the manual selection and use of pseudo-invariant features (PIFs) in the temporal series of images in order to mitigate differences in atmospheric conditions from date to date (described in Section 3.4).

3.3 Calculation of TOA Reflectance

The key step in the radiometric correction process was to compute the TOA reflectances for each pixel in each image portion of interest. This process takes into account i) radiometric calibration parameters for the relevant acquisition date, ii) the solar zenith angle and iii) the exo-atmospheric solar irradiance for the relevant acquisition date. To obtain data in physical units for SPOT data, the digital counts (Q) provided in image products were converted to TOA spectral radiance (L is in (W / m² sr µm)) using the following equation:

$$L^k = \frac{Q_k}{A_k G_k} \quad (2)$$

where:

A_k is the absolute calibration gain coefficient for band k estimated for the date of image acquisition.

G_k is the analog gain of on-board amplifier for spectral band k.

L^k was then divided by the exo-atmospheric solar irradiance to obtain the TOA reflectance (ρ^k). This was calculated by:

$$\rho^k = \frac{\Pi L^k d_s^2}{E^k . cos\theta_s} \tag{3}$$

where:

E^k is exo-atmospheric solar spectral irradiance[13,14] (W/ (m² μm)).

θ_s is the solar zenith angle in degrees.

d_s is the Earth-Sun distance in Astronomical Units.

The combination of equations (2) and (3) was used to convert SPOT image data from digital counts to TOA reflectance for all spectral bands for all images.

For Landsat images, Q can be converted to radiance L by the following equation:

$$L_K = \frac{Q_K - Q_{K0}}{G_K} \tag{4}$$

where G_k and Q_{k0} are calibration gain and bias for spectral band k, respectively. The combination of equations (3) and (4) were used to convert Landsat image digital counts to ρ^k for all spectral bands for all images.

[13] The exo-atmospheric solar irradiance for SPOT bands is available at http://www.spot.com/web/SICORP/445-sicorp-the-spot-satellites.php

[14] The exo-atmospheric solar irradiance for Landsat bands is available at http://landsathandbook.gsfc.nasa.gov/pdfs/L5_cal_document.pdf

3.4 Pseudo-Invariant Features

The best method for radiometric correction is to use field measurements of the reflectance of the targets of interest, but such data are rarely available. PIFs are ground targets whose reflectances are assumed to be constant over time. Selection of such ground targets for radiometric normalisation is dependent on the abilities and local knowledge of the analyst. There are some generally accepted criteria for a PIF or PIF set (Eckhardt et al., 1990): (i) the targets should contain only minimal amounts of vegetation because vegetation spectral reflectance is subject to change over time; (ii) the targets must be relatively flat areas so that changes in sun angle between images will produce the same proportional increases or decreases in insolation to all normalisation targets; (iii) the spatial pattern of the normalisation target should not change over time.

Features used as PIFs in previous studies have included lakes, beaches, asphalt, concrete and gravel (Elvidge et al., 1995). In some studies, the selection of appropriate PIF sets is not problematic, and reasonable radiometric correction is possible. In other areas, however, the presence of suitable PIFs can be confounded by any combination of variable cloud cover, variable weather leading up to the date of image capture, high topographic complexity in the terrain and lack of suitable targets. For this study, an airport runway (Brooks airport, 50°38′01″N, 111°55′33″W) served as a PIF for atmospheric normalisation (Figure 3.2), but for only a subset of the images available in the time series.

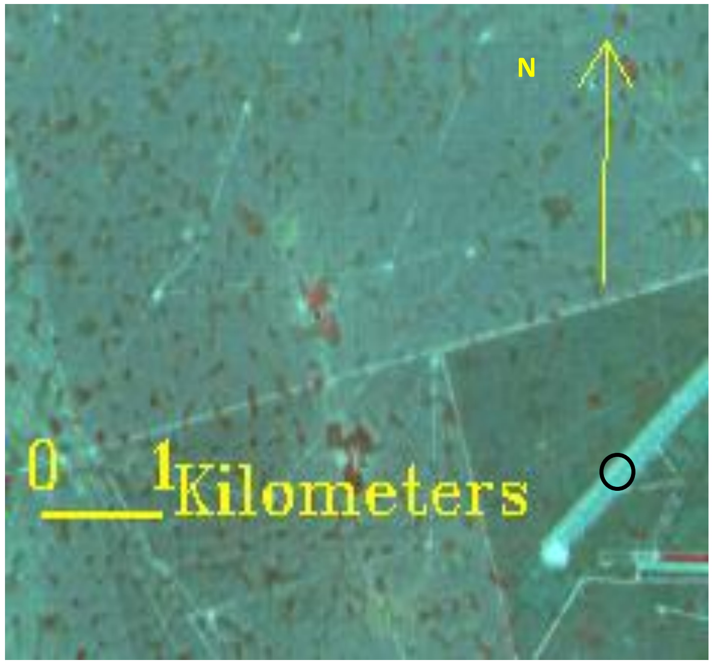

Figure 3.2: PIF (airport runway marked in circle) in the study area, SPOT-1 HRV 1 image June 24, 1986.

All the images were analysed visually to find the PIF and, finally, 17 Landsat and 8 SPOT images were used, because the same airport runway was found in these images only. The change in the TOA reflectance of the runway was not very high over the time span of interest. There were some other PIF pixels found, but those were not suitable because they had a slope (roof tops of buildings) and it was confirmed by the data pre-processing specialist (Xiaomeng Ren, personal communication). As there were some changes in the TOA reflectance of the airport runway over the time period of two decades, only one pixel, which was found consistent over the time, was used. Tables 3.1 and 3.2 contain information about the Landsat and SPOT images that included the PIF.

3.5 Reference Image

One image from the Landsat series was chosen as a reference to which all other images for both the Landsat and SPOT satellite series were normalised. This image should be the least cloud-contaminated, so that the image can be used as the reference for atmospheric normalisation. The reference image that was chosen for the PIF-based atmospheric normalisation is the Landsat image acquired on July 19, 1999. Figure 3.3 shows the chosen reference scene.

3.6 Atmospheric Normalization

All the Landsat and SPOT images were atmospherically normalized relative to the selected reference Landsat image. Based on the mean of the PIF pixels in each image, atmospheric normalization coefficients were calculated for all the images separately. Atmospheric normalization coefficients were calculated using the following formula:

$$\text{Atmospheric normalization coefficient} = \frac{Reference\ image\ PIF\ TOA\ reflectance}{Original\ image\ PIF\ TOA\ reflectance} \qquad (5)$$

Table 3.1: Landsat 30 meter images containing the airport runway PIF.

Image Number	Scene ID	Date	Sensor	Solar Zenith Angle (°)	Solar Azimuth Angle (°)
1	L5040025_02519870702	1987-07-02	Landsat 5 TM	34.2	132.8
2	L5040025_02519880720	1988-07-20	Landsat 5 TM	36.1	135.9
3	L5040025_02519890808	1989-08-08	Landsat 5 TM	40.5	138.2
4	L5040025_02519920731	1992-07-31	Landsat 5 TM	39.2	135.1
5	L5040025_02519940721	1994-07-21	Landsat 5 TM	37.7	131.7
6	L5040025_02519960811	1996-08-11	Landsat 5 TM	42.3	135.8
7	L5040025_02519970627	1997-06-27	Landsat 5 TM	33.3	134.7
8	L5040025_02519980716	1998-07-16	Landsat 5 TM	34.5	138.2
9	L5040025_02519990719	1999-07-19	Landsat 5 TM	35.1	138.2
10	L5040025_02520000705	2000-07-05	Landsat 5 TM	33.3	137.0
11	L5040025_02520010708	2001-07-08	Landsat 5 TM	33.2	138.3
12	L5040025_02520020711	2002-07-11	Landsat 5 TM	34.1	136.6
13	L5040025_02520030714	2003-07-14	Landsat 5 TM	34.4	137.3
14	L5040025_02520040716	2004-07-16	Landsat 5 TM	34.1	139.8
15	L5040025_02520050814	2005-08-14	Landsat 5 TM	37.4	144.72
16	L5040025_02520060807	2006-08-07	Landsat 5 TM	37.6	147.3
17	L5040025_02520080727	2008-07-27	Landsat 5 TM	35.8	142.7

Table 3.2: SPOT 20 meter images containing the airport runway PIF.

Image Number	Date	Sensor	Number of Bands	Solar Zenith Angle (°)	Azimuth Angle (°)	Incidence Angle (°)
1	1986-06-24	SPOT-1 HRV1	3	28.7	155.1	R2.4
2	1988-08-08	SPOT-1 HRV1	3	37.6	148.0	R31.1
3	1994-06-27	SPOT-2 HRV2	3	28.7	155.2	R0.9
4	1999-07-26	SPOT-4 HRVIR2	4	32.5	155.2	R0.6
5	2003-07-17	SPOT-2 HRV2	3	30.6	155.7	L3.0
6	2003-08-12	SPOT-2 HRV2	3	36.4	158.9	L3.0
7	2005-07-11	SPOT-5 HRG1	4	29.5	157.1	L8.6
8	2006-07-21	SPOT-5 HRG 1	4	32.0	152.0	R7.1

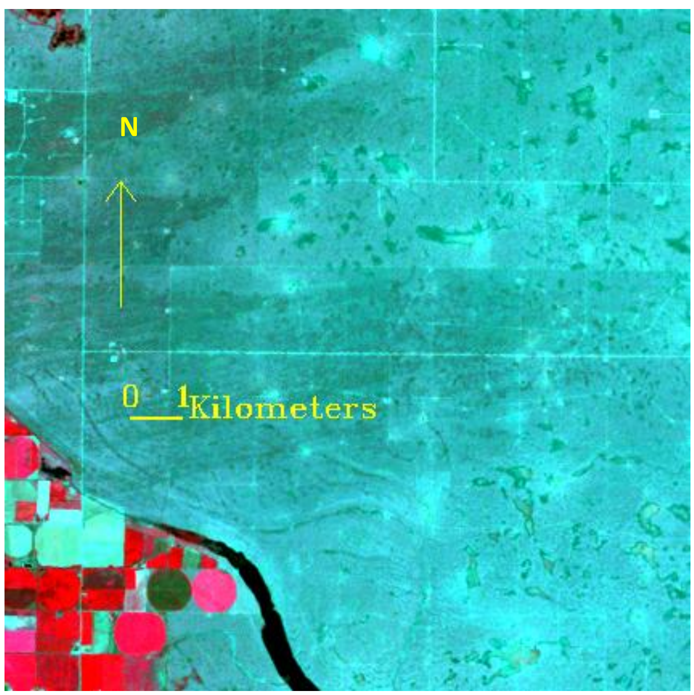

Figure 3.3: Landsat 5 TM image used as reference image, July 19, 1999.

Figure 3.4 shows the July 26, 1999 SPOT image. This figure is presented because it was acquired one week after the reference image was acquired. The Landsat reference image in Figure 3.3 and the SPOT-4 image in figure 3.4 look similar to each other.

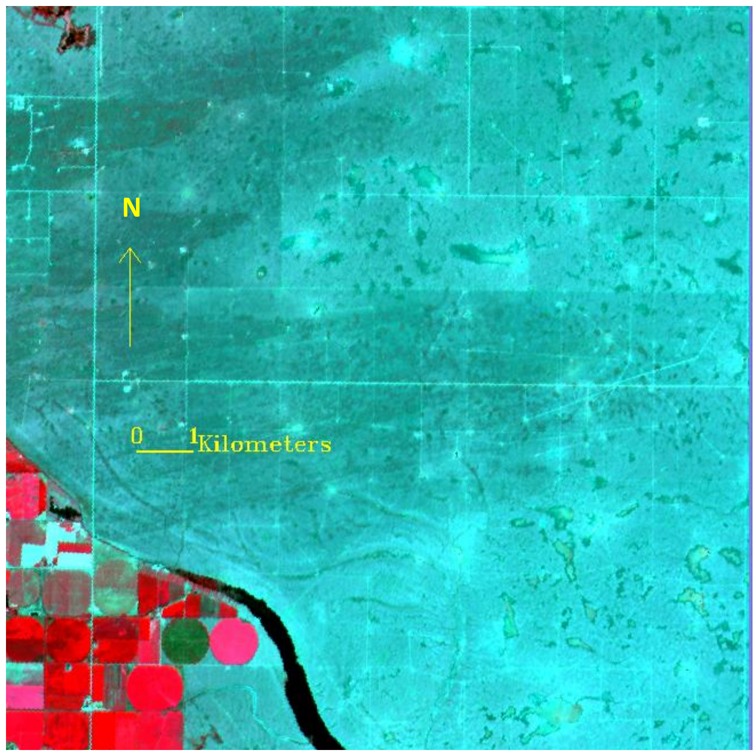

Figure 3.4: SPOT-4 HRVIR-2 image, July 26, 1999.

Tables 3.3 and 3.4 list the atmospheric normalization coefficients for the selected 17 Landsat and 8 SPOT images. The variation in TOA reflectance is caused by the differences in atmospheric conditions. The atmospheric normalization coefficient values in Tables 3.3 and 3.4 are within a reasonable range, indicating that the atmospheric effect is low.

Table 3.3: Atmospheric normalization coefficients for the Landsat images for the indicated dates and for the indicated spectral bands.

Landsat Image Acquisition Date	Band	Coefficient	Landsat Image Acquisition Date	Band	Coefficient
1987-07-02	B1	0.95	2000-07-05	B2	0.99
1987-07-02	B2	0.91	2000-07-05	B3	0.94
1987-07-02	B3	0.94	2000-07-05	B4	1.02
1987-07-02	B4	1.03	2000-07-05	B5	0.94
1987-07-02	B5	1.06	2000-07-05	B7	0.94
1987-07-02	B7	1.03	2001-07-08	B1	0.92
1988-07-20	B1	0.93	2001-07-08	B2	0.90
1988-07-20	B2	0.92	2001-07-08	B3	0.88
1988-07-20	B3	0.91	2001-07-08	B4	0.98
1988-07-20	B4	1.00	2001-07-08	B5	0.92
1988-07-20	B5	0.99	2001-07-08	B7	0.90
1988-07-20	B7	0.94	2002-07-11	B1	0.95
1989-08-08	B1	0.90	2002-07-11	B2	0.92
1989-08-08	B2	0.87	2002-07-11	B3	0.88
1989-08-08	B3	0.84	2002-07-11	B4	0.95
1989-08-08	B4	0.97	2002-07-11	B5	0.98
1989-08-08	B5	0.99	2002-07-11	B7	0.94
1989-08-08	B7	0.94	2003-07-14	B1	0.97
1992-07-31	B1	0.98	2003-07-14	B2	0.93
1992-07-31	B2	0.99	2003-07-14	B3	0.93
1992-07-31	B3	1.00	2003-07-14	B4	0.91
1992-07-31	B4	1.07	2003-07-14	B5	1.01
1992-07-31	B5	1.12	2003-07-14	B7	0.99
1992-07-31	B7	1.07	2004-07-16	B1	0.99
1994-07-21	B1	1.02	2004-07-16	B2	0.98
1994-07-21	B2	0.96	2004-07-16	B3	0.97
1994-07-21	B3	0.98	2004-07-16	B4	1.03
1994-07-21	B4	1.02	2004-07-16	B5	1.02
1994-07-21	B5	1.05	2004-07-16	B7	1.01
1994-07-21	B7	1.01	2005-08-04	B1	0.96
1996-08-11	B1	0.92	2005-08-04	B2	0.90
1996-08-11	B2	0.95	2005-08-04	B3	0.90
1996-08-11	B3	0.92	2005-08-04	B4	0.90
1996-08-11	B4	0.96	2005-08-04	B5	0.95
1996-08-11	B5	1.07	2005-08-04	B7	0.92
1996-08-11	B7	1.06	2006-08-07	B1	0.96
1997-06-27	B1	1.07	2006-08-07	B2	0.94
1997-06-27	B2	1.02	2006-08-07	B3	0.91
1997-06-27	B3	1.04	2006-08-07	B4	0.91
1997-06-27	B4	0.89	2006-08-07	B5	0.97
1997-06-27	B5	1.03	2006-08-07	B7	0.97
1997-06-27	B7	1.07	2008-07-27	B1	1.05
1998-07-16	B1	1.03	2008-07-27	B2	1.01
1998-07-16	B2	1.03	2008-07-27	B3	1.05
1998-07-16	B3	1.02	2008-07-27	B4	0.99
1998-07-16	B4	0.95	2008-07-27	B5	1.04
1998-07-16	B5	0.99	2008-07-27	B7	1.06
1998-07-16	B7	1.02			
1999-07-19	B1	1.00			
1999-07-19	B2	1.00			
1999-07-19	B3	1.00			
1999-07-19	B4	1.00			
1999-07-19	B5	1.00			
1999-07-19	B7	1.00			

Table 3.4: Atmospheric normalization coefficients for the SPOT images for the indicated dates and for the indicated spectral bands.

SPOT Image Acquisition Date	Sensor	Band	Coefficient
1986-06-24	SPOT-1 HRV 1	B1	0.90
1986-06-24	SPOT-1 HRV 1	B2	0.91
1986-06-24	SPOT-1 HRV 1	B3	0.94
1988-08-08	SPOT-1 HRV 1	B1	0.84
1988-08-08	SPOT-1 HRV 1	B2	0.85
1988-08-08	SPOT-1 HRV 1	B3	0.93
1994-06-27	SPOT-2 HRV 2	B1	0.91
1994-06-27	SPOT-2 HRV 2	B2	1.00
1994-06-27	SPOT-2 HRV 2	B3	1.00
1999-07-26	SPOT-4 HRVIR 2	B1	0.98
1999-07-26	SPOT-4 HRVIR 2	B2	0.99
1999-07-26	SPOT-4 HRVIR 2	B3	1.00
1999-07-26	SPOT-4 HRVIR 2	B4	0.97
2003-07-17	SPOT-2 HRV 2	B1	0.96
2003-07-17	SPOT-2 HRV 2	B2	0.97
2003-07-17	SPOT-2 HRV 2	B3	0.90
2003-08-12	SPOT-2 HRV 2	B1	0.87
2003-08-12	SPOT-2 HRV 2	B2	0.87
2003-08-12	SPOT-2 HRV 2	B3	0.91
2005-07-11	SPOT-5 HRG 1	B1	1.05
2005-07-11	SPOT-5 HRG 1	B2	1.04
2005-07-11	SPOT-5 HRG 1	B3	1.04
2005-07-11	SPOT-5 HRG 1	B4	0.93
2006-07-21	SPOT-5 HRG 1	B1	0.96
2006-07-21	SPOT-5 HRG 1	B2	0.90
2006-07-21	SPOT-5 HRG 1	B3	0.97
2006-07-21	SPOT-5 HRG 1	B4	0.83

To assess the extent to which the TOA reflectance of the PIF may have changed over time, the temporal coefficient of variation CV_t was computed via the following formula:

$$CV_t = 100\ [\frac{S_t}{M_t}] \quad [\%] \qquad (6)$$

where:

CV_t is the temporal coefficient of variation.

S_t is the standard deviation of the TOA reflectances.

M_t is the mean of the TOA reflectances.

The CVs of the TOA reflectance of the PIF are as follows:

Table 3.5: CV values based on the PIF TOA reflectance for Landsat images.

Band	**B1**	**B2**	**B3**	**B4**	**B5**	**B7**
CV (%)	0.06502	0.05210	0.05739	0.04940	0.05359	0.05496

Table 3.6: CV values based on the PIF TOA reflectance for SPOT images.

Band	**B1**	**B2**	**B3**	**B4**
CV (%)	0.06474	0.06944	0.04972	0.07296

The CV values indicate that the PIF variability is within 0.1% and, therefore, the PIFs are indeed invariant. There were only three SPOT images (one SPOT- 4 and two SPOT- 5 images), containing the SWIR band (band 4). Therefore, the CV value for SWIR band is higher compared to the other three bands for SPOT images. Only one pixel was used to calculate the CV values for Landsat and SPOT images, as only this pixel was found consistent over the two decades time period.

3.7 Digital Image Classification

The classification of the digital images was carried out using ENVI 4.7. The Support Vector Machine (SVM; Brown et al., 1999) classifier was used for supervised classification of the images into four classes: grassland, road infrastructure (oil and gas, transportation and oil wells), crops, and water. SVM is a learning machine classifier in which input vectors are mapped in a non-linear, high-dimensional space (Cortes and Vapnik, 1995).

The SVM classifier has been well known for some time in the field of machine learning and pattern recognition, and it was introduced more recently to the field of remote sensing (Huang et al., 2002; Melgani and Bruzzone, 2004). It is based on generating a hyperplane between the training samples that separates the two classes in multi-dimensional feature space. SVM was chosen in this research because it performs well with small training sets, even when high-dimensional datasets are classified, because it only considers training data close to the class boundary (Fauvel et al., 2006). The use of a kernel parameter in SVM influences the outome of the classification results by increasing the accuracy of remote sensing data processing. Kernel parameter is robust to noise and effective when dealing with low numbers of high-dimensional samples. It helps to produce accurate and robust classification results by linearizing data, even when the input data are non-linearly separable.

Texture analysis using occurrence texture measures in ENVI was also considered for extracting linear features like roads. The texture features included Data range, Mean, Variance, Entropy, and Skewness for each spectral band. Each texture feature was used in ENVI to identify roads and infrastructure. Data range, Mean and Variance appeared to identify more roads and infrastructure than Entropy and Skewness. It is better to extract more existing linear features so that existing road infrastructure and oil and gas exploration can be identified from the whole area and it will be easier to understand the fragmentation of the grassland. Therefore, Data range, Mean and Variance features of each spectral band were used together with the spectral bands of the original satellite images and then SVM classification was performed. Regions of interest (ROIs) were created for each land cover class and 50 % of the observations used for training of the classifier and 50 % for validation. The identification of the training and validation ROIs was done by visual examination of the images and with the help of local knowledge of the area from field expert. Figures 3.5 and 3.6 present the co-occurrence data range texture measure images of Landsat and SPOT images respectively.

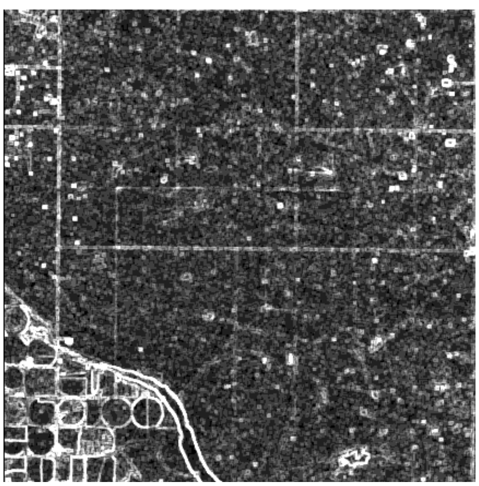

Figure 3.5: Occurence data range texture measure August 7, 2006, Landsat.

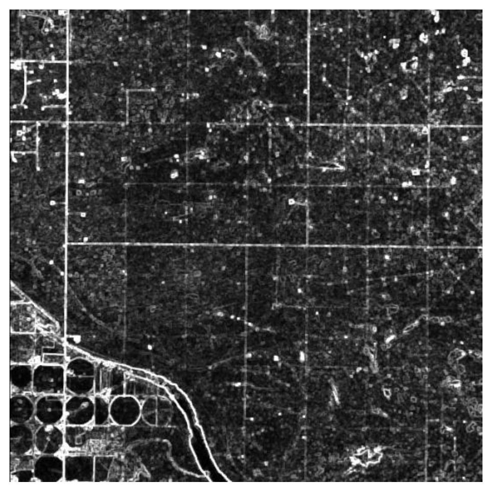

Figure 3.6: Occurence data range texture measure July 21, 2006, SPOT.

Occurrence data range texture measure images of Landsat (Figure 3.5) and SPOT (Figure 3.6) show that the linear features are easy to identify after performing the texture analysis. Existing road infrastructure can be extracted easily from the data range texture measure images of the study area.

3.8 Spatial Extent Estimation

The spatial extent of all the land cover classes was estimated from the SVM classification maps by calculating the amount of land covered by each class in the NCRA study area in hectares (ha). The statistics were computed from the satellite thematic maps produced after the SVM classification to find the number of pixels of each land cover class, then multiplied by the Landsat or SPOT pixel area to find the amount of land covered by each of the classes. Temporal analysis of the land cover amount in each class is presented in the results section.

3.9 Fragmentation Statistics Analysis

Fragmentation analysis was based on selected landscape metrics calculated using FRAGSTATS 3.3 for each individual land cover class as mapped by the image classification. FRAGSTATS offers a comprehensive choice of landscape metrics and has been used by investigators to quantify landscape structure (McGarigal et al., 2009). The fragmentation metrics involve qualitative and quantitative measures that express the characteristics of the landscape as a whole (Abdullah and Nakagoshi, 2006). The advantage of FRAGSTATS is that the calculations are implemented in a GIS framework and, consequently, the results are easy to apply to digital images and maps (McGarigal and Marks, 1995; Raines, 2002).

There are two versions of FRAGSTATS: one accepts Arc/Info polygon vector coverages and one accepts a raster image in various formats. The vector version of FRAGSTATS is in Arc/Info ARC Macro Language (AML), which is a high-level algorithmic language for generating applications in Arc/Info, developed on a SUN workstation running Arc/Info version 9.3. It will not run with earlier versions of Arc/Info. For this study, the raster version of FRAGSTATS was used.

FRAGSTATS provides a very comprehensive set of spatial statistics and descriptive metrics of patterns at the patch level (characteristics of an individual patch), class level (characteristics of one type of patch) and landscape level (characteristics of all classes in the landscape and their pattern) (Haines-Young and Chopping, 1996).

3.9.1 Metrics Computed in FRAGSTATS

Tables 3.6 to 3.13 outline the Area, Patch, Edge, Shape, Core, Nearest Neighbour, Diversity, Contagion, and connectivity metrics computed by the FRAGSTATS software.

Table 3.7: Fragstats area metrics.

Scale	Acronym	Metric (units)
Patch	Area	Area (ha)
Patch	LSIM	Landscape similarity index (percent)
Class	CA	Class area (ha)
Class/landscape	TA	Total landscape area (ha)
Class/landscape	LPI	Largest patch index (percent)

Table 3.8: Fragstats patch metrics.

Scale	**Acronym**	**Metric (units)**
Class/landscape	NP	Number of patches
Class/landscape	PD	Patch density (number/100 ha)
Class/landscape	MPS	Mean patch size (ha)
Class/landscape	PSSD	Patch size standard deviation (ha)
Class/landscape	PSCV	Patch size coefficient of variation

Table 3.9: Fragstats edge metrics.

Scale	**Acronym**	**Metric (units)**
Patch	PERIM	Perimeter (m)
Patch	EDCON	Edge contrast index (percent)
Class/landscape	TE	Total edge (m)
Class/landscape	ED	Edge density (m/ha)
Class/landscape	CWED	Contrast-weighted edge density (m/ha)

Table 3.10: Fragstats shape metrics.

Scale	**Acronym**	**Metric (units)**
Patch	Shape	Shape index
Patch	FRACT	Fractal dimension
Class/landscape	LSI	Landscape shape index
Class/landscape	MSI	Mean shape index
Class/landscape	AWMSI	Area-weighted mean shape index
Landscape	PAFRAC	Perimeter area fractal dimension

Table 3.11: Fragstats core area metrics.

Scale	**Acronym**	**Metric (units)**
Patch	CORE	Core area (ha)
Patch	NCORE	Number of core areas
Patch	CAI	Core area index (percent)
Class	C % LAND	Core area percentage of landscape
Class/landscape	TCA	Total core area (ha)

Table 3.12: Fragstats nearest neighbor metrics.

Scale	**Acronym**	**Metric (units)**
Patch	NEAR	Nearest neighbor distance (m)
Patch	Proxim	Proximity index
Class/landscape	MNN	Mean nearest neighbor distance (m)
Class/landscape	NNSD	Nearest neighbor standard deviation
Class/landscape	NNCV	Nearest neighbor coefficient of variation (m)
Class/landscape	ENN_MN	Euclidean nearest neighbor distance mean (m)
Class/landscape	ENN_SD	Euclidean nearest neighbor standard devaiation (m)
Class/landscape	Proximity_MN	Proximity index mean
Class/landscape	Proximity_SD	Proximity index standard deviation

Table 3.13: Fragstats diversity metrics.

Scale	**Acronym**	**Metric (units)**
Landscape	SHDI	Shannon's diversity index
Landscape	SIDI	Simpson's diversity index
Landscape	MSIDI	Modified Simpson's diversity index
Landscape	PR	Patch richness (number)
Landscape	PRD	Patch richness density (number/100 ha)

Table 3.14: Fragstats contagion and interspersion metrics.

Scale	Acronym	Metric (units)
Class/landscape	IJI	Interspersion and juxtaposition index (percent)
Landscape	CONTAG	Contagion index (percent)
Class	CLUMPY	Clumpiness index

Table 3.15: Fragstats connectivity metrics.

Scale	Acronym	Metric (units)
Class/landscape	PCI	Patch cohesion index
Class/landscape	CONNECT	Connectance index (percent)
Class/landscape	TRAVERSE	Traversability index (percent)

Amongst the many possibilities tabulated above, this research adopted a suite of 10 metrics commonly used to calculate vegetated land cover structure pattern metrics. These 10 metrics are used in a Berkeley document on vegetation baseline data[15] that are similar to the class of interest, which is grassland in this research. These metrics are:

(a) **Number of Patches (NP)**: Total number of patches in the landscape.

$$NP=N \tag{7}$$

where N is the total number of patches in the landscape.

(b) **Largest Patch Index (LPI)**: Area of the largest patch in the landscape, expressed as a percentage of the total landscape area.

15 http://gif.berkeley.edu/CE/Summer2007/GISanalysis_Exercise_August22_UCCE_Fragstats.pdf

$$\text{LPI} = \frac{max(a_{ij})}{A} 100\ \% \tag{8}$$

where

a_{ij} = area (m²) of patch ij and

A = total landscape area (m²).

(c) **Landscape Shape Index (LSI)**: A measure of total edge that adjusts for the size of the landscape.

$$\text{LSI} = \frac{.25\ \sum_{k=1}^{m} e^{*}{}_{\text{ik}}}{\sqrt{A}} \tag{9}$$

where

$e^{*}{}_{\text{ik}}$ = total length (m) of edge in landscape between patch types (classes) i and k.

A = total landscape area (m²).

(d) **Perimeter-Area Fractal Dimension (PAFRAC)**: Perimeter-area fractal dimension reflects shape complexity across a range of spatial scales (patch sizes).

$$PAFRAC = \frac{2}{\dfrac{\left[N\sum_{i=1}^{m}\sum_{j=1}^{n}(\ln p_{ij}\cdot \ln a_{ij})\right] - \left[\left(\sum_{i=1}^{m}\sum_{j=1}^{n}\ln p_{ij}\right)\left(\sum_{i=1}^{m}\sum_{j=1}^{n}\ln a_{ij}\right)\right]}{\left(N\sum_{i=1}^{m}\sum_{j=1}^{n}\ln p_{ij}^{2}\right) - \left(\sum_{i=1}^{m}\sum_{j=1}^{n}\ln p_{ij}\right)^{2}}} \tag{10}$$

where

a_{ij} = area (m^2) of patch ij,

p_{ij} = perimeter (m) of patch ij,

m = number of patch types,

n = number of patches, and

N = total number of patches in the landscape.

PAFRAC equals 2 divided by the slope of regression line obtained by regressing the logarithm of patch area (m^2) against the logarithm of patch perimeter (m), that is, 2 divided by the coefficient b_1 derived from a least squares regression fit to the following equation: ln(area) = $b_0 + b_1$ln(perim).

(d) **Proximity Index _MN :** The sum, across all patches of the corresponding patch type, of the corresponding patch metric values, divided by the number of patches of the same type. MN is given in the same units as the corresponding patch metric. Proximity index considers the size and proximity of all patches whose edges are within a specified search radius of the focal patch.

$$MN = \frac{\sum_{j=1}^{n} x_{ij}}{n_i} \tag{11}$$

where

X = proximity, which is,

PROX = $\sum_{s=1}^{n} \frac{a_{ijs}}{ijs}$

Where

a_{ijs} = area of patch ijs within a specified neighborhood of patch ij.

ijs = distance between patch ijs and patch ij based on patch edge –to-edge distance computed from cell centre to cell centre.

X_{ij} = area of patch ij and

n_i = number of patches of the same type.

(e) **Proximity Index_SD** : The square root of the sum of the squared deviations of each patch metric value from the mean metric value computed for all patches in the landscape, divided by the total number of patches, that is, the root mean squared error (deviation from the mean) in the corresponding patch metric.

$$SD = \sqrt{\frac{\sum_{i=1}^{m}\sum_{j=1}^{n}\left[x_{ij} - \left(\frac{\sum_{i=1}^{m}\sum_{j=1}^{n} x_{ij}}{N}\right)\right]^2}{N}} \tag{12}$$

(f) **Euclidean Nearest Neighbor_MN (ENN_MN):** The sum, across all patches in the landscape, of the corresponding patch metric values, divided by the total number of patches. MN is given in the same units as the corresponding patch metric. Euclidean nearest neighbor is a measure of the patch context and used extensively ro quantify patch isolation.

$$MN = \frac{\sum_{i=1}^{m}\sum_{j=1}^{n} x_{ij}}{N} \tag{13}$$

(g) **Euclidean Nearest Neighbor_SD (ENN_SD)**: The square root of the sum of the squared deviations of each patch metric value from the mean metric value of the corresponding patch type, divided by the number of patches of the same type; that is, the root mean squared error (deviation from the mean) in the corresponding patch metric.

$$SD = \sqrt{\frac{\sum_{j=1}^{n}\left[x_{ij} - \left(\frac{\sum_{j=1}^{n} x_{ij}}{n_i}\right)\right]^2}{n_i}} \tag{14}$$

(h) **Clumpiness Index (CLUMPY)**: The proportional deviation of the proportion of like adjacencies involving the corresponding class from that expected under a spatially random distribution. If the proportion of like adjacencies (G_i) is less than the proportion of the landscape comprised of the focal class (P_i) and $P_i < 0.5$, then CLUMPY equals G_i minus P_i, divided by P_i; else, CLUMPY equals G_i minus P_i, divided by 1 minus P_i.

Given $G_i = \frac{g_{ii}}{\sum_{k=1}^{m} \mathrm{g_{ik}}}$

$$\text{CLUMPY} = \frac{G_i - P_i}{1 - P_i} \qquad (15)$$

where,

g_{ii} = number of like adjacencies (joins) between pixels of patch type (class) i based on the double-count method.

$\mathrm{g_{ik}}$ = number of adjacencies (joins) between pixels of patch types (classes) i and k based on double count method.

P_i = proportion of the landscape occupied by the patch type (class) i.

(i) **Connectance Index (CONNECT)**: The number of functional joinings between all patches of the corresponding patch type (sum of c_{ijk} where $c_{ijk} = 0$ if patch j and k are not within the specified distance of each other and $c_{ijk} = 1$, if patch j and k are within the specified distance), divided by the total number of possible joinings between all patches of the corresponding patch type, multiplied by 100 to convert to a percentage.

$$\mathrm{CONNECT} = \left[\frac{\sum_{j \neq k}^{n} c_{ijk}}{\frac{n_i \, (n_i - 1)}{2}} \right] (100) \qquad (16)$$

Where

c_{ijk} = joining between patch j and k (0 = unjoined, 1 = joined) of the corresponding patch type (i), based on a user specified threshold distance and

n_i = number of patches in the landscape of the corresponding patch type (class).

Information about the metrics and the equations can be found on the University of Massachusetts web site[16]. The selected metrics are listed in order of patch, class and landscape in the following table.

[16] http://www.umass.edu/landeco/research/fragstats/documents/fragstats_documents.html

Table 3.16: Selected metrics in order of class and landscape.

Metric	**Scale**
NP	Landscape
LPI	Landscape
LSI	Landscape
PAFRAC	Landscape
Proximity_MN	Class
Proximity_SD	Landscape
ENN_MN	Landscape
ENN_SD	Class
CLUMPY	Class
CONNECT	Landscape

3.9.2 Input Data Formats

FRAGSTATS accepts several input data formats such as:

(1) ArcGrid created with Arc/Info.

(2) ASCII files without any header.

(3) 32-bit binary file without any header.

(4) 16-bit binary file without any header.

(5) 8-bit binary file without any header.

(6) ERDAS image files (.gis, .lan, and .img). FRAGSTATS accepts images from both ERDAS 7 (.gis and .lan) and ERDAS 8 (.gis, .lan, and .img).

(7) IDRISI image files (.rdc). IDRISI currently supports signed 8- or 16-bit integers and 32-bit floating point grids. This imposes some limitations when using FRAGSTATS on large grids.

In this study, ascii files were created from the satellite thematic raster maps. All the thematic maps were then saved in ascii format for input into FRAGSTATS for the fragmentation statistics analysis. The run parameter window of the FRAGSTATS software is given in Figure 3.7, which shows the options for input data type, class property files and output statistics to measure.

Class property files were created for fragmentation statistics analysis for each image date. FRAGSTATS software takes this file as an input of the class description, reads the class names (e.g., grassland), computes the fragmentation statistics, and produces the output files. An 8-cell patch neighbour rule was selected to consider 8 adjacent cells, including 4 orthogonal and 4 diagonal neighbours. Thus, 2 cells of the same class that are diagonally touching will be considered to be part of the same patch.

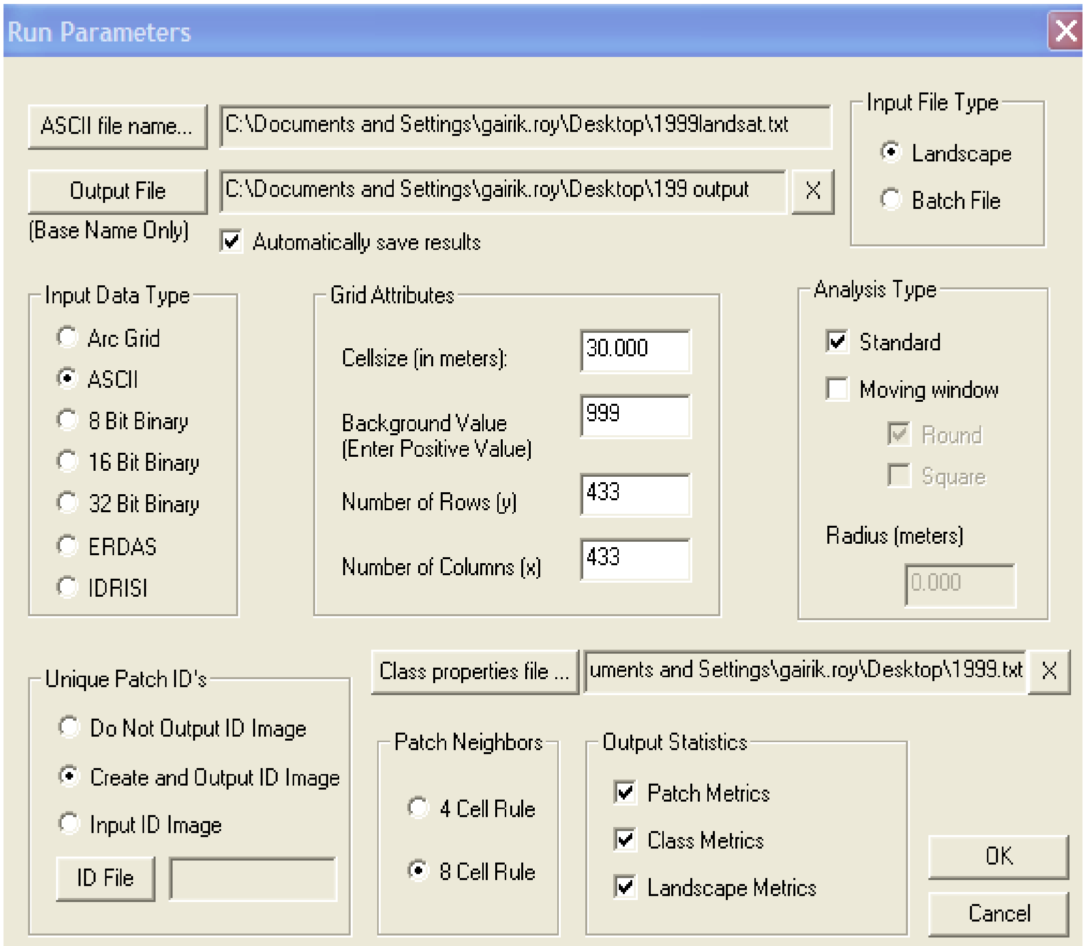

Figure 3.7: Run parameter window in FRAGSTATS software.

3.9.3 Output Files

FRAGSTATS creates four output files. A basename is given for the output files and FRAGSTATS appends the extensions .adj, .patch, .class, and .land to the basename. All files created are comma-delimited ASCII files and viewable. These files are named and formatted to facilitate input into database management programs.

The basename.adj file contains a simple header in addition to one record for each class in the landscape and is given in the form of a two-way matrix. Specifically, the first record contains the input file name, including the full path. The second record and first column contain the class IDs and the elements of the matrix, which are the tallies of cell adjacencies for each pairwise combination of classes.

- The basename.patch file contains the patch metrics for a landscape. The file contains one record for each patch in the landscape.
- The basename.class file contains the class metrics. The file contains one record for each class in the landscape.
- The basename.land file contains the landscape metrics. The file contains one record for the landscape.

4 RESULTS AND DISCUSSION

Tables 4.1 and 4.2 show accuracy results extracted from the confusion matrices for the 17 Landsat image classifications and 8 SPOT image classifications. ROIs were created for each land cover type and 50 % of the ROIs were used for training of the classifier and 50 % for validation. The classification results showed an average of 98.2 % overall accuracy for Landsat images and 98.2 % for SPOT images. The classification accuracies being high is normal as half of the ROIs were used for validation. Also, the classes of interest in this study (grassland, road and oil infrastructure, crops and water) are so different from each other that it is easy to recognise the difference between grassland and non-grassland areas in the image data and to select the ROIs accordingly. The pixels-correct ratio in the tables indicates the total number of pixels that were correctly classified for all the classes.

To intercompare Landsat versus SPOT results, the 17 Landsat and 8 SPOT thematic maps were reduced to 6 Landsat and SPOT thematic map same year pairs. These thematic map results are shown in this section. All the other thematic maps are shown in Appendix A.

Table 4.1: Overall accuracy of Landsat images classified by the SVM classifier.

Results from Confusion Matrices		
	Overall Accuracy	
Image Date	**Pixels Correct Ratio**	**Percentage Correct (%)**
July 02, 1987	(5198/5312)	97.8
July 20, 1988	(4966/5066)	98.0
August 08, 1989	(5588/5649)	98.9
July 31, 1992	(5509/5561)	99.0
July 21, 1994	(5821/5906)	98.5
August 11, 1996	(3568/3650)	97.7
June 27, 1997	(3259/3429)	95.0
July 16, 1998	(4167/4308)	96.7
July 19, 1999	(4605/4696)	98.0
July 05, 2000	(4638/4739)	97.8
July 08, 2001	(3462/3630)	95.3
July 11, 2002	(2541/2546)	99.8
July 14, 2003	(5052/5114)	98.7
July 16, 2004	(2258/2266)	99.6
August 4, 2005	(2827/2835)	99.7
August 7, 2006	(3027/3030)	99.9
July 27, 2008	(3556/3569)	99.6

Table 4.2: Overall accuracy of SPOT images classified by the SVM classifier.

Results from Confusion Matrices		
	Overall Accuracy	
Image Date	**Pixels Correct Ratio**	**Percentage Correct (%)**
June 24, 1986	(9475/9551)	99.2
August 8, 1988	(10025/10043)	99.8
June 27, 1994	(4219/4236)	99.5
July 26, 1999	7616/7671)	99.2
July 17, 2003	(4854/4983)	97.4
August 12, 2003	(4968/4983)	99.6
July 11, 2005	(5205/5579)	93.3
July 21, 2006	(8666/8873)	97.6

4.1 Image Classification Results

The thematic maps resulting from the Landsat and SPOT image classifications are shown in Figures 4.1- 4.12. The classification results have errors of commission, because the spectral signatures of bare patches and blow-out areas are similar to that of road infrastructure, such that class confusion led to errors. Oil and gas wells or roads are linear or regularly shaped features. In the classification process, the non-linear shaped features, which were mapped as road infrastructure, are not related to road infrastructure. Some years during the satellite image time series were drier than the average of a 25-year period. Less moisture resulted in the lack of vegetation growth and, thus, bare patches and blow-out areas appeared. These bare patches and blow-out area pixels were classified as road infrastructure.

In the July 1988 Landsat thematic map (Figure 4.1), more road infrastructure pixels (red spots) can be seen compared to the August 1988 thematic map (Figure 4.2). Many of these red spots are not part of a linear feature and they are not related to road infrastructure. As noted above, it is known, based on field inspections (A.M. Smith, personal communication), that lack of moisture prevents the growth of the vegetation such that bare patches and blow-out areas appeared in those areas and those pixels were classified as road infrastructure. The July 1994 Landsat (Figure 4.3) and June 1994 SPOT (Figure 4.4) thematic maps differ in terms of road infrastructure in many areas. In these thematic maps (Figures 4.5 and 4.6), some areas include many pixels classified as road infrastructure (red spots) that are not related to road infrastructure, as they are non-linear or irregularly shaped features. Differences in road infrastructure are evident between the July 2003 Landsat and SPOT thematic maps, even though the images were acquired only

3 days apart (Figures 4.7 and 4.8). Similar differences can be seen between the Landsat-based and SPOT-based thematic maps of 1988 (Figures 4.1 and 4.2), 2005 (Figures 4.9 and 4.10), and 2006 (Figures 4.11 and 4.12).

Clearly, the pixels classified as road infrastructure differ between the Landsat-based and SPOT-based thematic maps. The different image captured dates (Tables 4.1 and 4.2) possibly have an impact on this, because there may be differences in land cover on the different dates of any given same-year pair, typically approximately 3 weeks apart (see Tables 4.1 and 4.2). It is not possible to say which one is better between Landsat-based and SPOT-based thematic maps without further data and analyses beyond the scope of this study. However, grassland in the Newell County area is generally dry and brown and changes very little with time in the absence of significant rain events. Therefore, it is likely though unproven that the differences between the Landsat and the SPOT results are due to the significant differences in spatial resolution (the surface area represented by SPOT pixels is less than half the surface area of Landsat pixels).

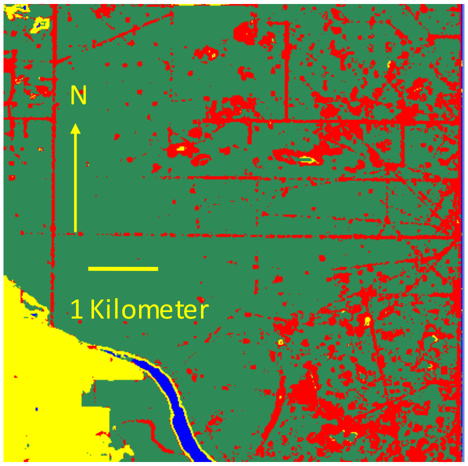

Figure 4.1: July 20, 1988 Landsat thematic map.

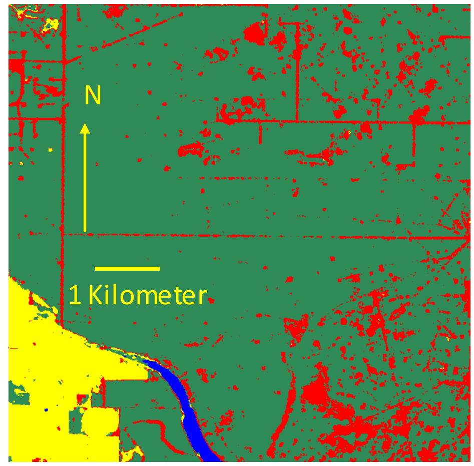

Figure 4.2: August 8, 1988 SPOT thematic map.

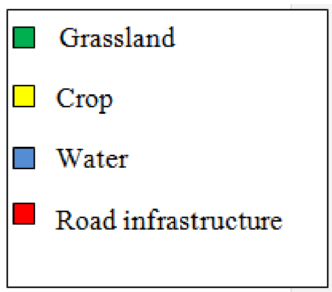

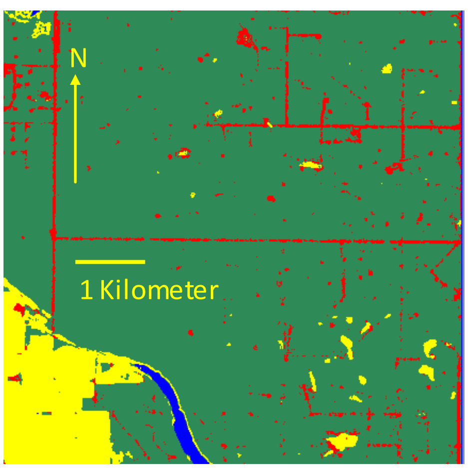

Figure 4.3: July 21, 1994 Landsat thematic map.

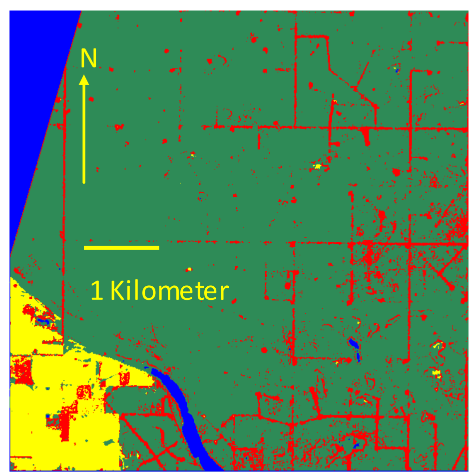

Figure 4.4: June 27,1994 SPOT thematic map.

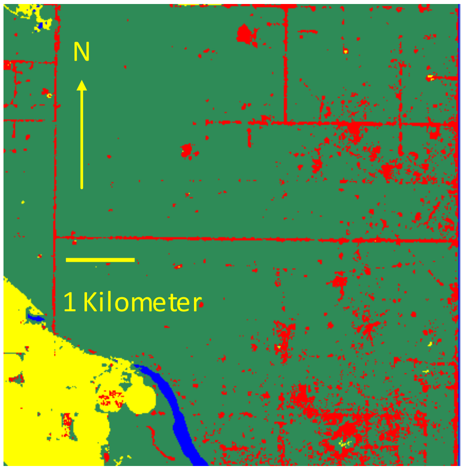

Figure 4.5 July 19, 1999 Landsat thematic map.

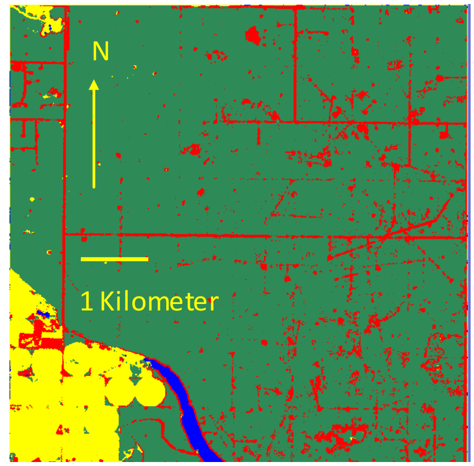

Figure 4.6: July 26, 1999 SPOT thematic map.

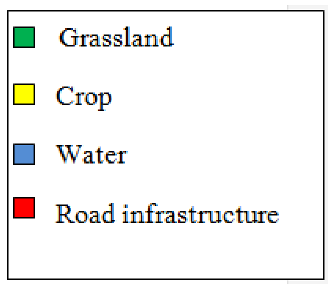

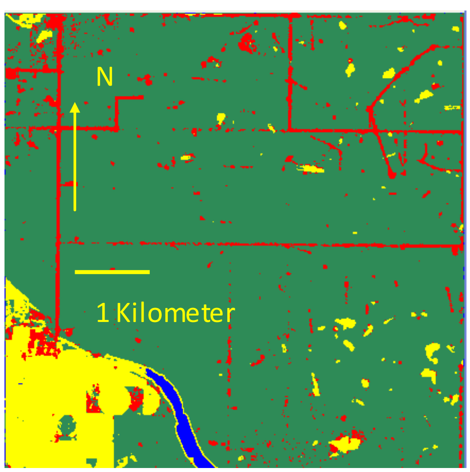

Figure 4.7: July 14, 2003 Landsat thematic map.

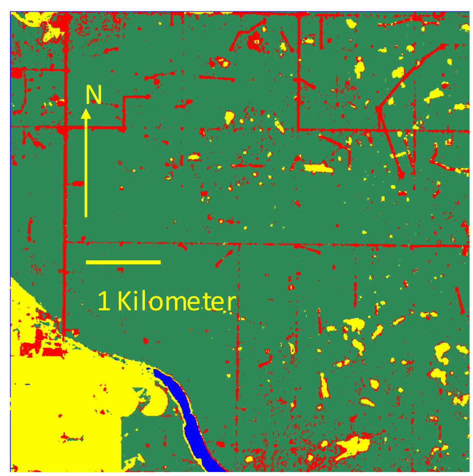

Figure 4.8: July 17, 2003 SPOT thematic map.

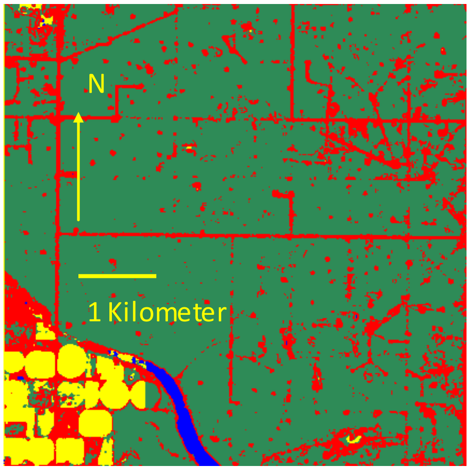

Figure 4.9: August 4, 2005 Landsat thematic map.

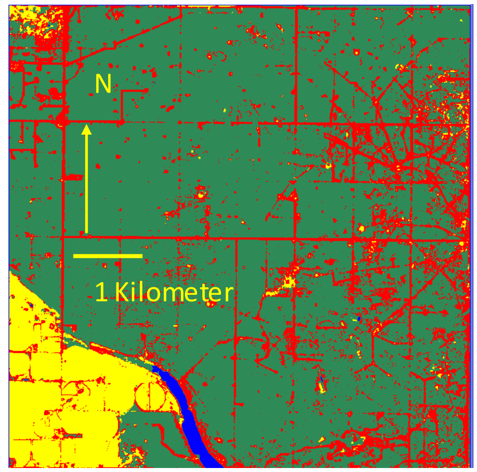

Figure 4.10: July 11, 2005 SPOT thematic map.

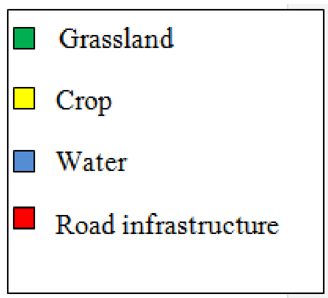

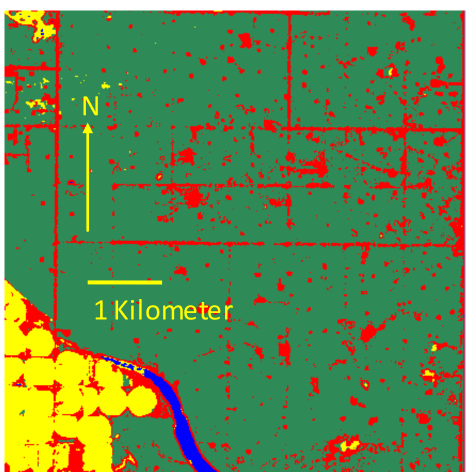

Figure 4.11: August 7, 2006 Landsat thematic map.

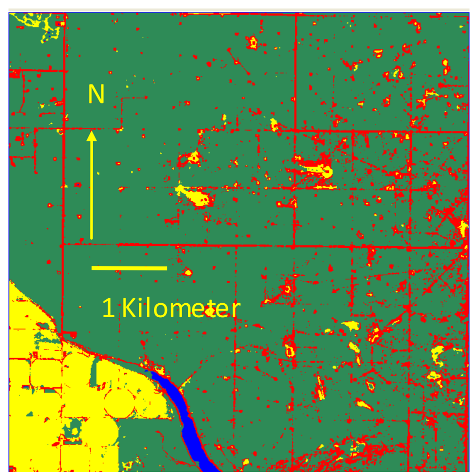

Figure 4.12: July 21, 2006 SPOT thematic map.

4.2 Spatial Extent Estimation

Spatial extent information was estimated from each of the 17 Landsat and 8 SPOT thematic maps. The number of points of each land cover class, derived from the SVM classification, was multiplied by the Landsat and SPOT pixel sizes to calculate the amount of land covered by each class. Landsat pixels are 30 m by 30 m, hence 900 m^2 in area. SPOT pixels are 20 m by 20 m, hence 400 m^2 in area, less than half the area of Landsat pixels. Note that the SPOT-5 images were rescaled to 20-m spatial resolution. Figure 4.13 presents the temporal behaviour, from 1985 to 2008 based on the 17 Landsat images, of the spatial extent of grassland and road infrastructure within the 13-km by 13-km ROI. These two classes are shown because their spatial extents are of greater interest than those of crops and water.

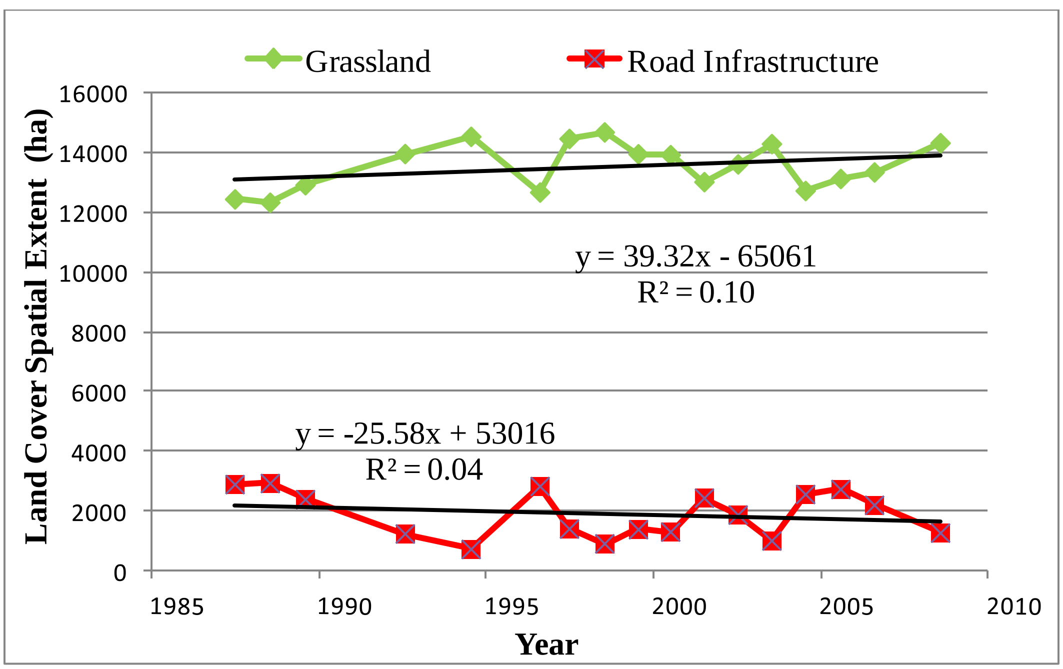

Figure 4.13: Landsat-derived land cover spatial extent in hectares (ha).

The results in Figure 4.13 show that, for both grassland and road infrastructure classes, the coefficients of determination (R^2) and the slopes are very low, indicating that no statistically significant change in spatial extent can be detected from Landsat image data from 1985 to 2008 for either class. Here, only a linear trend was examined. The images were captured on different dates in the various years. Therefore, there may be seasonal differences in the amount of grassland growth at the different times.

While there is no significant change over the time span, there are indications of year-to-year variations in spatial extent of both grassland and road infrastructure and that the changes in the two land cover types tend to mirror each other. Therefore, the Landsat-based spatial extents of grassland and road infrastructure land cover are compared to each other in Figure 4.14. In this figure, the negative correlation is clear, the high R^2 indicating that the reduction in grassland is almost certainly due to the gain in road infrastructure.

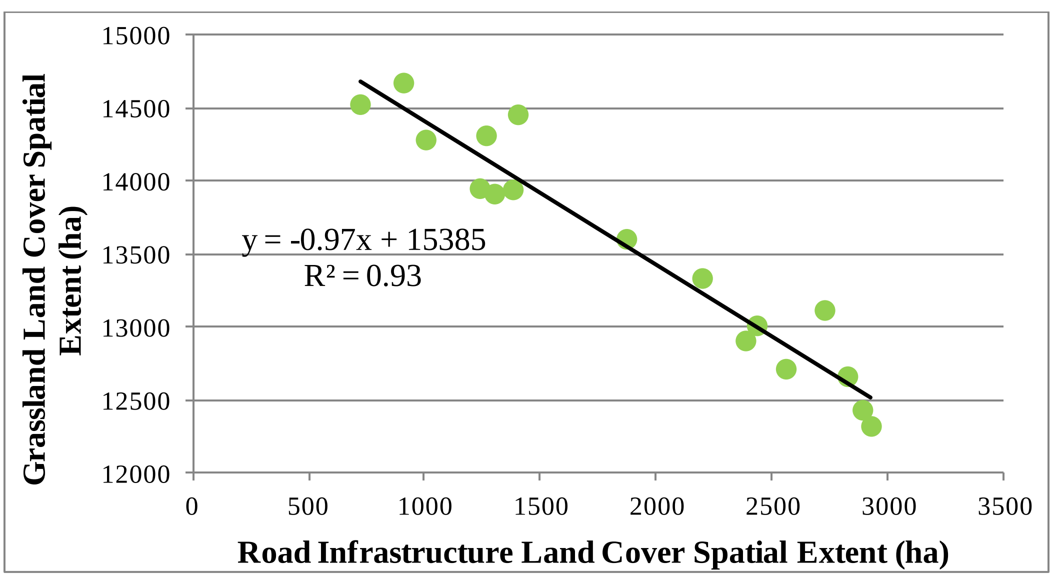

Figure 4.14: Landsat-derived land cover spatial extent comparison between grassland and road infrastructure.

Land-cover spatial extent information was also derived from the 8 SPOT-based thematic maps as shown in Figure 4.15.

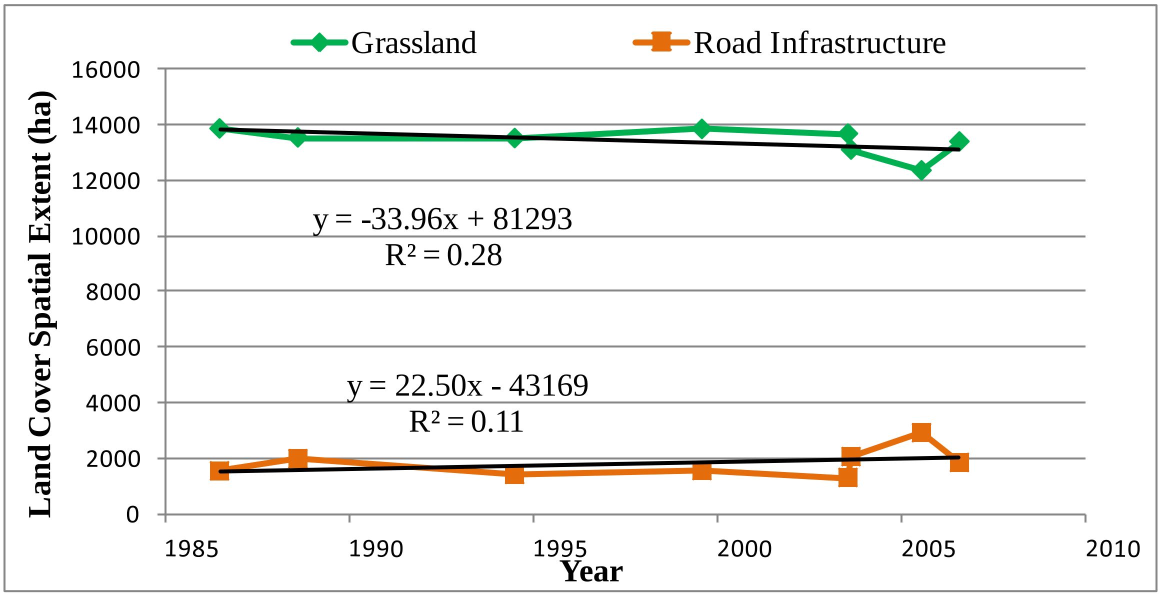

Figure 4.15: SPOT-derived land cover spatial extent in hectares (ha).

The results in Figure 4.15 show that, as for Landsat, the spatial extent of both grassland and road infrastructure classes over time have low R^2 and the slopes are small. Similar to Landsat images, SPOT images were also captured on different dates in the various years. Therefore, seasonal changes might have an impact on the grassland growth at the different times. Compared to the Landsat case, given the more limited temporal sampling, there are fewer indications of significant year-to-year variations in spatial extent of both grassland and road infrastructure, but the changes for the two land cover categories still tend to mirror each other for SPOT-derived results. Therefore, the spatial extents of grassland and road infrastructure land cover types were compared to each other for the SPOT-base results in Figure 4.16. The negative correlation in the spatial extents of grassland and road infrastructure is clear (R^2 = 0.84)

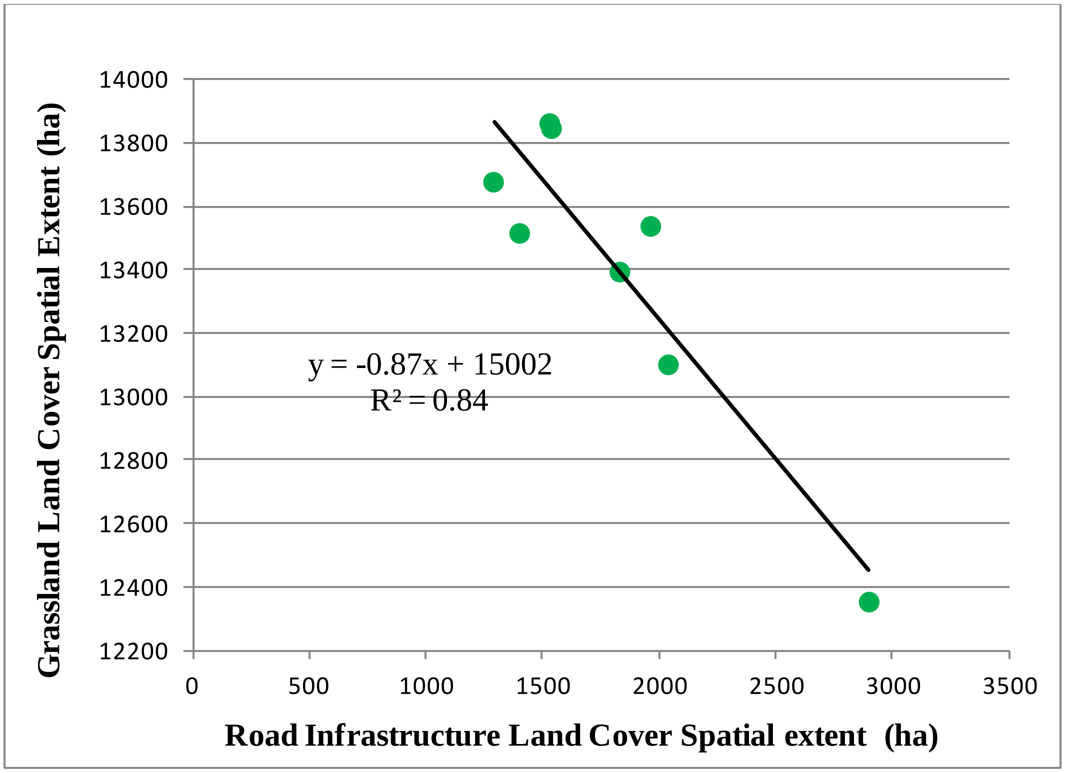

Figure 4.16: SPOT-derived land cover spatial extent comparison between grassland and road infrastructure.

The temporal behaviours of the Landsat-based and SPOT-based spatial extents were examined (Figure 4.17) for the 6 years in common. The findings indicate that the coefficients of determination and the slopes are low for both classes for both image types.

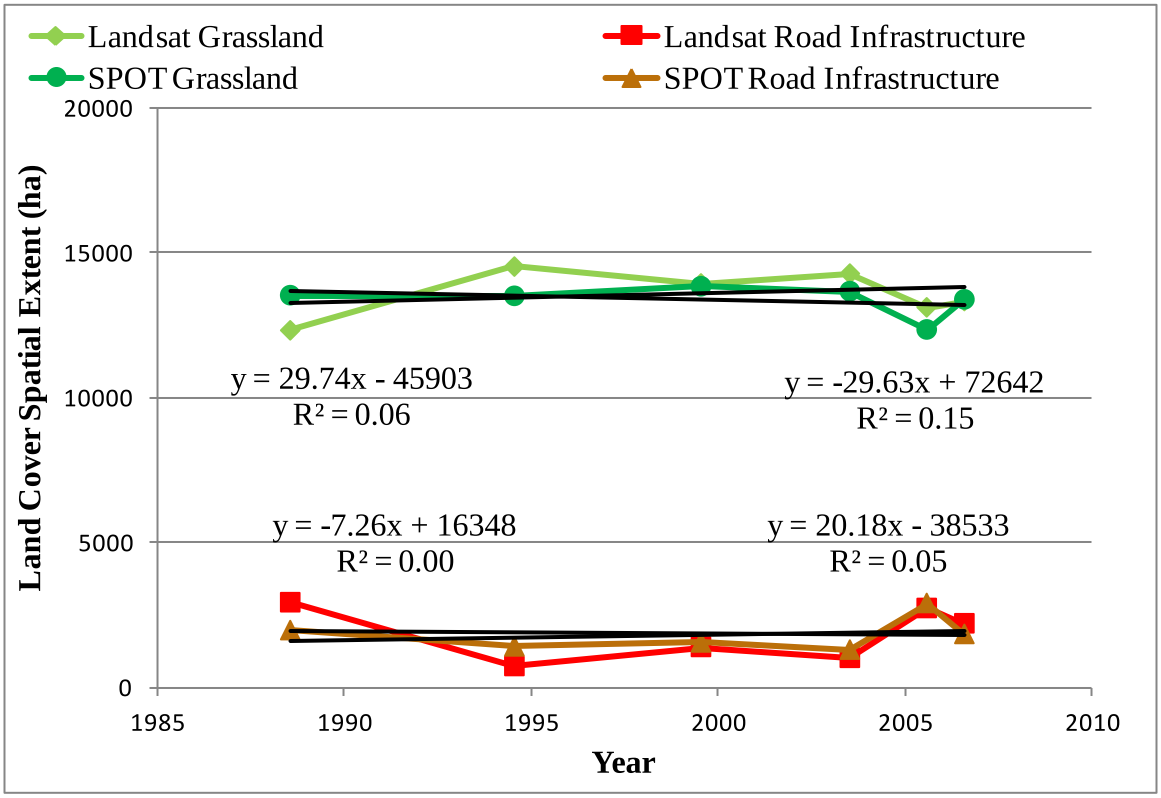

Figure 4.17: Land cover spatial extent comparison between results based on Landsat and SPOT.

Figure 4.18 compares the Landsat-based and SPOT-based grassland spatial extent for the same years. The R^2 is low and the slope is far from unity, indicating the Landsat-based and SPOT-based results differ. As noted earlier, the different image captured dates and/or the different pixel sizes may be the cause of this, but there is no way of verifying these possibilities.

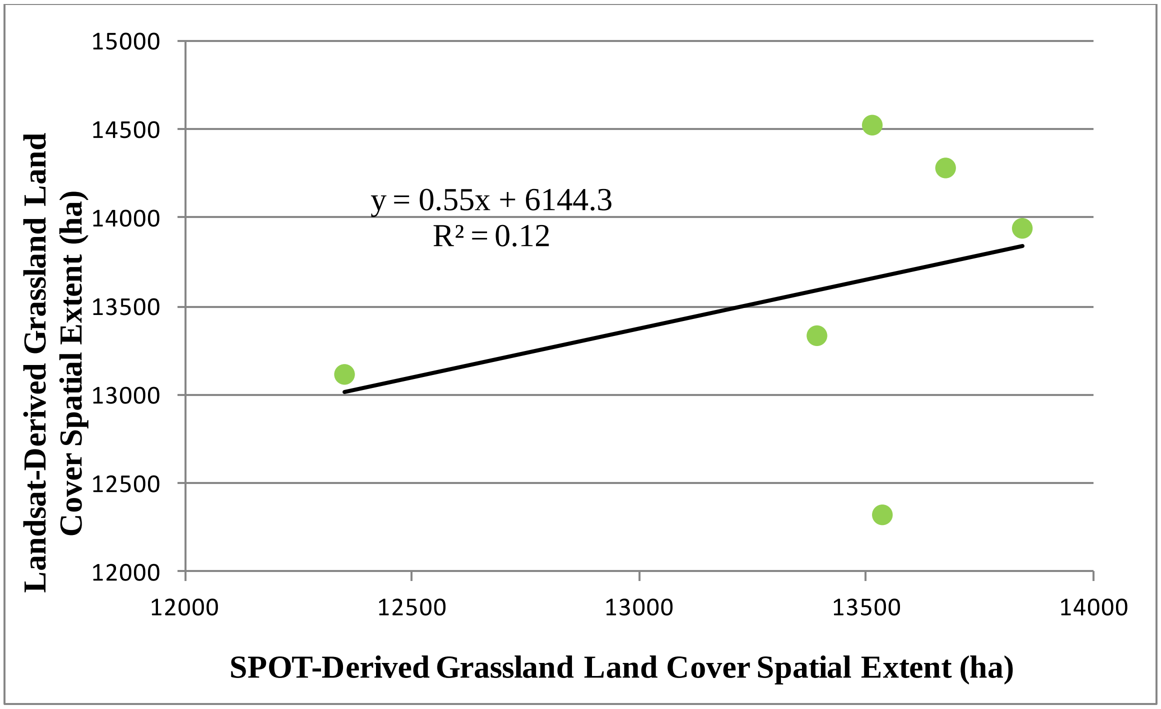

Figure 4.18: Grassland land cover spatial extent - Landsat versus SPOT for the same years.

Figure 4.19 compares the Landsat-based and SPOT-based road infrastructure spatial extent for the same years. Here, the R^2 is higher than the value for grassland in Figure 4.18 and, hence, the results based on Landsat and SPOT are correlated to some extent. The slope is far from unity, however, and so actual spatial extent results from Landsat and SPOT differ. The characteristics of road infrastructure are such that the rate of its change over time is not very high, whereas it is more common to have changes in grassland land cover in a short period of time. Therefore, it is likely that time differences in image acquisition in a given year did not affect the road infrastructure spatial extent comparison in Figure 4.19.

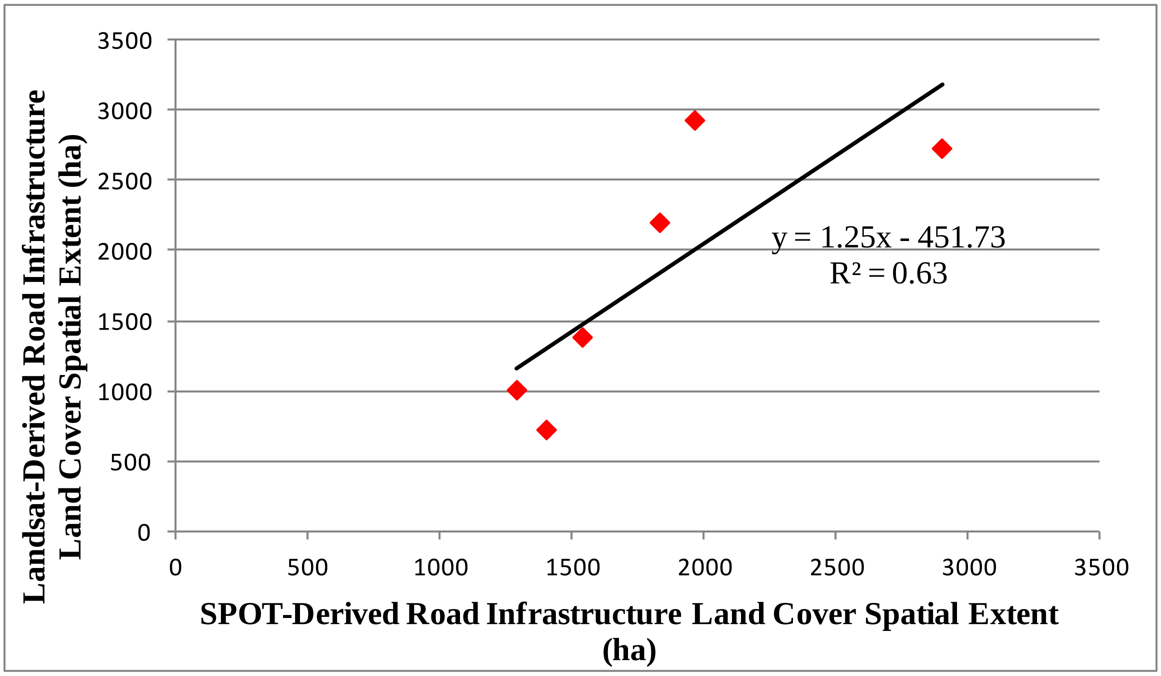

Figure 4.19: Road infrastructure land cover spatial extent - Landsat versus SPOT for the same years.

4.3 Precipitation Levels

Precipitation levels were checked for the years spanned by this study to see if it has any relation with the grassland growth. For this purpose, Brooks weather station data were obtained from the Environment Canada website[17]. This is the nearest weather station to the Newell County study area. Precipitation data were summed cumulatively from September 1 of the previous year to August 31 of the image capture year. This process was done for the years from 1985 to 2007. These precipitation sums were compared to grassland spatial extents based on Landsat (Figure 4.20) and SPOT (Figure 4.21) to determine if there was any relation between the grassland spatial extent and precipitation levels.

[17] http://www.weatheroffice.gc.ca/canada_e.html

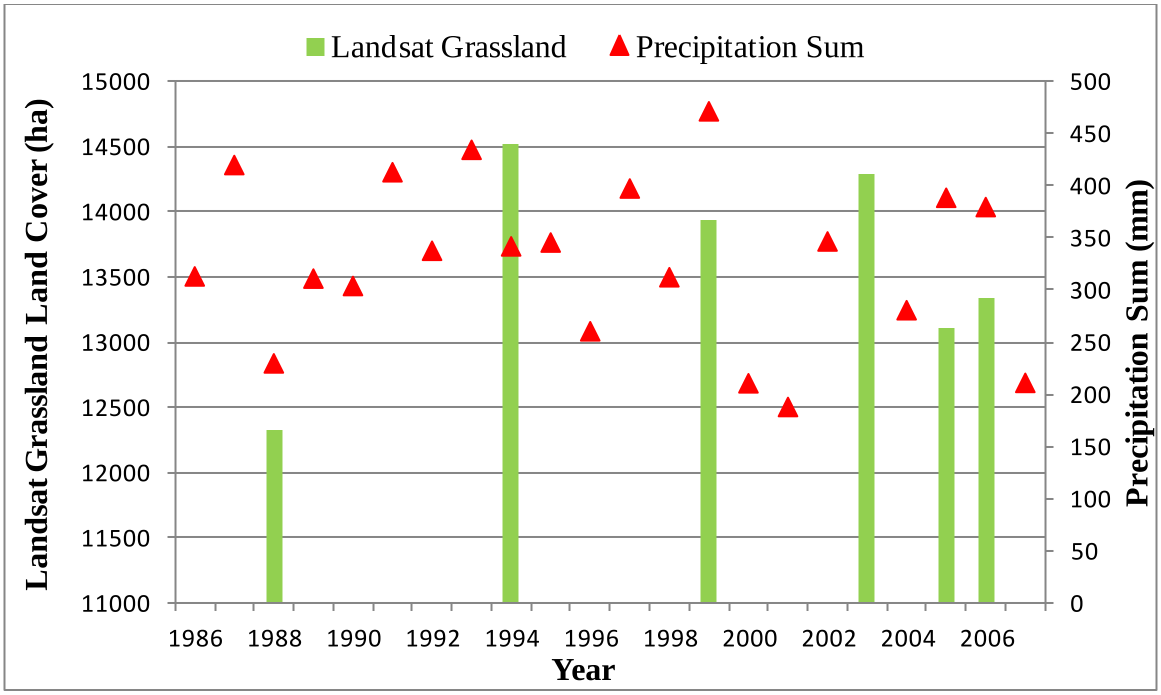

Figure 4.20: Accumulated precipitation from September 31 of previous year to August 31 of image capture year versus Landsat-derived grassland land cover.

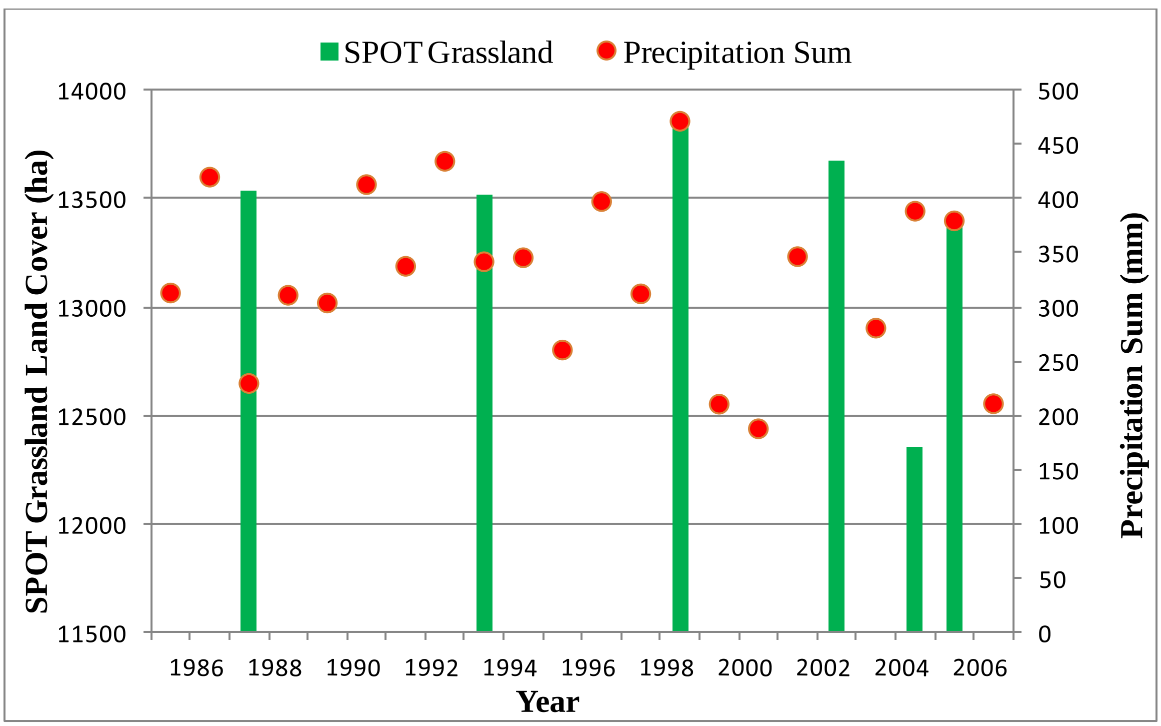

Figure 4.21: Accumulated precipitation from September 31 of previous year to August 31 of image capture year versus SPOT-derived grassland land cover.

The graphs show that, from the given image data sets, the grassland growth is not related in any obvious way to precipitation levels. Nevertheless, it is known, based on field inspections (A.M. Smith, personal communication), that the frequency and timing of rainfall events relative to the grassland growth cycle, and lack of moisture can result in diminished grassland growth. Thus, bare patches and blow-out areas can appear in places where grassland growth was less, leading to possible classification of those patches as road infrastructure instead of grassland.

4.4 Fragmentation Statistics

Fragmentation statistics were computed from the Landsat and SPOT thematic maps for each land cover class using the FRAGSTATS 3.3 software. In this section, fragmentation results for the Number of Patches (NP) are presented.

The NP values for the grassland and road infrastructure classes derived from Landsat are presented in Figure 4.22.

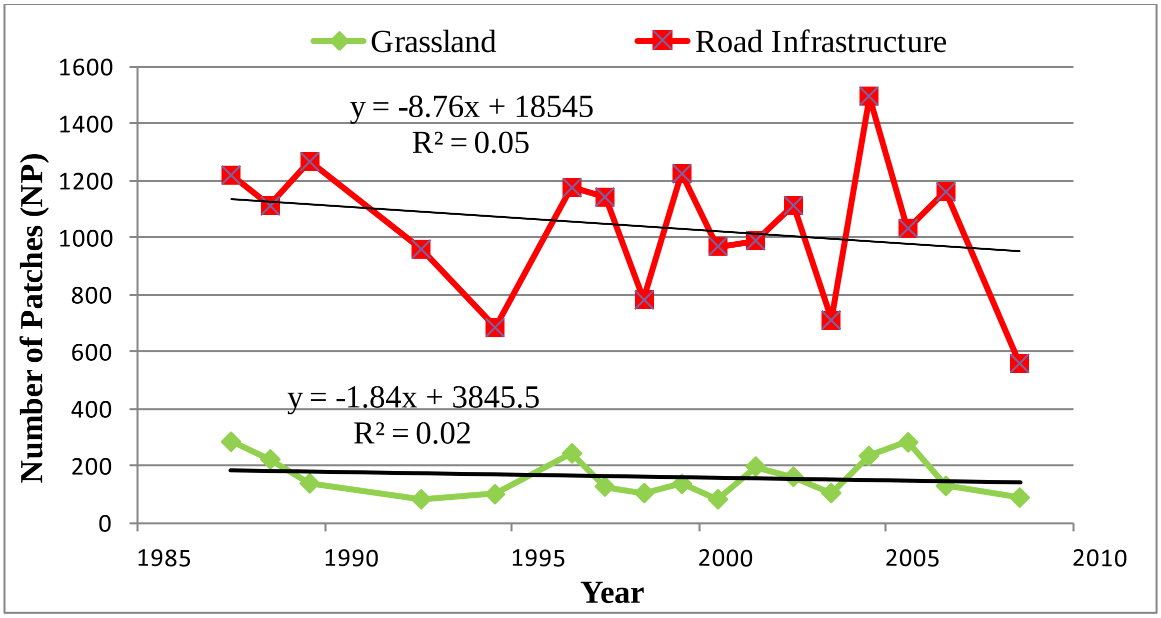

Figure 4.22: Number of patches (NP) fragmentation metric derived from Landsat.

Only a linear trend is examined in Figure 4.22, and it shows that there is no statistically significant change in either class over the two decades encompassed by the image data set. There appear to be year-to-year variations in NP for both classes, but, unlike the case for spatial extent, there is no hint of a mirror-like relationship between the grassland NP and the road infrastructure NP. This suggests that the gains or losses in the number of grassland patches are not attributable to losses or gains in the number of road infrastructure patches. Instead, there are hints in Figure 4.22 that the year-to-year variabilities of the two classes may be slightly positively correlated. Figure 4.23 compares NP for grassland to NP for road infrastructure derived from Landsat thematic maps. The low R^2 proves, based on the information available, that the gains or losses in the number of grassland patches are not attributable to losses or gains in the number of road infrastructure patches.

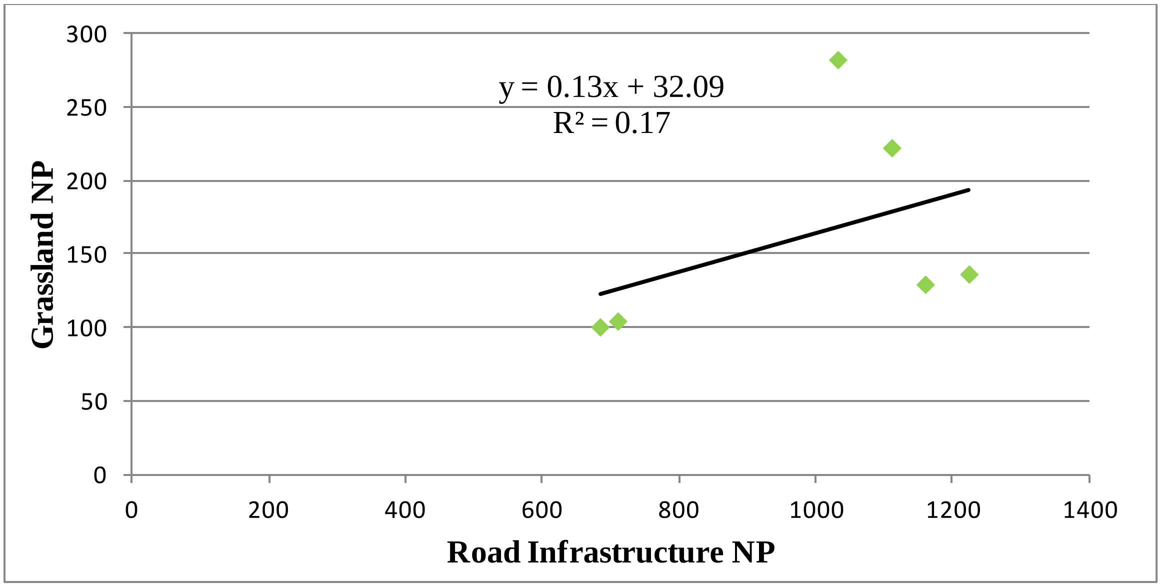

Figure 4.23: Landsat-based NP for grassland versus NP for road infrastructure.

Figure 4.24 presents the NP for grassland and road infrastructure classes over time as derived from SPOT imagery. It also shows a linear trend and the results indicate that there has been a significant change, especially for road infrastructure. However, the R^2s are such that only part of the change is explained by data.

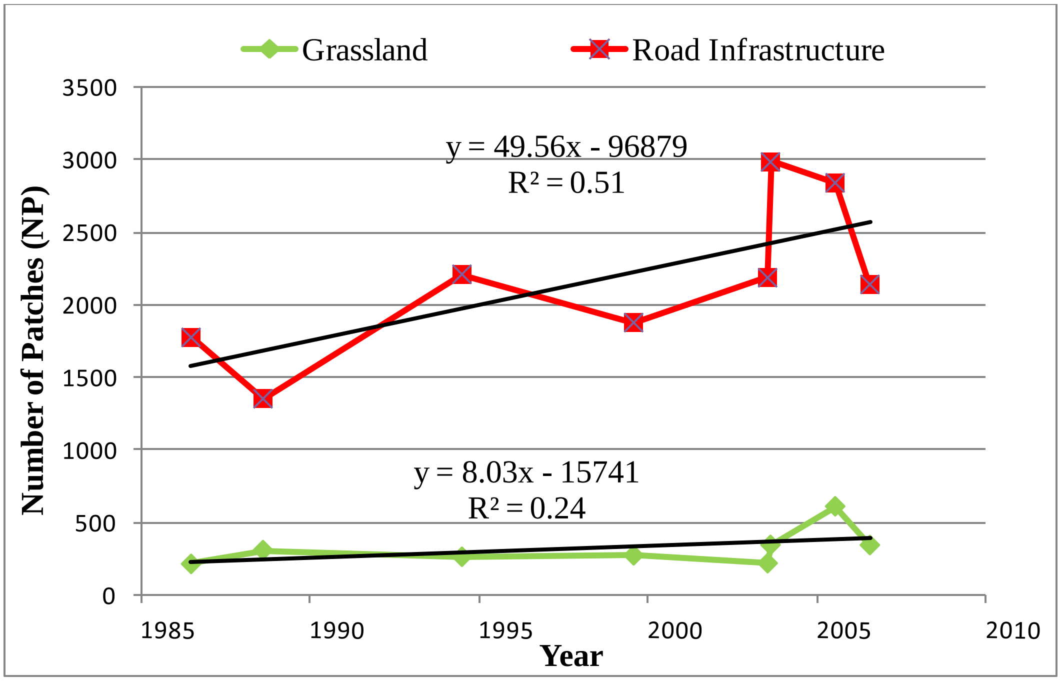

Figure 4.24: Number of patches (NP) fragmentation metric derived from SPOT.

Figure 4.25 compares NP for grassland to NP for road infrastructure derived from SPOT thematic maps. The low R^2 proves that the gains or losses in the number of grassland patches are not attributable to losses or gains in the number of road infrastructure patches. However, the R^2 is not very low compared to the plot in Figure 4.23, because of the 2005 year.

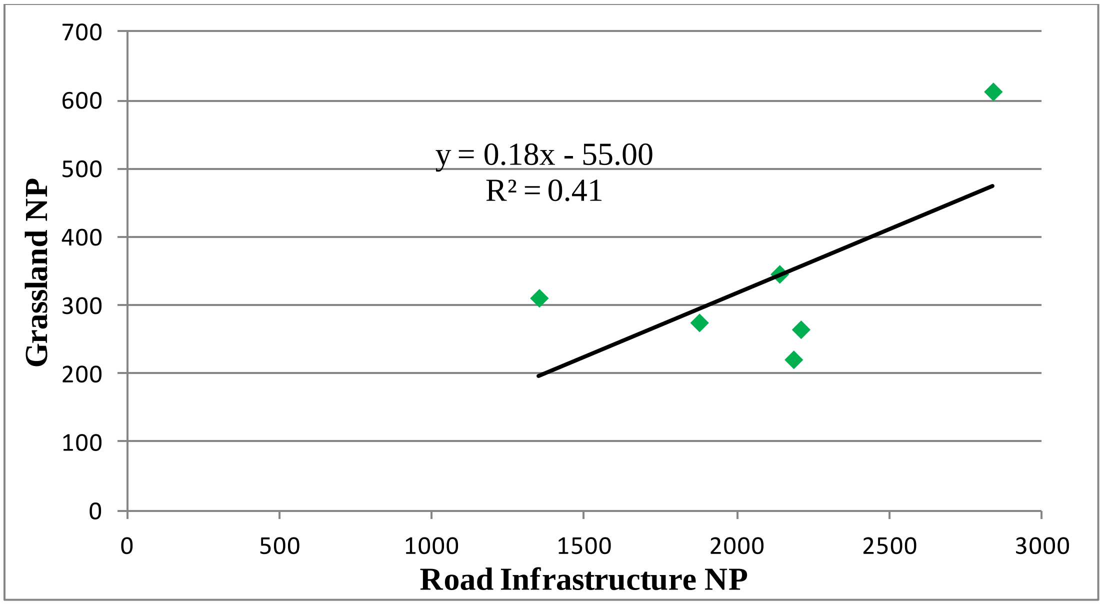

Figure 4.25: SPOT-based NP for grassland versus NP for road infrastructure.

Figure 4.26 compares Landsat-based and SPOT-based NP for grassland for the same years. The relatively high R^2 shows positive correlation between Landsat and SPOT-based grassland NP. However, this high R^2 is anchored by the 2005 year. Note that the slope is far from unity and, while the Landsat-based and SPOT-based NP results are correlated, the actual values differ by approximately a factor of 2. Therefore, based on the information available, Landsat and SPOT cannot be expected to yield comparable grassland NP fragmentation values.

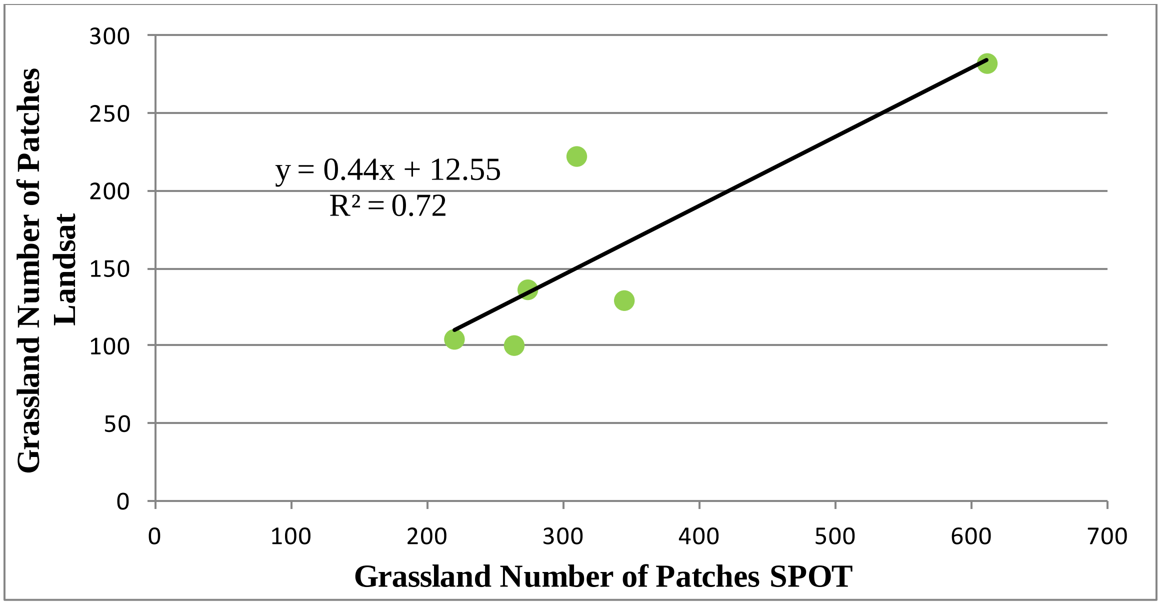

Figure 4.26: Grassland NP-Landsat versus SPOT for same years.

Figure 4.27 compares Landsat-based and SPOT-based NP for road infrastructure for the same years. Unlike the grassland comparison (Figure 4.26), the R^2 is low. Thus, Landsat and SPOT yield very dissimilar and uncorrelated NP fragmentation values for the road infrastructure.

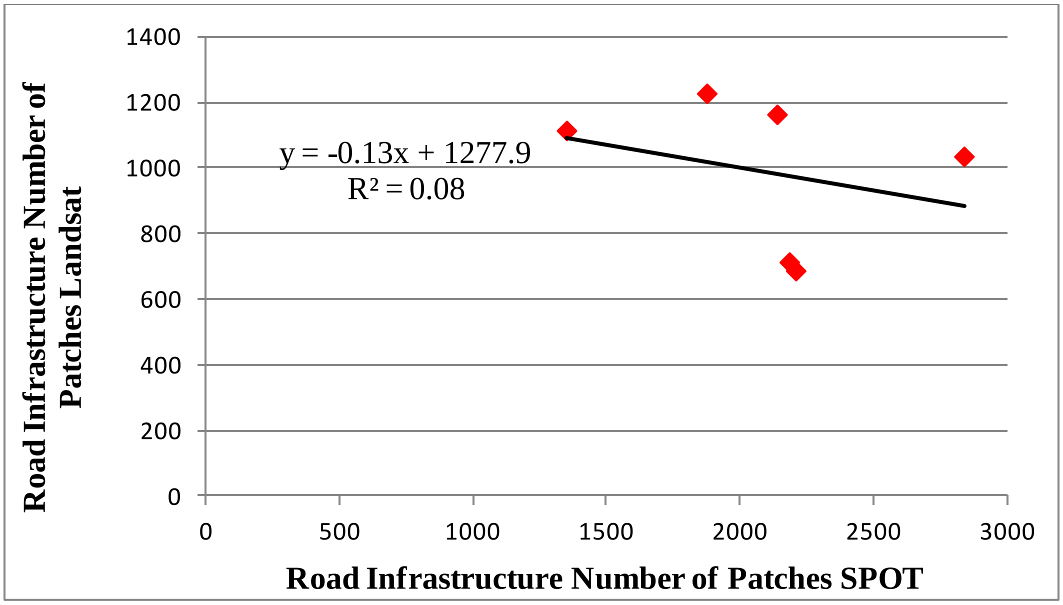

Figure 4.27: Road infrastructure NP-Landsat versus SPOT for same years.

As for the spatial extent results, there is no way of ascertaining, in this study, why the Landsat and SPOT results for NP differ as much as they do. While it is likely that the different pixel sizes are the cause, there is no way of verifying this likelihood. Also, there may be seasonal differences in the land cover due to different image acquisition dates, which might have an impact on the results.

Figure 4.28 presents the Largest Patch Index (LPI) values for grassland and road infrastructure derived from Landsat. LPI is an important metric in terms of fragmentation analysis in this research, as it quantifies the percentage of total landscape area comprised by the largest patch of a given class and, therefore, it provides information about which land cover class patch is predominant in that landscape area.

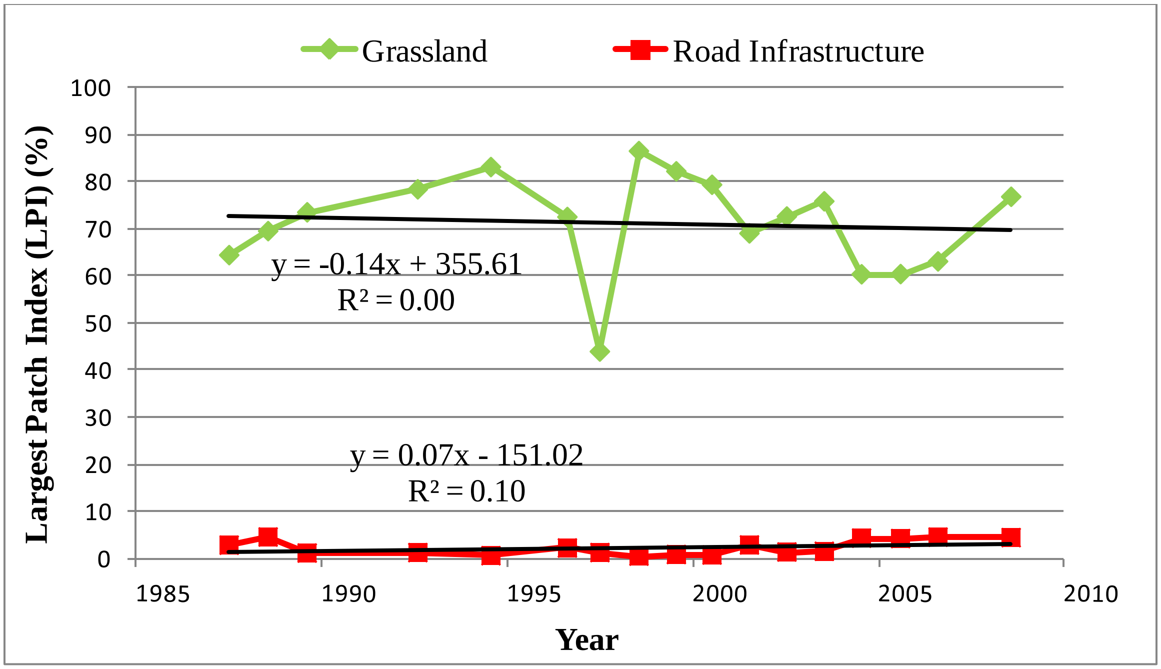

Figure 4.28: Largest Patch Index (LPI) fragmentation metric derived from Landsat.

Only a linear trend is examined in Figure 4.28, and it shows that there is almost no statistically significant change in either land cover class over the two decades encompassed by the image data set. However, the loss in grassland LPI in 1997 from 1996 and the gain in grassland LPI in 1998 from 1997 are significant individually. But in these years gains or losses in the grassland LPI are not attributable to the losses or gains in the road infrastructure LPI.

Figure 4.29 compares LPI for grassland to LPI for road infrastructure derived from Landsat thematic maps. It shows high R^2 and a negative correlation, which indicates that the gains or losses in the Landsat-based LPI of grassland may be attributable to losses or gains in the LPI of road infrastructure. Only six similar years were found containing Landsat and SPOT data and there was no data available for groups of years which fall in the middle of the trend. This anchored the high R^2 value. The result suggests that the largest patch of grassland occupies almost 85% of the total grassland area compared to the largest patch of road infrastructure occupying 0.5% in 1994. In cases the largest road infrastructure patch approaches 5% compared to the largest grassland patch occupying almost 70% of the total grassland area in 1988. Therefore, it can be concluded that the gains or losses in the Landsat-based LPI of grassland may be attributable to losses or gains in the LPI of the road infrastructure.

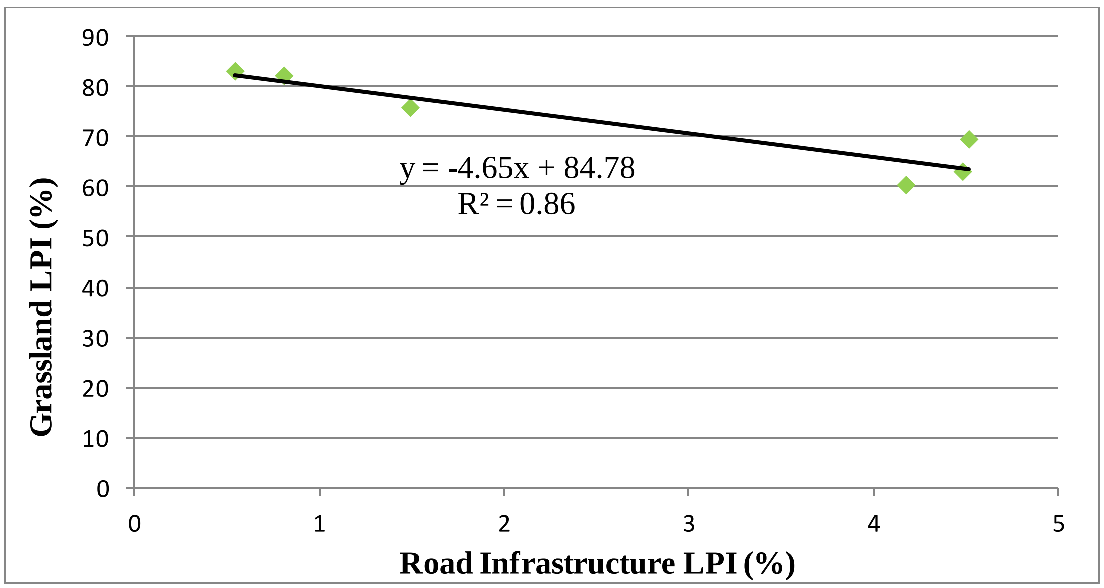

Figure 4.29: Landsat-based LPI for grassland versus LPI for road infrastructure.

Figure 4.30 presents the LPI values for grassland and road infrastructure derived from SPOT. The R^2 is low for both grassland and road infrastructure. LPI derived from SPOT shows almost no significant change in either land cover class over the two decades encompassed by the image data set. Figure 4.30 suggests that the loss of grassland LPI in 2005 is likely attributable to the gain in road infrastructure LPI, although there is no way to verify this.

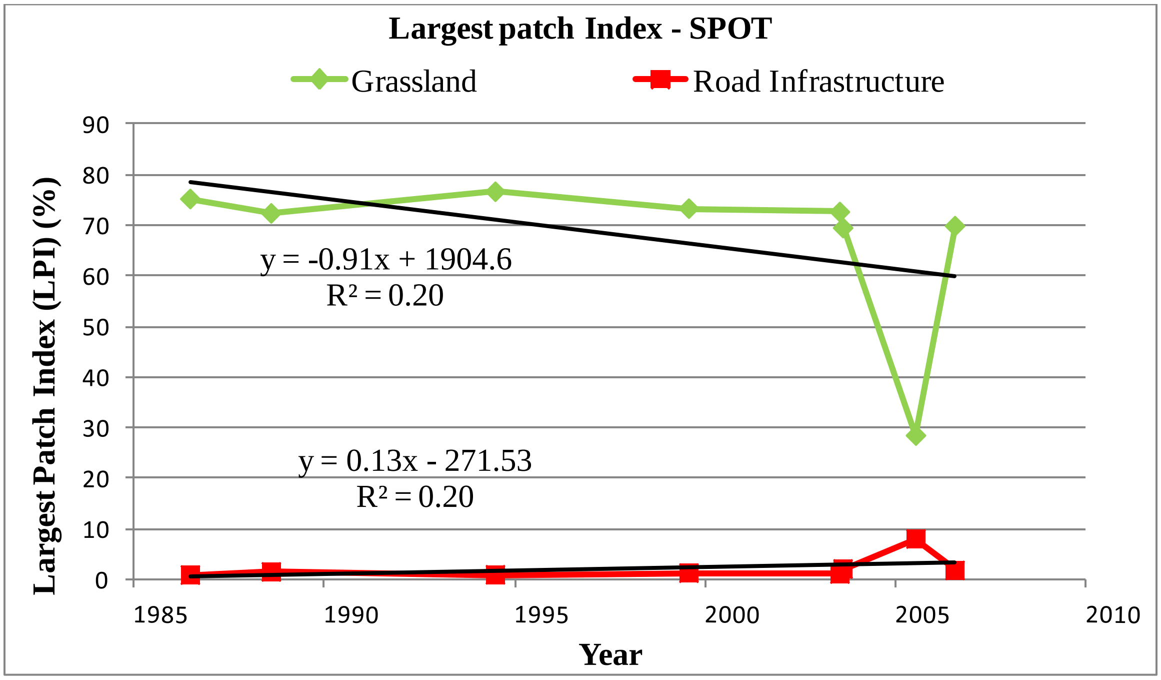

Figure 4.30: Largest Patch Index (LPI) fragmentation metric derived from SPOT.

Figure 4.31 compares LPI for grassland to LPI for road infrastructure derived from SPOT thematic maps. It shows a negative correlation and very high R^2, similar to the Landsat case (Figure 4.29), which indicates that the gains or losses in the SPOT-based LPI of grassland may be attributable to losses or gain in the LPI of road infrastructure. The distribution of the points is peculiar in the plot because only six similar years were found containing Landsat and SPOT data and there is no data available for groups of years in the middle of the trend. Also, the very high R^2 is anchored by the 2005 year.

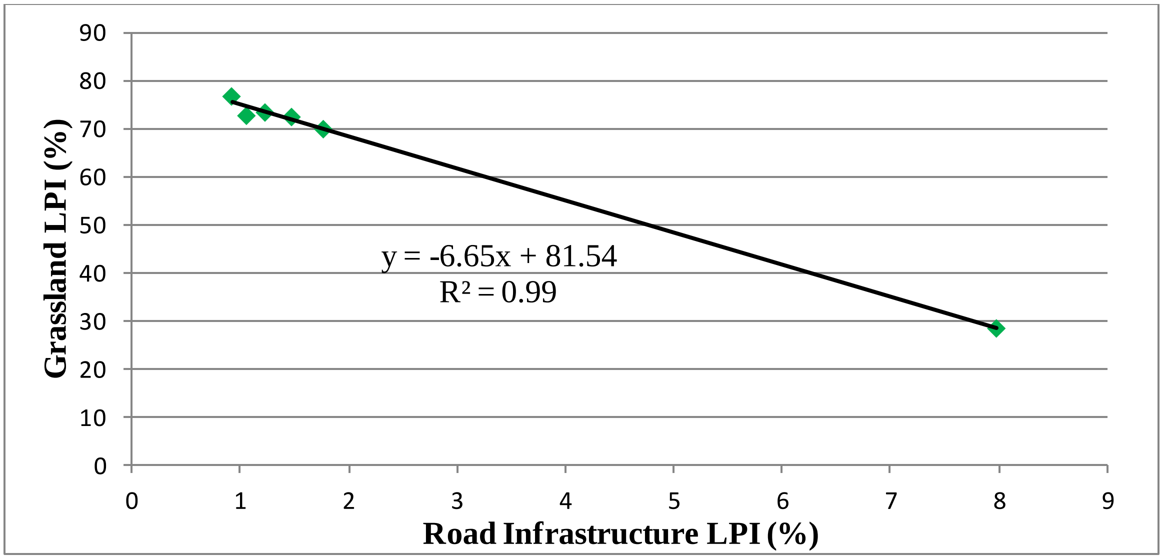

Figure 4.31: SPOT-based LPI for grassland versus LPI for road infrastructure.

Figure 4.32 compares Landsat-based and SPOT-based LPI for grassland for same years. The distribution of the points is unusual because only six similar years were found containing Landsat and SPOT data, and the 2005 year is anchoring the low R^2.

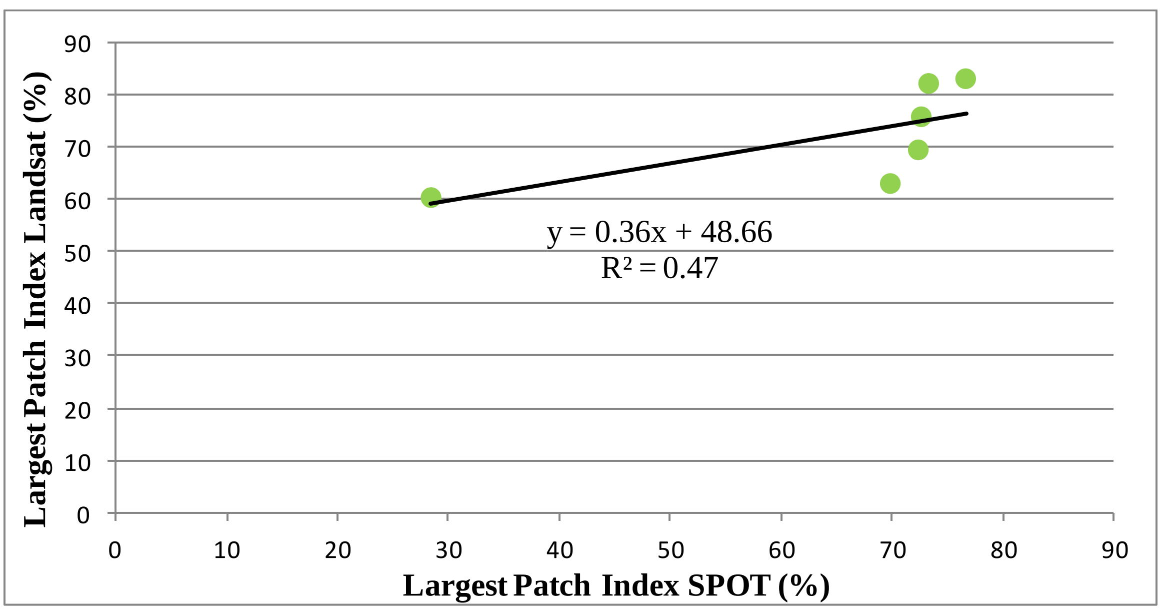

Figure 4.32: Grassland LPI - Landsat versus SPOT for the same years.

Figure 4.33 compares Landsat-based and SPOT-based LPI for road infrastructure for the same years. In this Figure, all the points are showing big differences between Landsat and SPOT road infrastructure LPI. The distribution of the points is so unusual because only six similar years were found containing Landsat and SPOT data and, therefore, there is no data available for groups of years in the middle of the trend and the 2005 year is anchoring the low R^2.

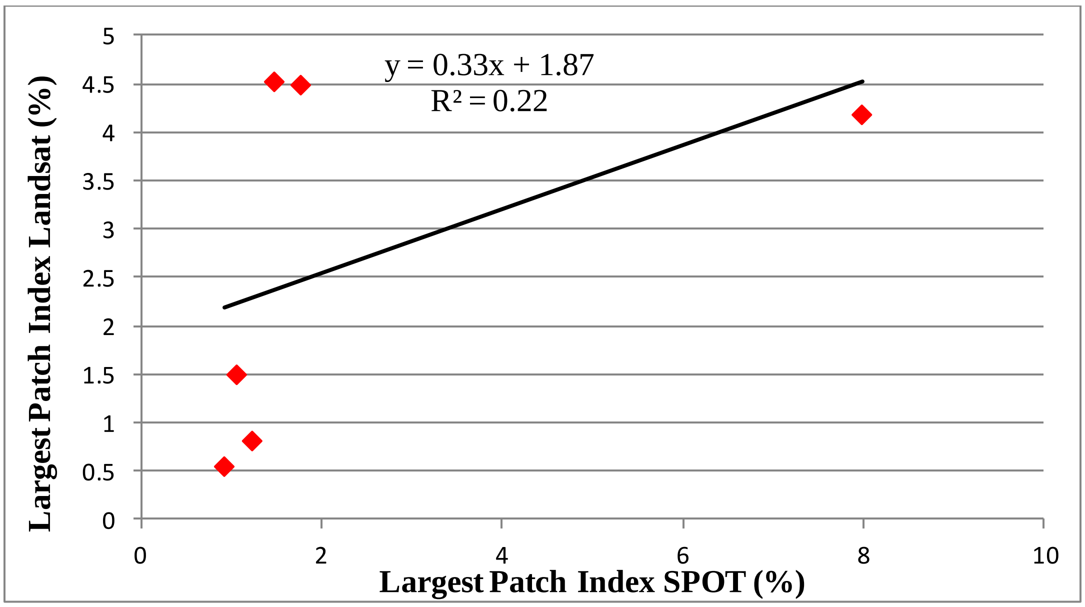

Figure 4.33: Road infrastructure LPI - Landsat versus SPOT for same years.

The differences between the Landsat-based and SPOT-based LPI results for grassland and road infrastructure are possibly due to the different image acquisition dates and spatial resolutions of the two sensors.

The fragmentation results presented in this section are for NP and LPI. The relationship between grassland and road infrastructure results, and the differences between Landsat-based and SPOT-based results are similar generally for the other fragmentation metrics (Appendix B).

5 CONCLUSIONS

Remote sensing technology is useful in monitoring grassland health for planning and improving both economic and social uses. This work requires appropriate data for identifying grassland for accurate classifications. The thesis research goals were to estimate the spatial extent of grassland and the fragmentation of grassland, as well as their changes over time mainly as a result of road infrastructures due to oil and gas exploration and other transportation purposes using multi-year multispectral satellite imagery. The classes of interest for this research are grassland, road infrastructure, crops and water. The SVM classifier was used for the image classification process. The classification results showed an average of 98.2 % overall accuracy for Landsat images and 98.2 % for SPOT images.

Based on the resulting thematic classifications, spatial extent was estimated for all four land cover classes. The results are presented for grassland and road infrastructure classes because their spatial extents and fragmentations are of greater interest than those of crops and water.

The first objective of this research was to estimate the spatial extent of native grasslands using multi-year, multi-spectral satellite imagery and, then, to estimate quantitatively the rate and location of grassland change. The results present the changes of spatial extent of grassland over 25 years. Based on Landsat and SPOT satellite image data, the results say that in Newell County there is almost no significant change found in the grassland and road infrastructure land cover in over two decades. Significant year-to year variations in spatial extent of both grassland and road infrastructure are found and the changes in the two land cover types are negatively correlated, indicating that the reduction in grassland is almost certainly due to the gain in road infrastructure. Therefore, the findings suggest that, in each specific year of the time period of two decades, grassland reduced to the gain in road infrastructure. Hence, the merit of the methodology is proved.

The second objective of this research was to estimate the fragmentation of grassland as a result of road infrastructures due to oil and gas exploration and other transportation. Fragmentation metrics were computed using the FRAGSTATS 3.3 software. The overall temporal trend results of over two decades show that there is no significant change in number of patches (NP) results derived from Landsat. However, NP results derived from SPOT show some significant change. There appears to be year-to-year variations in NP results for both classes, but, unlike the case for spatial extent, there is no mirror-like relationship between the grassland NP and the road infrastructure NP. If anything, the correlation between the two classes is slightly positive. It is found that the gains or losses in the number of grassland patches are not attributable to losses or gains in the number of road infrastructure patches. So it cannot be said that that the grassland was fragmented by the road infrastructure. Therefore, the second objective of estimating fragmentation of grassland as a result of road infrastructure is not met in this research with the provided data sets. The overall trend results for LPI over two decades show that there is no significant change in LPI results derived from either Landsat or SPOT. Also, it is found from the results, that gains and losses in Landsat and SPOT-based LPI of grassland are attributable to the losses or gains in the LPI of road infrastructure. While it is likely that the differences between the Landsat-based and SPOT-based fragmentation metrics occur may be due to the different image acquisition dates (Landsat and SPOT images were captured a few weeks apart), which may have resulted in the differences of the land cover, and also the spatial resolution differences of the Landsat and SPOT (the surface area represented by SPOT pixels is less than half the surface area of Landsat pixels), there is no way of verifying these factors.

Three factors affected the results in this research. The first factor that may have significant impact on the results is the weather. It is known that the frequency of rain events and amount of rainfall in southern Alberta can affect grassland growth. The spectral reflectance signatures of bare patches due to lack of moisture and blow-out areas are similiar to that of road infrastructure such that bare patches and blow-out areas were classified as road infrastructure.

The second factor that possibly had an impact on the results is the spatial resolution of the sensors. The Landsat-based and SPOT-based results for spatial extent and fragmentation metrics differ may be due to the spatial resolution. Road infrastructure can be extracted more accurately from SPOT images compared to Landsat images because of the higher spatial resolution of SPOT images. The surface area represented by SPOT pixels is less than half the surface area of Landsat pixels. Hence, spatial resolution of the sensors possibly had an impact on the fragmentation results, but there is no way of proving this.

The last factor that may have affected the results is the image acquisition date. The Landsat and SPOT images were captured a few weeks apart in most cases, which may have resulted in differences in the land cover, grassland in particular. However, there is no information available to ascertain whether or not this factor affected the results for spatial extent and/or fragmentation.

This research examined new ways of quantifying native grassland change and providing information on the spatial extent and fragmentation of native grasslands. This research will help to assess the current and future status of native grasslands, particularly in the prairie region of Canada and also the land managers and government agencies to provide input into decision support systems and land management programs. Remote sensing is known to be useful for estimating the spatial extent of vegetated areas such as grassland. The research presented in this thesis advanced this capability to estimate the spatial extent of grassland for over 25 years of span. The possibility that remote sensing image data can be used to obtain fragmentation statistics for analysis was also explored. The results indicate that it is possible to estimate fragmentation of grassland in a study area using remote sensing image data. However, it cannot be concluded that the fragmentation of the grassland was due to the road infrastructure.

Given the data sets and the results of the spatial extent and fragmentation statistics, the first hypothesis, that remote sensing provides an unique opportunity to assess and monitor fragmentation of grassland, is accepted. Using remote sensing, satellite images of over two decades were classified and thematic maps were produced. Fragmentation metrics were calculated for the land cover classes from the Landsat and SPOT thematic maps of over two decades and fragmentation of grassland was estimated.

Landsat and SPOT image data yield spatial extent and fragmentation results that differ. While it is likely that the SPOT-based results are better, the limited number of data sets for comparison (six) is such that this question could not be answered within the scope of this study. Hence, the second hypothesis, that better spatial extent and fragmentation results can be achieved with SPOT rather than Landsat due to SPOT's higher spatial resolution, is not accepted.

Future research should be done with higher spatial resolution images, which can help to extract linear features like roads more accurately and potentially yield better results. Also, it is possible to use linear feature extraction, which will helpt to extract linear features and better results can be achieved. Increased frequency in image capture times may improve the process of tracking spatial extent and fragmentation of the classes of interest.

6 REFERENCES

Abdullah, S. A., and Nakagoshi, N., 2006, Changes in landscape spatial pattern in the highly developing state of Selangor, peninsular Malaysia. **Landscape and Urban Planning**, 3: 263–275.

Butterfield, H. S., and Malmstrom, C.M., 2006, Experimental use of remote sensing by private range managers and its influence on management decisions. **Rangeland Ecology and Management**, 59: 541-548.

Brown, M., Gunn, S. R., and Lewis, H. G., 1999, Support vector machines for optimal classification and spectral unmixing. **Ecological Modelling**, 120: 167-179.

Cakir, G., Sivrikaya, F., and Keles, S., 2007, Forest cover change and fragmentation using Landsat data in Macka State Forest Enterprise in Turkey. **Environmental Monitoring Assessment,** 137: 51-66.

Castelli, O., Fent, L., McEwan, D., Adams, B., Orr, R. and McNeil, R., 2005, **Grassland Vegetation Inventory (GVI) Final Report**. GVI committee, Lethbridge, Alberta, pp. 1-67.

Cortes, C., and Vapnik, V., 1995, Support-vector networks. **Machine Learning**, 20: 273-297.

Eckhardt, D. W., Verdin, J.P., and Lyford, G.R., 1990, Automated update of an irrigated lands GIS using SPOT HRV imagery. **Photogrammetric Engineering and Remote Sensing**, 56: 1515-1522.

Elvidge, C.D., Yan, D., Ridgeway, D. W., and Lunetta, R.S., 1995, Relative radiometric normalization of Landsat Multispectral Scanner (MSS) data using an automatic scattergram-controlled regression. **Photogrammetric Engineering and Remote Sensing**, 61: 1255-1260.

Fauvel, M., Chanussot, J., and Benediktsson, J.A., 2006, Evaluation of kernels for multiclass classification of hyperspectral remote sensing data. In **ICASSP 2006, Proceedings of the IEEE International Conference on Acoustics, Speech and Signal Processing**, 14-19 May 2006, Toulouse, France. IEEE New York. 2: 813-816.

Galaty, J.G., and Johnson, D.L., 1990, Introduction: pastoral systems in global perspective. In: Galaty, J.G., Johnson, D.L. (Eds.). **The World of Pastoralism: Herding Systems in Comparative Perspective**, The Guilford Press, New York, pp. 1-32.

Guo, X., Monitoring grassland health with remote sensing approaches, 2003, **Prairie Perspectives**, pp. 11-22.

Haines-Young, R. and Chopping, M., 1996, Quantifying landscape structure: a review of landscape indices and their application to forested landscapes. **Progress in Physical Geography**, 20: 418–445.

Harris, A.T., and Asner, G.P., 2003, Grazing gradient detection with airborne imaging spectroscopy on a semi-arid rangeland. **Journal of Arid Environments**, 55: 391-404

Hobbs, N.T., Galvin, K.A., Stokes, C.J., Lackett, J.M., Ash, A.J., Boone, R.B., Reid, R.S., and Thornton, P.K., 2008, Fragmentation of rangelands: Implications for humans, animals, and landscapes, **Global Environmental Change,** 18: 776-785.

Huang, C., Davis, L.S., and Townshend, J.R., 2002, An assessment of support vector machines for land cover classification. **International Journal of Remote Sensing**, 23(4): 725-749.

Hunt, E.R., Jr., Everitt, J.H., Ritchie, J.C., Moran, M.S., Booth, D.T., Anderson, G.L., Clark, P.E., and Seyfried, M.S., 2003, Applications and research using remote sensing for rangeland management. **Photogrammetric Engineering & Remote Sensing,** 69(6): 675-693.

James, L.F., Young, J.A., and Sanders, K., 2003, A new approach to monitoring rangelands. **Arid Land Research and Management,** 17: 319-328.

Janzen, H.H., Campbell, C.A., Gregorich, E.G., and Ellert, B.H., 1997, Soil carbon dynamics in Canadian ecosystems. In Lal, R., Kimble, J.M., Follet, R.F., and Stewart, B.A., (Eds.). **Advances in Soil Science: Soil Process and the Carbon Cycle,** CRC Press Inc., Chapter 5, pp. 57-80.

Jensen, J. R., 2007, **Remote Sensing of the Environment: An Earth Resource Perspective** (2 ed.). Upper Saddle River, NJ: Pearson Education, Inc, 592 pages.

Lund, H.G., 2007, Accounting for the world's rangelands. **Rangelands**, 29(1): 3-10.

McGarigal, K., and Marks, B. J., 1995, FRAGSTATS: Spatial pattern analysis program for quantifying landscape structure. **U.S. Forest Service General Technical Report,** PNW 351. Sci. 260: 1905-1910.

McGarigal, K., Tagil, S., and Cushman, A, S., 2009, Surface metrics: an alternative to patch metrics for the quantification of landscape structure. **Landscape Ecology,** 24: 433-450.

Marsett, R.C., Qi, J., Heilman, P., Biedenbender, SH., Watson, M.C., Amer, S., Weltz, M., Goodrich, D., and Marsett, R., 2006, Remote sensing for grassland management in the arid southwest. **Rangeland Ecology & Management,** 59(5): 530-540.

Melgani, F., and Bruzzone, L., 2004, Classification of hyperspectral remote sensing images with support vector machines. **IEEE Transactions on Geoscience and Remote Sensing**, 42(8): 1778-1790.

Millennium Ecosystem Assessment (MEA), 2005, **Ecosystems and Human Wellbeing: Synthesis**. Island Press, Washington, DC, 64 pages.

Mitchell, G.J., and Somoliak, S., 1971, Antelope range characteristics and food habits in Alberta. **The Journal of Wildlife Management,** 35(2): 238-250.

Norse, D. and Tschirley, J.B., 2000, Links between science and policy making. **Agriculture, Ecosystems and Environment**, 82: 15-26.

Olsen, B.D., 1994, Alberta's prairie vegetation: past and present use. **Rangelands,** 16(2): 58-62.

Owens, R.A., and Myers, M.T., 1973, Effects of agriculture upon populations of native passerine birds of an Alberta fescue grassland. **Canadian Journal of Zoology,** 51: 697-713.

Perkins, J.S., and Thomas, D.S.G., 1993, Spreading deserts or spatially confined environmental impacts? Land degradation and cattle ranching in the Kalahari Desert of Botswana. **Land Degradation and Rehabilitation** 4, 179–194.

Price, J.C., 1994, How unique are spectral signatures? **Remote Sensing of Environment**, 49: 181-186

Pyke, D.A., and Herrick, J.E., 2003, Transitions in rangeland evolutions. **Rangelands,** 25(6): 22-30.

Raines, G. L., 2002, Description and comparison of geologic maps with FRAGSTATS - A spatial statistics program. **Computers and Geosciences** 28: 169-177.

Rasmussen, G.A., and Bunson, M.W., 1996, Strategies to manage conflicts among multiple users. **Weed Technology**, 10(2): 447-450.

Richter, R., 1990, A fast atmospheric correction algorithm applied to LandsatTM images. **International Journal of Remote Sensing**, 11: 159–166.

Roth, E., Fratkin, E. (Eds.), 2005, **As Pastoralists Settle: Social, Economic, and Health Consequences of Pastoral Sedentarization in Northern Kenya**, Kluwer Academic Publishers, Amsterdam, Volume 1, 280 pages.

Schott, J.R., 2007, **Remote Sensing The Image Chain Approach** (2 ed.), Oxford University Press, Inc, 666 pages.

Smith, A.M., and Kloppenburg, C., 2010, Remote sensing tools for mapping native grassland change in western Canada. **Proceedings of the 31st Canadian Symposium on Remote Sensing / Canadian Association of Geographers (CAG) Annual Conference**, Piwowar, J. M. (Editor), pp. 293-296.

Smith, A.M., Larson, G.L., Kloppenburg, C., Hill, B.D., and Teillet, P.M., 2009, Mapping native grassland change using single date multi-spectral satellite imagery. **Proceedings of the 30th Canadian Symposium on Remote Sensing**, Lethbridge, Alberta, Coburn, C.A., and Peddle, D. R. (Editors), paper # 564, pp. 659-665.

Smyth, A.J., and Dumanski, J., 1993, **FESLM: An International Framework for Evaluating Sustainable Land Management.** World Soil Resources Report. Rome, Italy: Food and Agriculture Organization of the United Nations, pp. 73-74.

Song, C., Woodcock, C.E., Seto, K.C., Pax Lenney, M., and Macomber, S.A., 2001, Classification and change detection using Landsat TM data: when and how to correct atmospheric effects? **Remote Sensing of Environment**, 75: 230–244.

Southworth, J., Munroe, D., and Nagendra, H., 2004, Land cover change and landscape fragmentation- comparing the utility of continuous and discrete analyses. **Agriculture, Ecosystems and Environment,** 101(2004): 185-205.

Stoddart, L.A., 1967, What is range management? **Journal of Range Management,** 20(5): 304-307.

Teillet, P.M., 2010, Sensor webs: A geostrategic technology for integrated Earth sensing, **IEEE Journal of Selected Topics in Applied Earth Observations and Remote Sensing**, 3(4): 473- 480.

Teillet, P.M., Gauthier, R.P., and Chichagov, A., 2001, Towards Integrated Earth Sensing: The Role of In Situ Sensing, **First International Workshop on Future Intelligent Earth Observing Satellites (FIEOS)**, G. Zhou, O. Baysal, M. Kafatos, and R. Yang, Eds. Pottstown, PA: Hierophantes Pub., 2003, Ch. 2, pp. 19-30.

Ustin, S., Roberts, D.A., Gamon, J.A., Asner, G.P., and Green, R.O., 2004, Using image spectroscopy to study ecosystem processes and properties. **BioScience,** 54(6): 523-534.

Yuan, D., Elvidge, C.D., and Lunetta, R.S., 1998, Survey of multispectral methods for land cover change analysis, **Remote sensing change detection: Environmental monitoring methods and applications,** Michigan: Ann Arbor Press, pp. 21-39.

7 APPENDICES

7.1 Appendix A: Additional thematic maps from Landsat and SPOT.

This appendix contains the rest of the Landsat-based and SPOT-based thematic maps other than the thematic maps decribed in the results. Thematic classification maps from 11 Landsat and 2 SPOT images are presented here. In the figures that follow, some pixels in otherwise grassland areas have been classified as road infrastructure (red spots in the thematic maps), as discussed earlier. For example, more pixels are classified as road infrastructure in the 1989 Landsat thematic map than in the 1992 Landsat thematic map. The 1997 Landsat thematic map shows a lower amount of road infrastructure compared to 1996. The 2004 Landsat and 2003 SPOT thematic maps show large amounts of road infrastructure development.

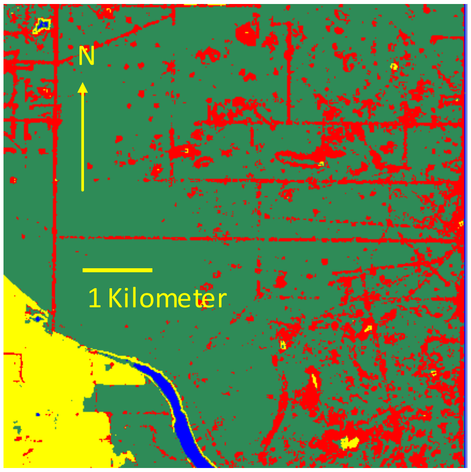

Appendix Figure 1: July 2, 1987
Landsat thematic map.

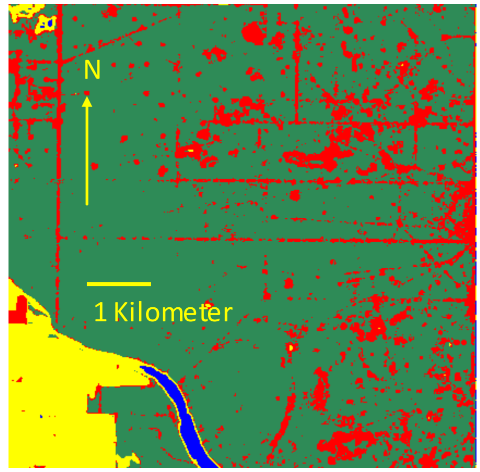

Appendix Figure 2: August 8, 1989
Landsat thematic map.

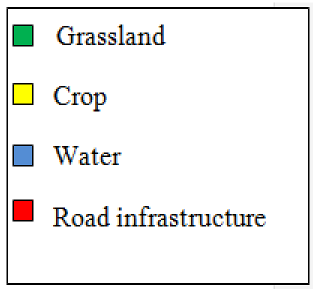

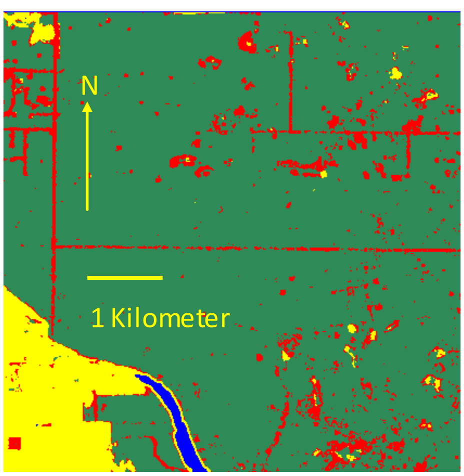

Appendix Figure 3: July 31, 1992
Landsat thematic map.

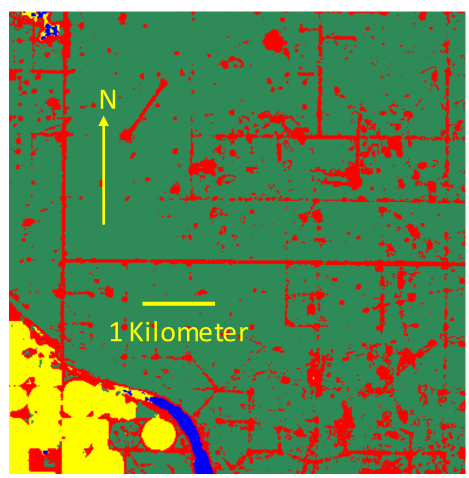

Appendix Figure 4: August 11, 1996
Landsat thematic map.

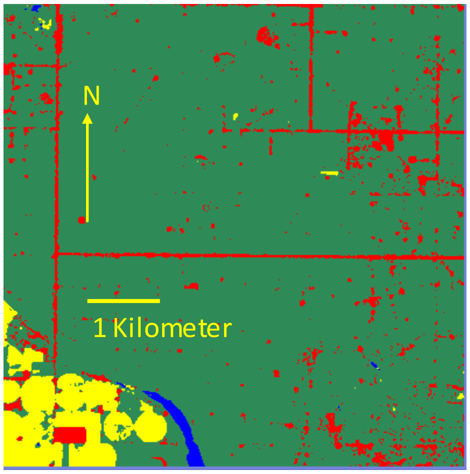

Appendix Figure 5: June 27, 1997
Landsat thematic map

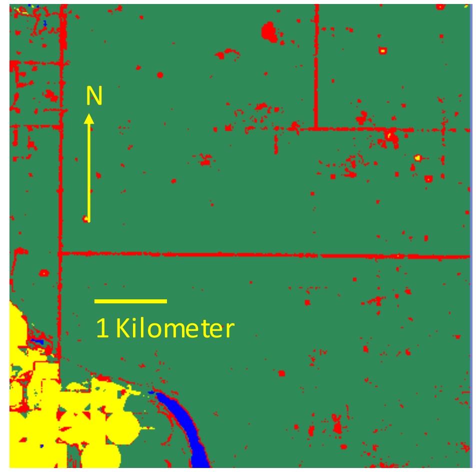

Appendix Figure 6: July 16, 1998
Landsat thematic map.

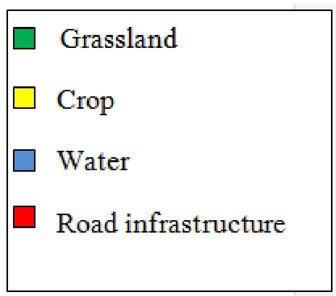

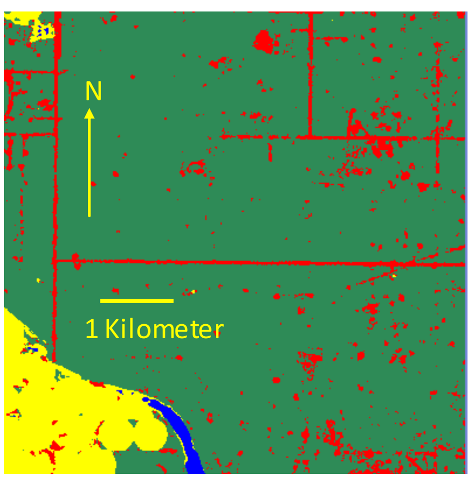

Appendix Figure 7: July 5, 2000
Landsat thematic map.

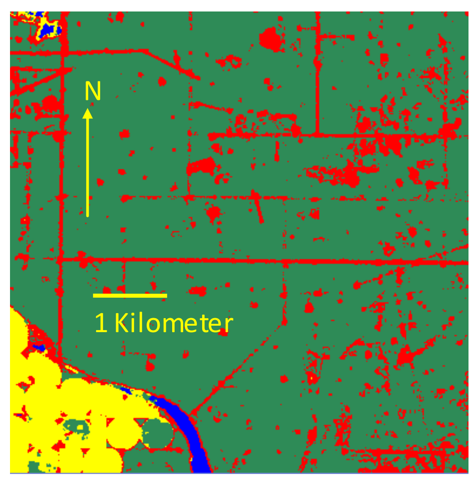

Appendix Figure 8: July 8, 2001
Landsat thematic map.

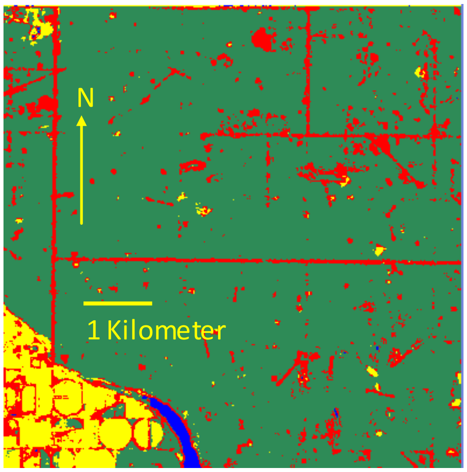

Appendix Figure 9: July 11, 2002
Landsat thematic map.

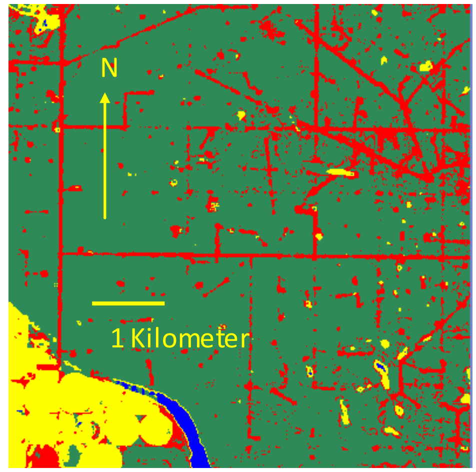

Appendix Figure 10: July 16, 2004
Landsat thematic map.

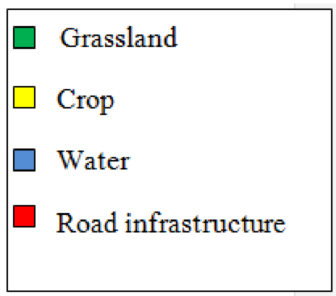

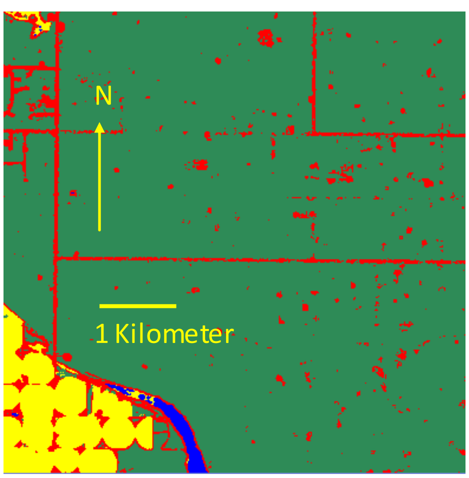

Appendix Figure 11: July 27, 2008
Landsat thematic map.

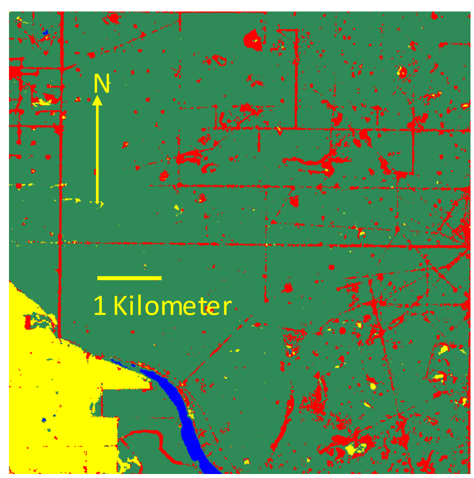

Appendix Figure 12: June 24, 1986
SPOT thematic map.

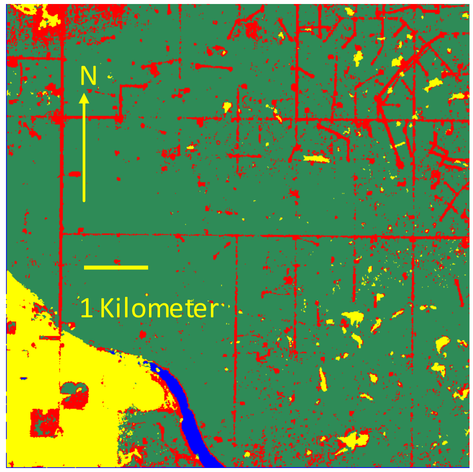

Appendix Figure 13: August 12, 2003 SPOT thematic map

Grassland

Crop

Water

Road infrastructure

7.2 Appendix B: Additional fragmentation statistics results.

This section contains fragmentation metric results derived from the temporal Landsat and SPOT image sequences other than Number of Patches (NP) and Largest Patch Index (LPI), which were described in the results section. The differences between the fragmentation metrics for Landsat-based and SPOT-based results are likely due to the differences in the spatial resolutions of the sensors and possibly due to the differences in image capture times. Some grassland and road infrastructure metrics are numerically similar. Also, some metrics have highly variable grassland and very little variation in road infrastucture. Possibly, differences in spatial resolution of the sensors and also the differences in acquired image times are reasons behind these findings. However, further research would be required to confirm these possible explanations.

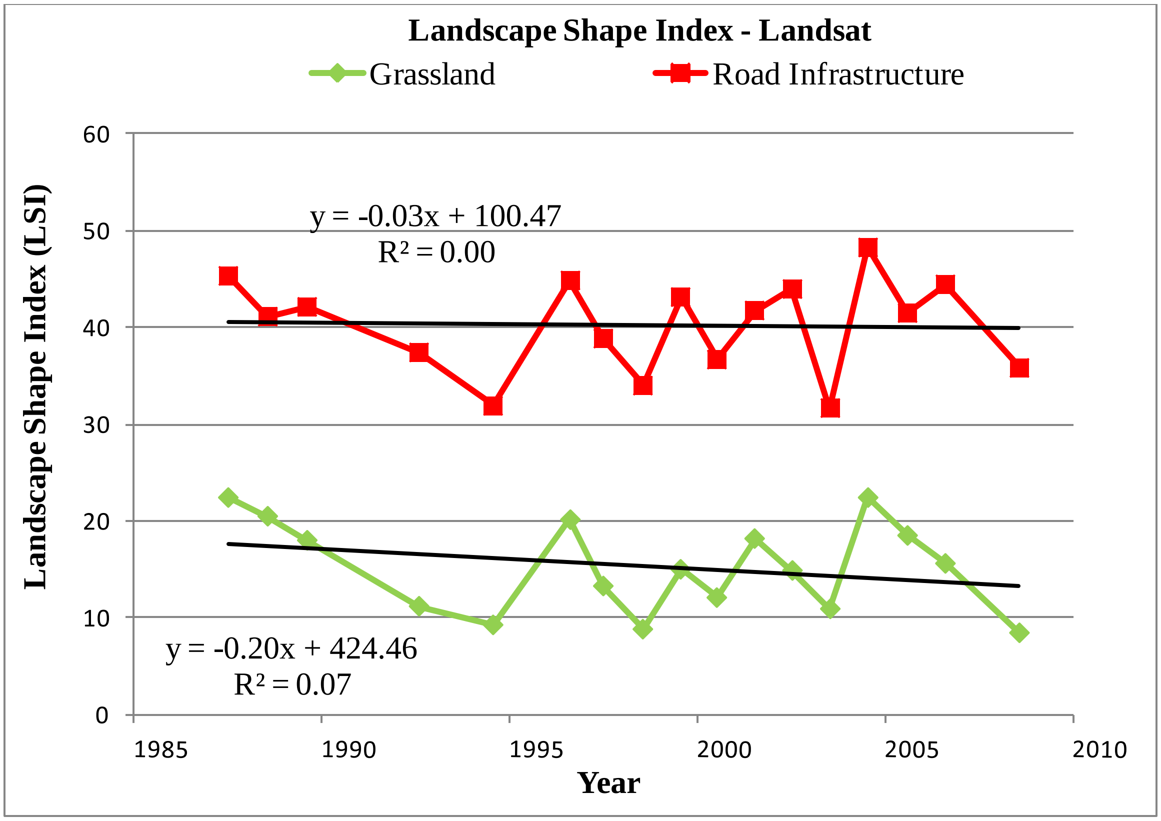

Appendix Figure 14

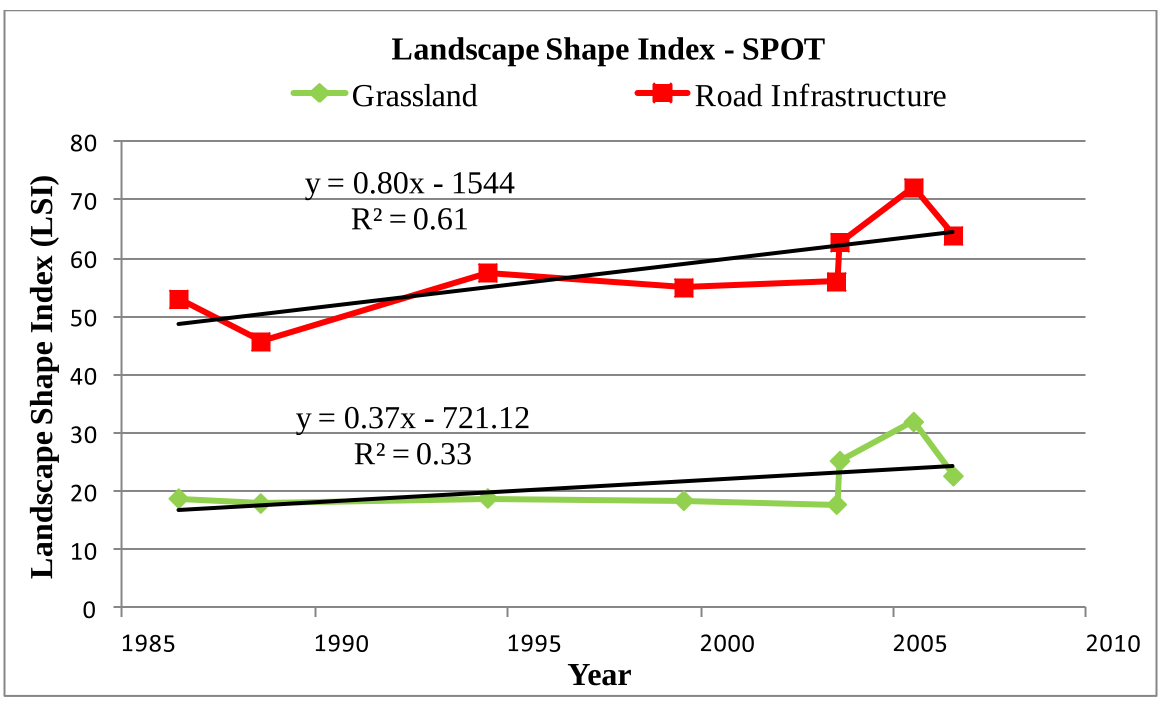

Appendix Figure 15

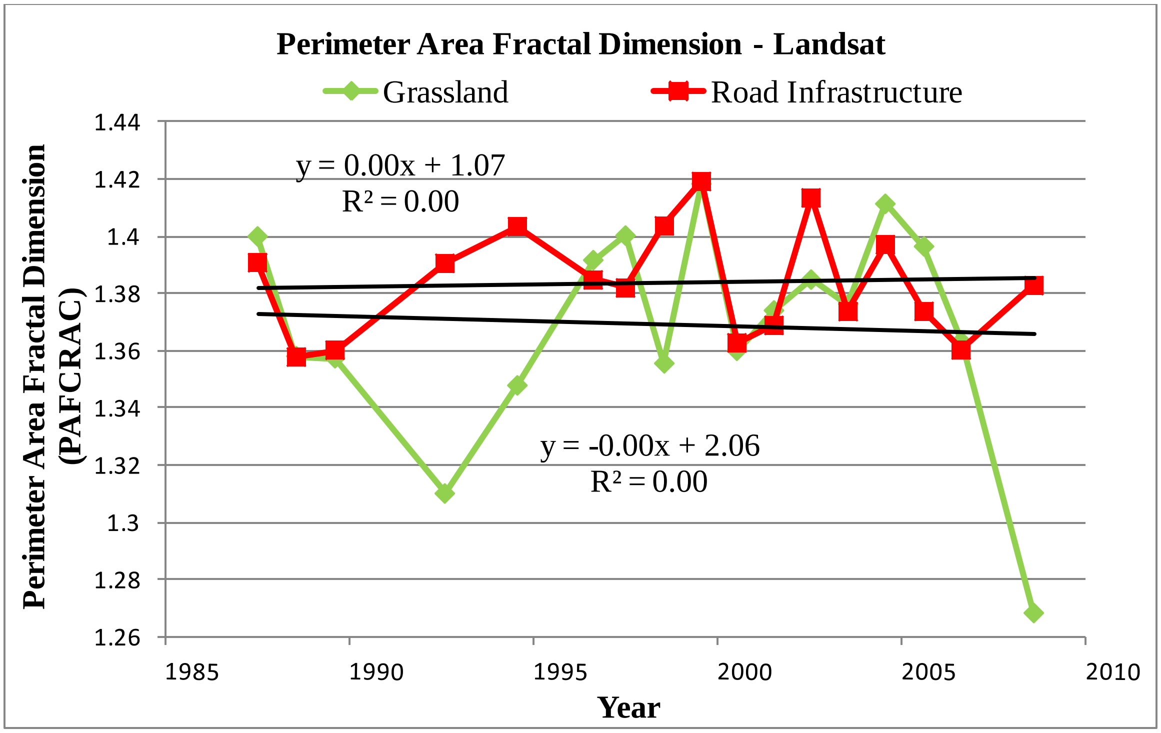

Appendix Figure 16

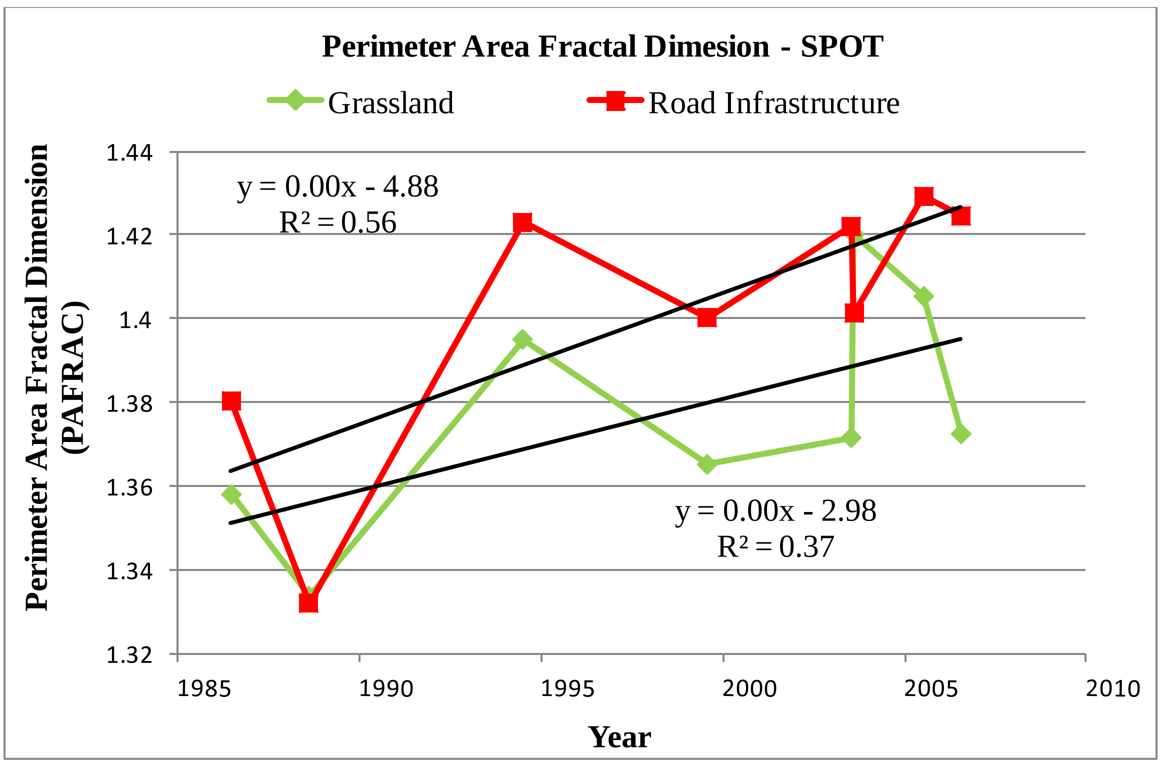

Appendix Figure 17

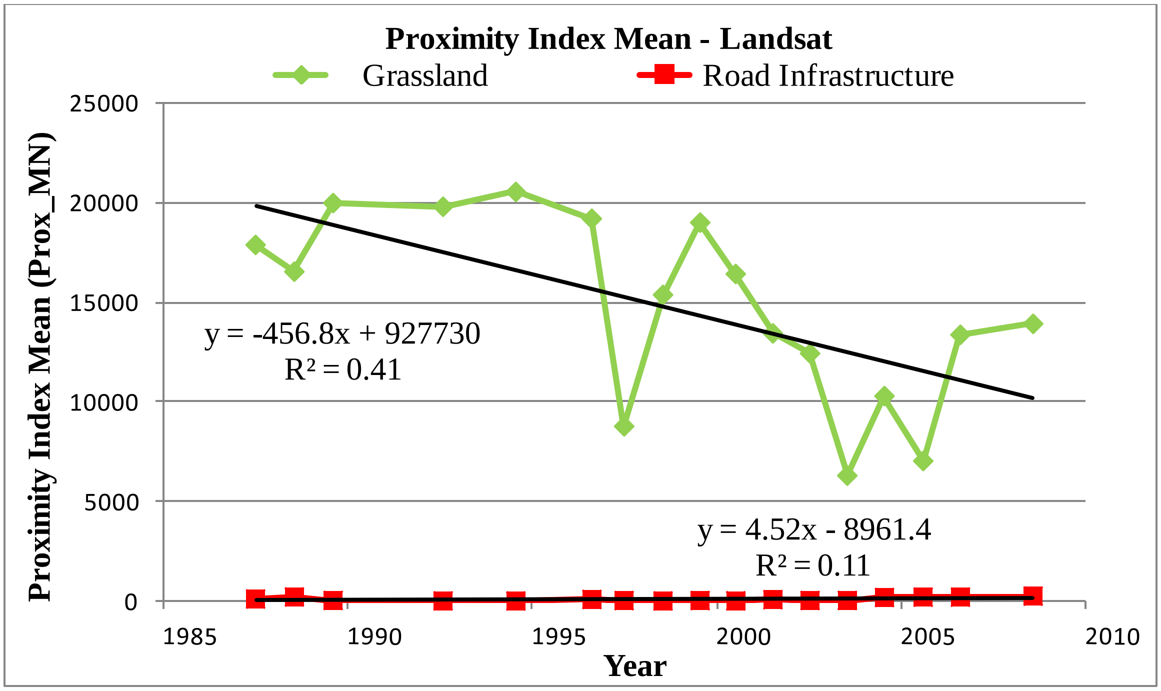

Appendix Figure 18

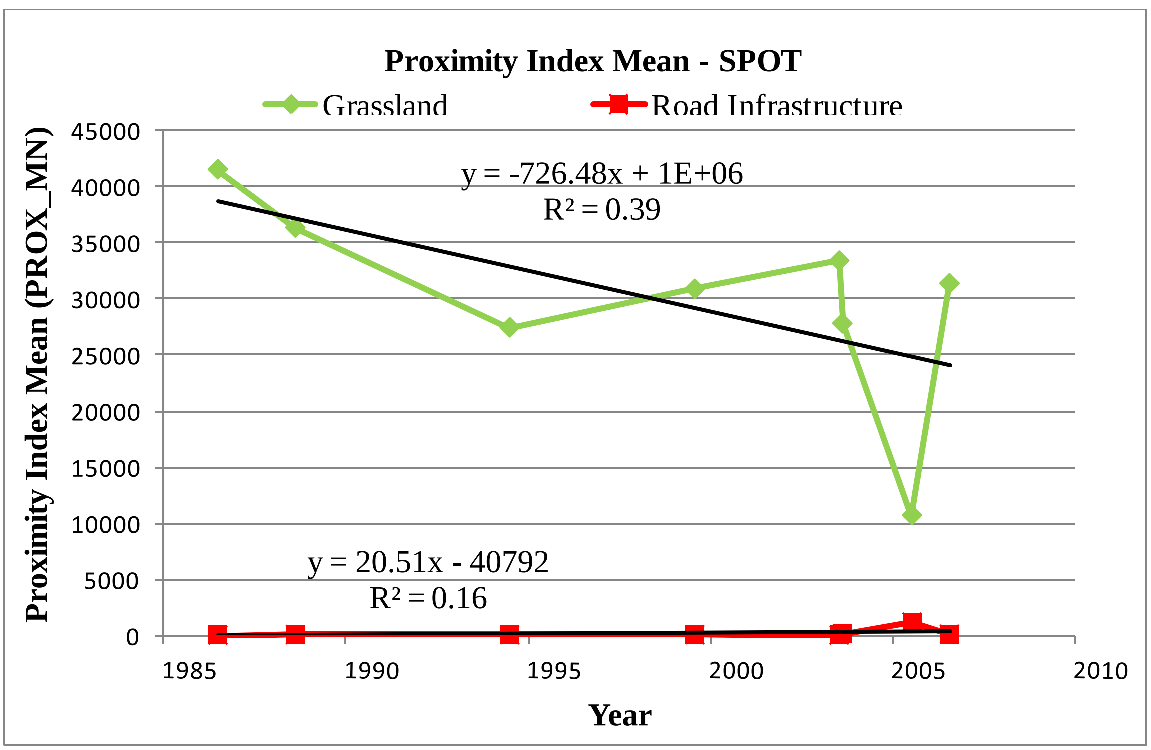

Appendix figure 19

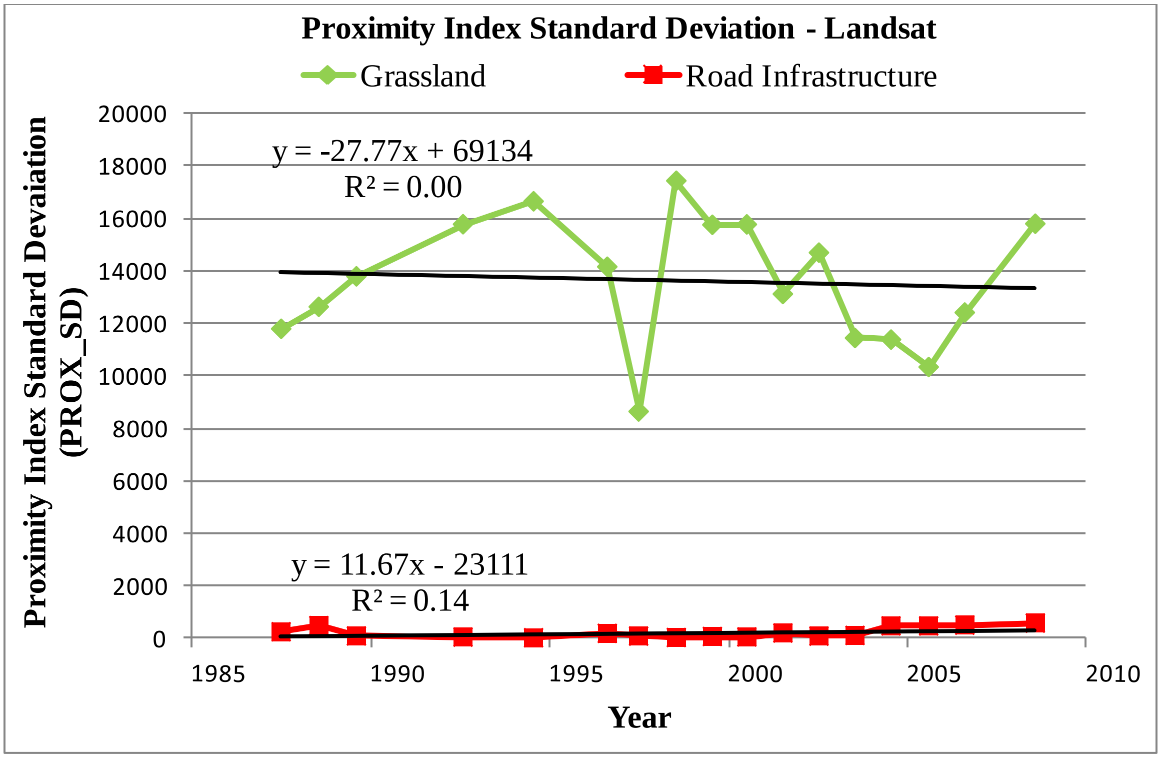

Appendix Figure 20

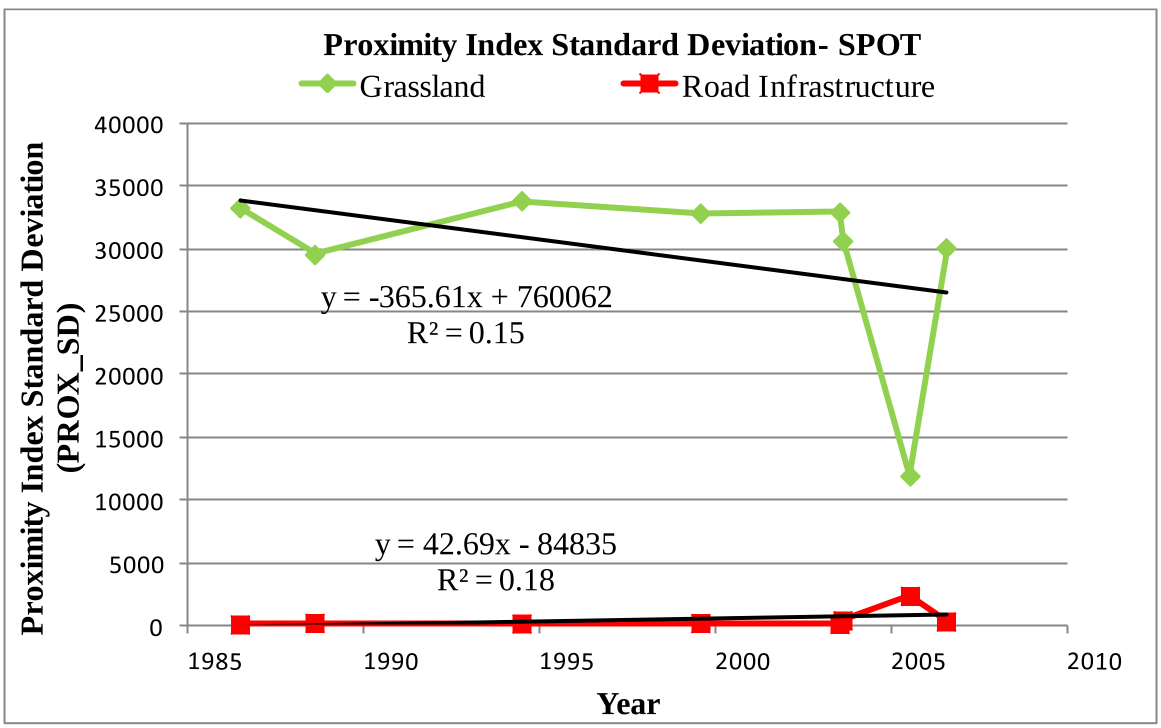

Appendix Figure 21

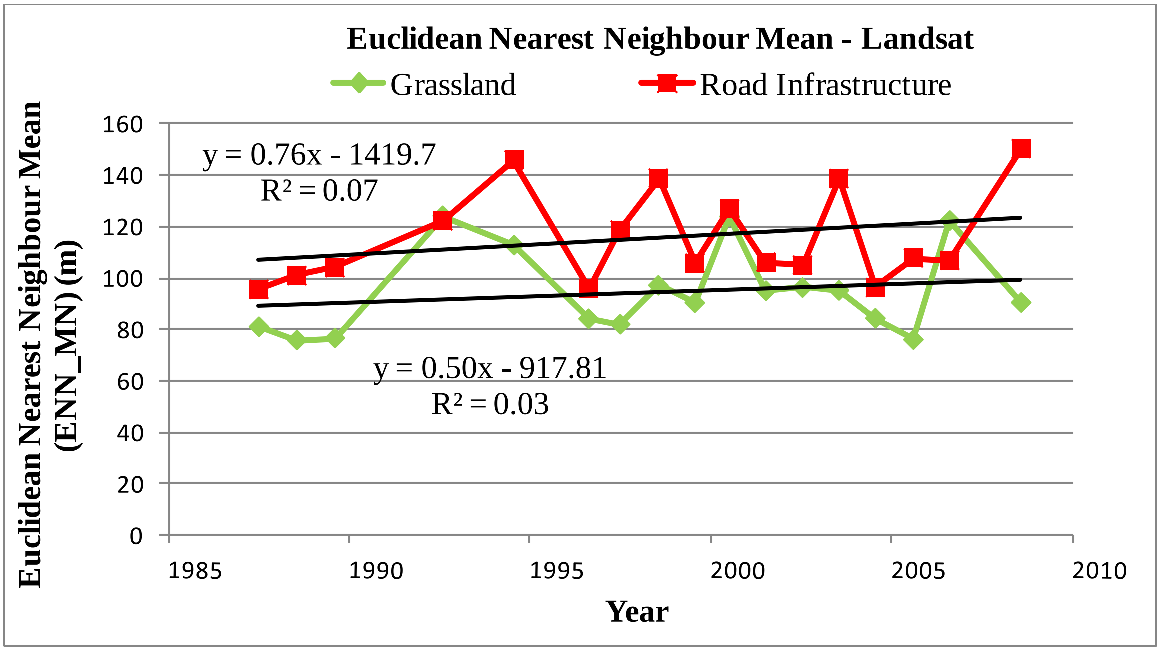

Appendix Figure 22

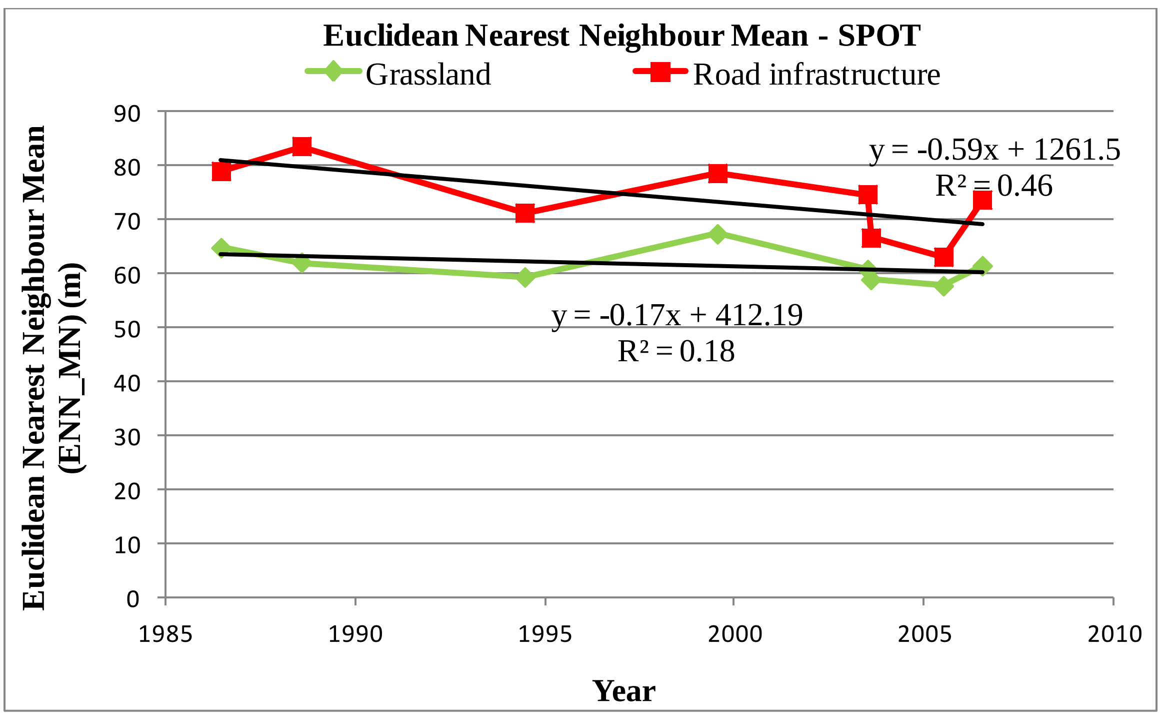

Appendix Figure 23

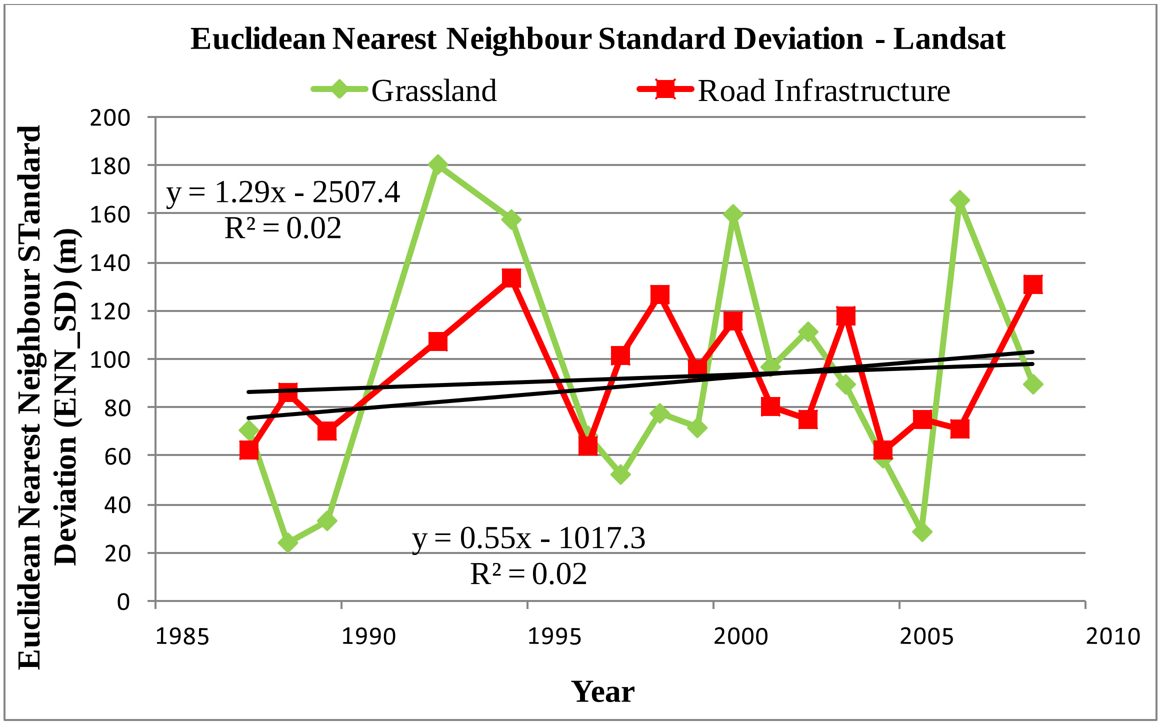

Appendix Figure 24

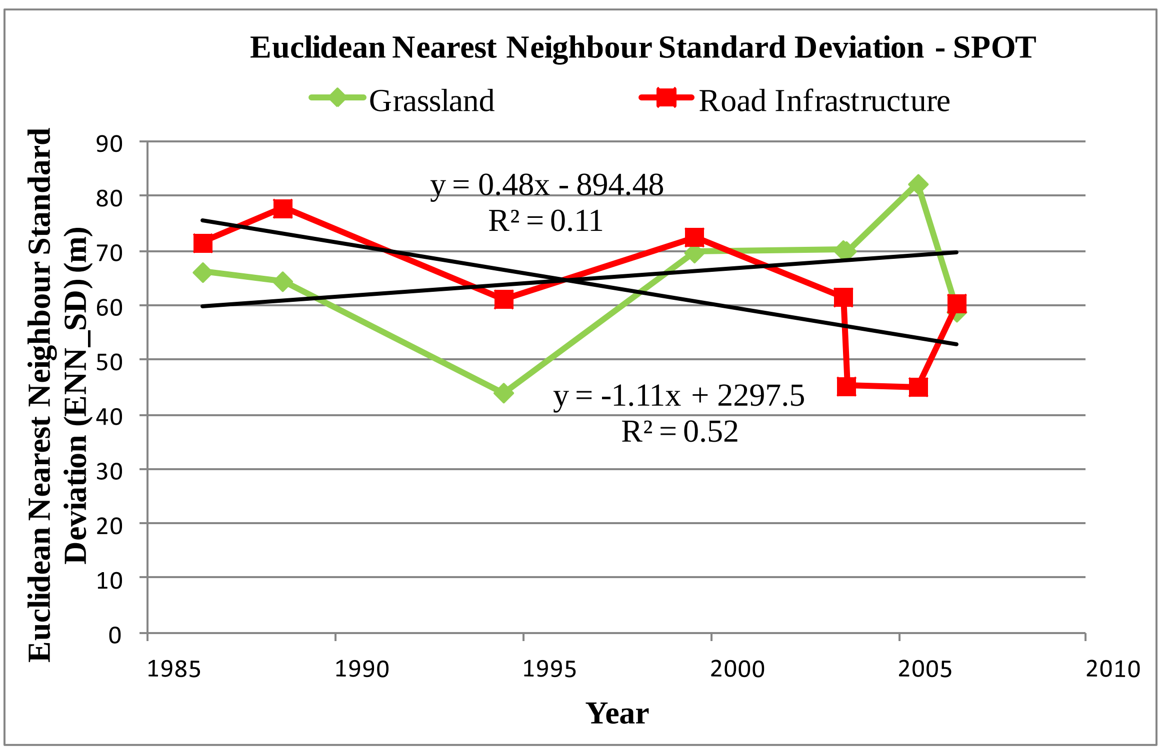

Appendix Figure 25

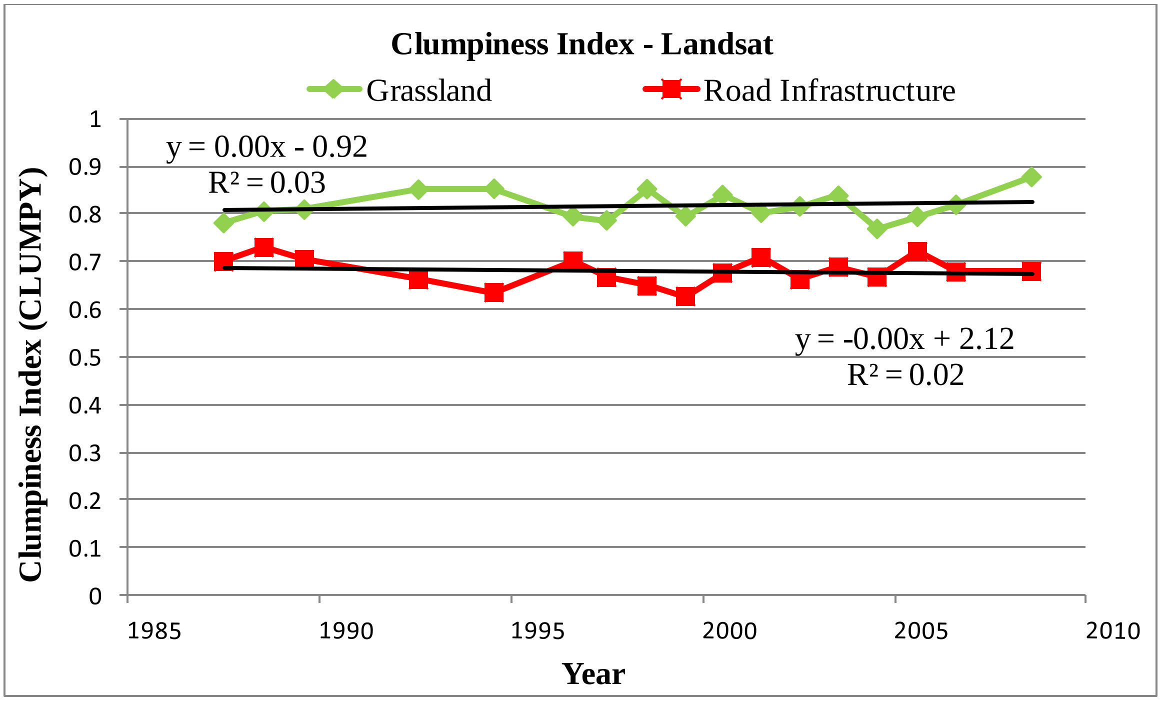

Appendix Figure 26

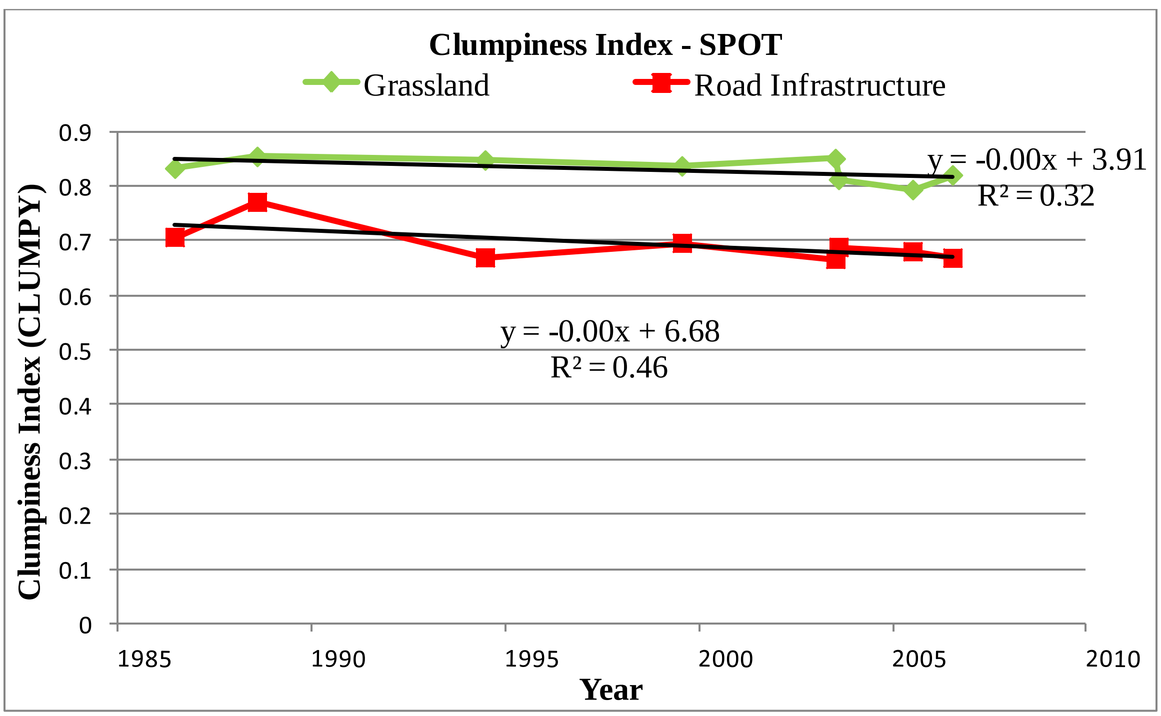

Appendix Figure 27

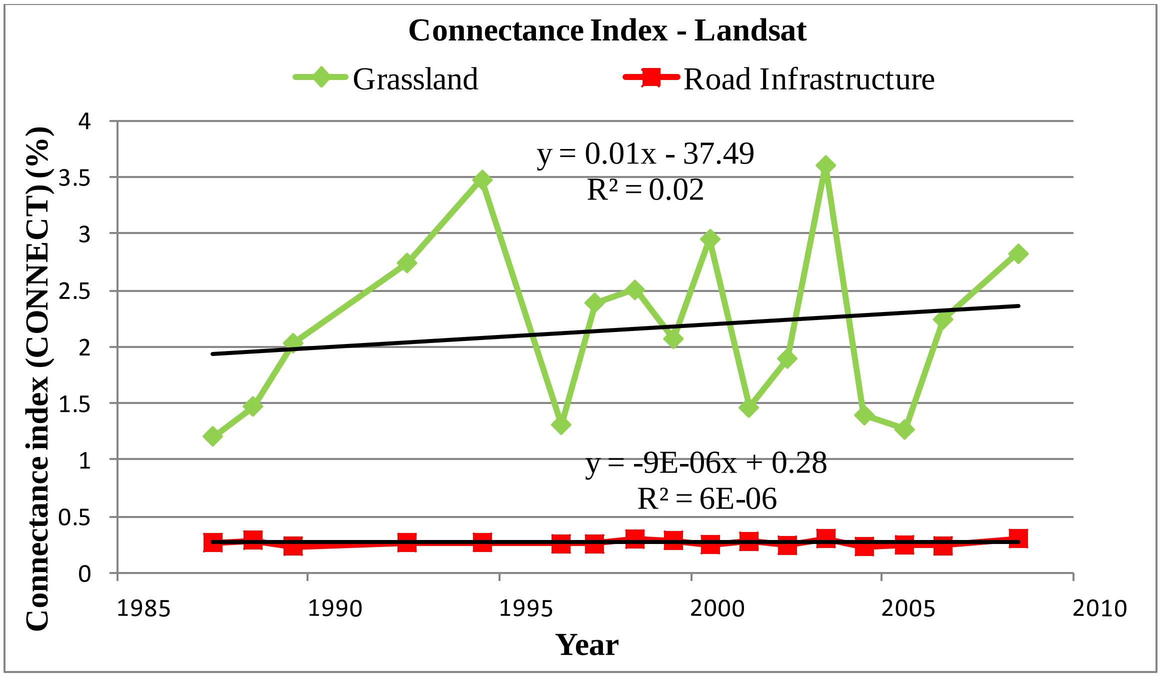

Appendix Figure 28

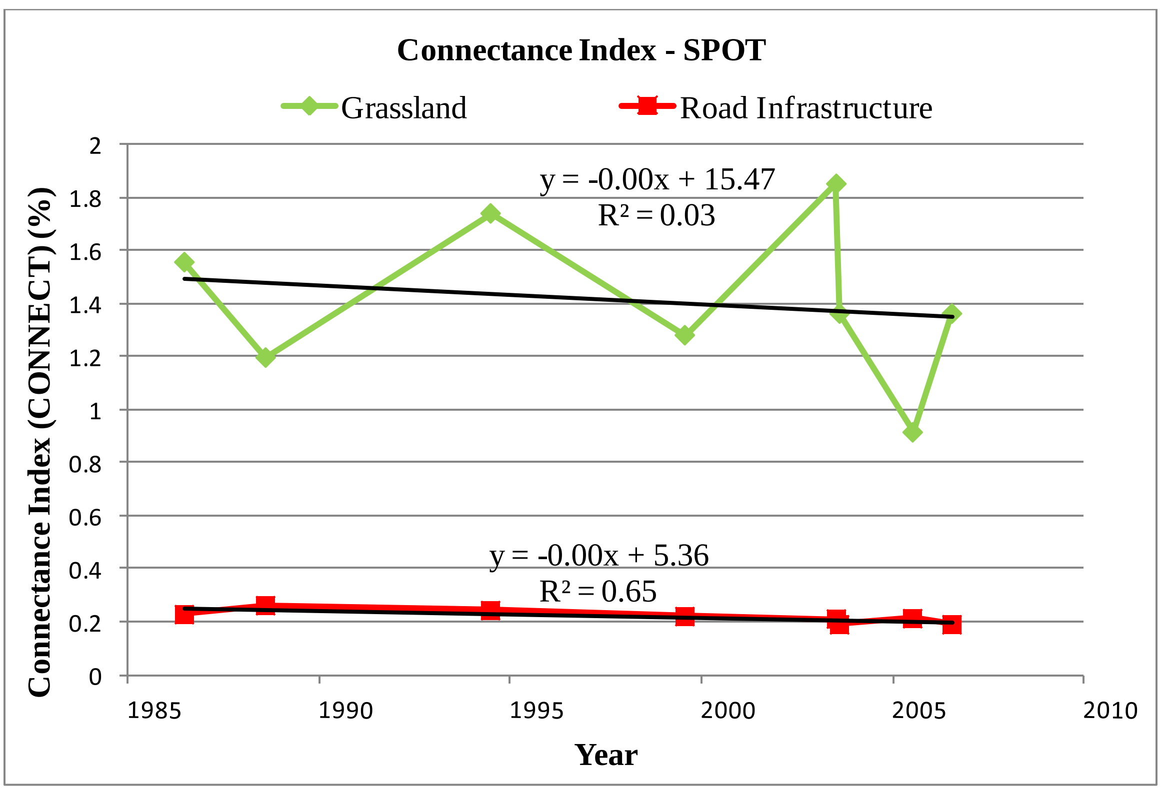

Appendix Figure 29